DISSERTATION

Titel der Dissertation

„Coarse-graining, structure and rheology of

polymer nanocomposites“

Verfasserin

Daniela Marzi, BSc MSc

angestrebter akademischer Grad

Doktorin der Naturwissenschaften (Dr. rer. nat.)

Wien, 08.04.2014

Meinen Eltern

"One never notices what has been done; one can only see what remains to be done."

(Marie Curie, 1894)

Summary

In this Doctoral Thesis, we present investigations on mixtures of polymer stars with a number of arms f and hard, colloidal additives in the nanocomposite limit, in which the colloids are smaller than the polymers. In particular, with $R_{g,S}$ denoting the gyration radius of the stars and R_C the colloid radius, we focus on size ratios $q \equiv R_{g,S}/R_C > 1$. In a first step, we derive the effective pair potential between star polymers and colloids, leading, together with the known star-star and colloid-colloid pair interaction, to a fully coarse-grained description of the binary system. The coarse-grained model is based on scaling arguments for the star polymer, and the effective potentials are confirmed by full-monomer Monte Carlo (MC) simulations. These effective interactions are employed in a two component Rogers Young integral equation theoretical approach to obtain structural data on the system, which show excellent agreement with an experimental realization for one specific system ($f = 214$ and $q = 3$) and are confirmed and extended by MC and Molecular Dynamics simulations. An addition of colloids leads to a melting of the polymer glass, in quantitative and parameter-free agreement with experiments. While already the above mentioned effective interactions allow for studying large systems in computer simulations to obtain structural and thermodynamical results, it is possible with the help of the commonly known depletion picture, to further coarse-grain the system. In this second-level coarse-graining, the colloidal particles are traced-out leaving a pure star-polymer system, interacting by means of a renormalized effective Hamiltonian in a depletion picture. The depletion interaction is derived by inversion of integral equations and it is further confirmed by the method of superposition approximation. Using the depletion approach, we are able to determine the binodal demixing lines for the system, which show that the binary system demixes much easier, the higher the functionality f of the star or the smaller q, i.e., the bigger the colloids and less asymmetric the size ratio is. This is in agreement with the results that were obtained from calculating the non-additivity parameter of the interactions. The results offer a variety of possibilities for comparison with and designing of experiments, for employing large scale simulations and to present an accurate theory valuable for such a tuneable system of star polymers and colloids, which only depends on the parameters f and q.

Zusammenfassung

Die vorliegende Dissertation befasst sich mit Mischungen von Sternpolymeren mit Funktionalität f (d.h., Anzahl der Arme ist f) und harten Kolloidteilchen im sogenannten *Nanokompositbereich*, in dem die Kolloide kleiner als die Polymere sind. Das bedeutet, dass wir uns mit Größenverhältnissen $q \equiv R_{g,S}/R_C > 1$ beschäftigen, wobei $R_{g,S}$ der Gyrationsradius der Sterne und R_C der Kolloidradius ist. Zuerst vereinfachen wir die Beschreibung dieser Mischung, indem wir effektive Paarwechselwirkungen zwischen Sternpolymeren und Kolloiden einführen und die bekannten Paarwechselwirkungen für die harten Kugeln und für die Sternpolymere verwenden. Im Detail ersetzen wir die Monomerdarstellung der Sternpolymere durch eine vereinfachte Beschreibung, die auf einer Skalierungstheorie für Polymerlösungen basiert, und vergleichen die Paarwechselwirkungspotentiale mit Ergebnissen aus monomeraufgelösten Monte-Carlo-Simulationen, was beeindruckende Übereinstimmungen für theoretische und numerische Ergebnisse liefert. Mithilfe von Integralgleichungen wird die Struktur des Systems untersucht, in denen die effektiven Wechselwirkungen über die Rogers-Young-Beziehung Einfluss nehmen. Die erhaltenen Strukturfaktoren stimmen mit denen aus Monte-Carlo-Simulationen überein und die durch die Modekopplungstheorie erhaltenen theoretischen Zustandsdiagramme spiegeln experimentelle Ergebnisse für eine bestimmte Mischung ($f = 214$ und $q = 3$) qualitativ und quantitativ wieder. Die Zugabe von Kolloiden führt zu einem Schmelzen des Sternpolymerglases. Mithilfe der effektiven Paarwechselwirkungen ist es nun einerseits möglich, auch eine große Anzahl von Teilchen in Computersimulationen zu simulieren und damit strukturelle und thermodynamische Ergebnisse der Mischung zu bestimmen. Andererseits kann das System mithilfe weiterer theoretischer Betrachtungen weiter vereinfacht werden, z.B. durch eine Betrachtung, wie die zugegebenen Kolloide die Region um ein Sternpolymer "verarmen". Die Mischung wird dann nur noch durch Sternpolymere dargestellt, die über einen veränderten, effektiven Hamiltonoperator interagieren. Dieser enthält den Einfluss der Kolloide, ohne dass diese weiterhin explizit in der Mischung dargestellt werden. Dazu werden erneut Integralgleichungen invertiert und mit einer weiteren Methode (der sogenannten Superpositionsnäherung) verglichen. Der Vergleich bestätigt unseren theoretischen Ansatz und wir können mithilfe der effektiven Einteilchenbeschreibung nun Binodalen berechnen, die aufzeigen, für welche Parameter sich die Mischung phasentrennt. Dies ist im Besonderen für hohe Funktionalität, d.h. weniger weiche Sternpolymere, und für ähnlich große Mischungskomponenten der Fall, d.h., wenn $q \gtrsim 1$ ist. Dieselbe Beobachtung konnten wir bereits durch Berechnung des Nichtadditivitätsparameters der Paarwechselwirkungen machen, so dass auch diese Vorhersage bestätigt werden kann und unseren Ansatz zur Vereinfachung der Komplexität der Mischung validiert. Die Ergebnisse eröffnen viele Möglichkeiten, theoretische Berechnungen und experimentelle Daten zu vergleichen, aber auch die Gestaltung, welche Parameter in Experimenten interessante Eindrücke liefern werden, ist bereits vorhersehbar. Nicht zu vernachlässigen ist die Nutzung der effektiven Wechselwirkungen in Vielteilchensimulationen und die exakte theoretische Beschreibung eines einstellbaren Polymer-Kolloid-Komposites, die nur von der Funktionalität der Sternpolymere und dem Größenverhältnis der beiden Komponenten abhängt.

List of (published) manuscripts

This thesis is based on the following original articles:

Chapter 2

Coarse graining of star-polymer – colloid nanocomposites,
Daniela Marzi, Christos N. Likos, and Barbara Capone,
J. Chem. Phys. **137**, 014902 (2012).

Original abstract: We consider mixtures of self-avoiding multiarm star polymers with hard colloids that are smaller than the star polymer size. By employing computer simulations, and by extending previous theoretical approaches, developed for the opposite limit of small star polymers [1], we coarse-grain the mixture by deriving an effective cross-interaction between the unlike species. The excellent agreement between theory and simulation for all size ratios examined demonstrates that the theoretical approaches developed for the colloidal limit can be successfully modified to maintain their validity also for the present case of the protein limit, in contrast to the situation for mixtures of colloids and linear polymers. We further analyze, on the basis of the derived interactions, the non-additivity parameter of the mixture as a function of size ratio and star functionality and delineate the regions in which we expect mixing as opposed to demixing behavior. Our results are relevant for the study of star-colloid nanocomposites and pave the way for further investigations of the structure and thermodynamics of the same.

Chapter 3

Glassy States in Asymmetric Mixtures of Soft and Hard Colloids,
Domenico Truzzolillo, Daniela Marzi, John Marakis, Barbara Capone, Manuel Camargo, Abdul Munam, Firmin Moingeon, Mario Gauthier, Christos N. Likos, and Dimitris Vlassopoulos,
Phys. Rev. Lett. **111**, 208301 (2013).

This Chapter contains results from theoretical and experimental investigations. The particles were synthesized by Mario Gauthier et al at the University of Waterloo, while the experiments were performed at F.O.R.T.H. in the University of Crete by Domenico Truzzolillo and coworkers. The MD results were obtained by Manuel Camargo at the University of Bogota.

Original abstract: By employing rheological experiments, Mode Coupling Theory and computer simulations based on realistic coarse-grained models, we investigate the effects of small, hard colloids on the glassy states formed by large, soft colloids. Multiarm star polymers mimic hard and soft colloids by appropriately varying the number and size of their arms. The addition of hard colloids leads, depending on their concentration, to either

melting of the soft glass or the emergence of two distinct glassy states. We explain our findings by depletion of the colloids adjacent to the stars, which leads to an arrested phase separation when the repulsive glass line meets the demixing binodal. The parameter-free agreement between experiment, theory, and simulations suggests the generic nature of our results and opens the route for designing soft-hard colloidal composites with tunable rheology.

Chapter 4

Glassy states and melting in polymer star - colloid mixtures,
Daniela Marzi, Manuel Camargo, Barbara Capone, and Christos N. Likos
In preparation.

Original abstract: We investigate the effects of hard colloidal particles on star polymer glasses by employing Rogers Young integral equations and ergodicity factors coming from mode coupling theory based on a coarse-grained picture of this binary mixture. We find that, depending on the size ratio $q = R_{g,S}/R_C$ of the stars and the colloids, the functionality f of the stars and on the concentration of added colloids, either a melting of the soft glass takes place or no effect at all occurs, if the mixture is highly asymmetric. Our results can be explained by understanding the small colloidal particles as depletants for the polymeric stars, where the effect of reducing the repulsions can lead to a glass melting. The validity of the initial star-star structure factors, coming from Rogers-Young integral equation theory was proven with the help of coarse-grained Monte Carlo simulations. Our results have shown to be relevant in experimental systems and will lead to a deeper understanding of such polymer composite materials.

Chapter 5

Depletion interactions in binary polymer star - colloid mixtures,
Daniela Marzi, and Christos N. Likos
In preparation.

Original abstract: We study the influence of small colloidal additives on the effective star polymer interaction and determine the depletion interaction they induce on the stars. By employing the two-component Rogers-Young integral equation theory based on the recently introduced effective star-colloid interaction (see Chapter 2) [2], we compare its accuracy with that of the superposition approximation. We further investigate the effects of the size ratio and colloid density on the colloid-modified star-star interactions. These modified interactions are sensitive on the star polymer - colloid size ratio, the density of the added colloids and the number of arms of the stars. Finally, we employ a mean-field approximation to calculate the free energy and determine demixing binodal lines for different star functionalities and size ratios.

Contents

Chapter 1

Introduction

Soft matter systems or *complex fluids* constitute a research field that aims in describing materials and phenomena, which are important in our everyday life [3, 4] and of interest in biology and industrial applications. The terminology complex fluids is somewhat misleading, in the sense that such systems are not necessarily fluid, as we will also see in the course of this thesis, where we deal with glassy materials.

Although it is not at first sight visible what cosmetic products like gels, cream and toothpaste, cells like viruses and blood cells, food like mayonnaise, milk and honey or ink and paint have in common, it is their macroscopic behaviour which is dominated by mesoscopic lengths scales in the range of $1\text{nm} - 1\mu\text{m}$, stemming from the interactions between the relevant mesoscopic components in the system [5]. The importance that soft matter systems will have in medical applications can already be predicted, since specific systems are possible candidates for drug delivery and advanced medical techniques [6, 7].

The relevant mesoscopic constituents of a complex fluid range from simple colloidal particles with usually few internal degrees of freedom, to complex structures like synthesised polymers which can have various degrees of freedom [4, 5]. The word *colloid* is a composition of the Greek words κόλλα (glue) and εἶδος (kind). The length scales of soft matter systems allow for observation of particles and thereby a direct validation of theoretical predictions by experiments with visible light in, e.g., confocal microcopy or scattering experiments.

The terminology *polymer* is constructed of the two Greek words πολύ (many) and μέρος (parts), representing the structure of such a mesoscopic particle: A polymer is composed of large numbers of chemically attached *monomers*, where a monomer usually is a hydrocarbon unit. The number N of monomers is called the *degree of polymerisation* and various architectures like chains, stars or dendrimers are possible [8–10]. Those constituents (colloids, polymers, etc.) usually are then dissolved in a molecular or atomic solvent, which makes the whole system very complex in terms of length- and time scales. The constituents itself can also self organise in the solution leading to aggregates in the solution,

while synthesised polymers or proteins are already itself in the range of $1\text{nm} - 1\mu\text{m}$ [3]. This complexity of soft matter systems built of large colloids dissolved in small solvent molecules, leading to an enormous amount of highly asymmetric degrees of freedom, is the challenge in the theoretical description of such systems. The main task lies in bridging the gap between the different length scales and finding ways to decide which properties have to be taken into account explicitly and which scales can be treated on a *coarse-grained* level, i.e., a pre-averaging, in which some degrees of freedom have been traced out, leaving the overall thermodynamic relations of the system invariant [5, 11, 12]. Then it is possible to use methods of statistical mechanics [13] and standard simulation techniques [14–16] to investigate the macroscopic behavior of a specific soft matter system.

The complexity of soft matter systems results on the other hand into a large variety of interesting phenomena, which are studied in a joint effort of theoretical and experimental physicists, chemists, engineers and all natural sciences, and have a high potential for pioneering inventions. Research in this fascinating field can lead to great achievements in everyday life situations, in industry, medicine and pharmaceutics and therefore it is important to understand soft matter compositions from a theoretical point of view to predict the behavior of mixtures that have not been realised yet. One property of soft matter systems, also referred to as *colloidal dispersions*, is the possibility of synthesising the components in such complex fluids and therefore design materials with desired properties [17, 18].

One way of studying colloidal dispersions is the concept of *effective interactions* [5, 19], where uninteresting degrees of freedom are integrated out and a mesoscopic Hamiltonian is obtained. It is often important to describe the behavior of the largest constituent in a complex fluid, while we are not interested in the solvent or other (small) particles. The behavior of such particles is often uninteresting, and just their influence on the interesting component has to be included in the effective Hamiltonian. In Chapter 2, we have introduced an effective interaction between star-polymers and colloids in a binary mixture by developing a coarse-grained description. Such effective interactions are very useful in the further theoretic considerations, but also in building coarse-grained simulations and for comparing with experimental results, as we have done in Chapters 2 and 3. Effective interactions can for example implicitly include the influence of solvent molecules and other particles which are uninteresting for the specific investigations.

One famous example for such a coarse-graining is the Asakura Oosawa model [20] for colloid-polymer mixtures. In this model, all degrees of freedom of the polymers are traced out and an effective interaction between the colloids is obtained, mapping the system to an effective one-component system. In this description the effective attraction, the so-called depletion force, arises due to the increasing available volume for the polymers in the solution, when the big colloids approach each other close enough. This depletion

model, still being the reference system for any type of depletion interactions, has been used to explain the equilibrium phase behaviour of colloid-polymer mixtures [21], as well as the specific phenomena in such mixtures like clustering, gelation, glass transitions, etc. [22].

Soft matter systems can be found in liquid or solid states. One interesting feature, which is important for studying new materials, is the glass formation of soft matter systems, where the solutions feature solid-like dynamical behaviour, but a fluid-like structure [22–25]. The glass transition is a very interesting phenomenon in soft matter physics, since it differs from the glass transition in atomic systems: In atomic systems the effect of dynamical arrest leads to the slowing down of the dynamics in dense systems and to a liquid-like structure while the viscosity increases by several orders of magnitude and non-relaxing density fluctuations occur. In soft matter systems a different observation arises: arrested states in soft matter can be divided into (repulsive and attractive) glasses and gels [22, 26]. Until today, the ideal hard sphere system is still the reference system for investigations of soft matter systems and especially for the glass transition [26]. One important tool for investigating the glass transition is the *mode coupling theory of the glass transition* (MCT) by Götze, which we have used in Chapters 3 and 4. We present a brief exposure on the one-component MCT in Appendix B.

It is important that soft matter systems are also of great relevance in constructing model systems for physical problems. The focus for modelling physical systems lies on how specific constituents behave in the desired experiments, and how they can be tailored for individual needs, while in such considerations it is unimportant, what these particles are from a chemical point of view.

One of these model systems is the concept of a *polymer star*. They are an easily tuneable model system of colloidal particles, being able by changing their number of arms f to model a wide range of ultrasoft up to hard spherical particles. They have been widely studied in experiments [27–29], theory [30–32] and simulations [33–35]. It has been shown, how to derive an effective interaction for such star polymers [5, 32] and a lot of research has been done in understanding the static and dynamical behavior of star polymers, showing for example the rich phase diagram [33]. In Chapter 2 we have shown how to replace star polymers in a binary mixture of star polymers and hard spheres by effective point particles, that interact with the colloids via an effective interaction potential with the help of scaling theory [31].

Usually, soft matter systems are composed of multiple components of different kinds, i.e., polymers and colloids, which on one hand, makes the description even more challenging, but on the other hand leads to the rich phase behavior, only mixtures can offer. Each of the components can separately undergo a crystallisation, glass forming [22, 36] or also a demixing can occur [37–40]. The complexity of colloidal dispersions in the sense of the

different size and length scales is extended, when dealing with mixtures.

Mixtures of star polymers with other components promise to have interesting features. So far, mixtures of polymers with hard colloidal particles, where the colloids are bigger than the stars [1], mixtures of star polymers with linear chains [41, 42] and star-star mixtures have been studied. In this dissertation we present our investigations on star-polymer – colloid mixtures, where the smaller, hard colloidal additives are added to a star polymer solution. We focus on the glass melting of a star polymer glass and the depletion effect of the colloids on the stars.

The chapters of this dissertation are structured as follows:

In Chapter 2 we introduce our model system consisting of big, soft colloids represented by star polymers and hard colloidal additives. Here, the coarse-graining lies in replacing the star polymer consisting of monomers by a spherical region that exerts an osmotic pressure on a colloid, that reaches inside this region. We present the effective interaction between stars and colloids and by making use of the effective-hard sphere mapping and the non-additivity parameter we make first predictions on the phase separation of the binary mixture, depending on the size ratio $q = R_{g,S}/R_C$ of the stars and colloids and the functionality f, i.e., the number of arms of the polymeric stars. Here, $R_{g,S}$ denotes the radius of gyration of the polymer stars and R_C the radius of the hard colloids. The effective interaction is confirmed by Monte-Carlo computer simulations, leading to a coarse grained theoretical description of the system consisting of the three effective pair interactions between stars and colloids.

The effective interactions are subsequently used in an integral equation theory approach with the help of the Rogers-Young closure to obtain structural information on the system and investigate with the help of mode coupling theory the glass melting upon increasing the amount of colloids in the system. In Chapter 3 the theoretical methods are carried out on specific parameters of an experimental setup which was synthesized by Munam *et al* at the University of Waterloo in Canada. The experiments of Truzzolillo and coworkers at FORTH in Crete led to excellent agreement between theory, simulations and experiments [43]. The parameter choices of f and q are then extended in Chapter 4, leading to systematic predictions on how the size ratio and functionality can influence the rheological behavior of the system.

Finally, with the help of the depletion interaction idea [20] and perturbation theoretical calculations, we present binodal demixing lines for the system at hand, paving the way for mapping the complex star-polymer – colloid binary mixture to an effective one-component system in Chapter 5.

Chapter 6 summarises our results and provides and outlook to possible further research.

Chapter 2

Coarse graining of star-polymer − colloid nanocomposites

2.1 Introduction

Mixtures of colloids and non-adsorbing polymers have been a topic of extensive and detailed investigations during the last two decades [44–47]. The main focus of the research has been on the so-called *colloid limit* of these systems, for which the size ratio between the polymer coils and the colloidal particles (to be defined more precisely in what follows) is smaller or even much smaller than unity. For such cases, the approach of modeling the polymer coils as effective soft spheres, which mutually repel each other as well as the colloidal particles, is usually adopted [1, 48–51]. As a result, an entropic depletion attraction emerges between the colloidal particles, which, under circumstances depending on the concentration and size ratio between the two components, can drive a macroscopic de-mixing transition in the system [51]. A great deal of work along these lines has been based on a simplified picture of ideal (i.e., non-interacting) polymers in the framework of the Asakura-Oosawa model [52–54]. However, it has been demonstrated that quantitative agreement with experimental findings, both for the bulk and for the interfacial properties of such mixtures, requires a more accurate approach, in which the polymer-polymer and polymer-colloid interactions are taken into account in a realistic fashion [51, 55, 56].

As mentioned above, a parameter of crucial importance for the behavior of colloid-polymer mixtures is the size ratio $q \equiv R_{g,S}/R_c$ between the polymers and the colloids, whereby $R_{g,S}$ is the gyration ratio of the former and R_c denotes the radius of the latter, which are usually modeled as hard spheres. The term 'colloid limit' usually refers to $q < 1$, whereas the opposite case, $q > 1$, is known (though not universally) as the *protein limit* [57–60]. Considerably less work has been done in the protein limit, for good reasons: here, the polymer is a long chain when measured against the colloidal size, so that it

cannot be modeled as a spherical globule that depletes the hard spheres. Accordingly, the approaches applied in this case are more involved: from the computational point of view, extensive simulations of long, self-avoiding walks on a lattice have been employed to study the phase behavior of the mixture, whereas the most successful and robust theoretical approach involves the PRISM-theory of Fuchs and Schweizer [61], in which indeed a monomer-by-monomer resolution of the polymer chain is employed. Results on the phase behavior of colloid-polymer (CP) mixtures in the protein limit have been compared also with those from experiments [60]. Closely related to the protein limit of CP mixtures is also the highly topical and rapidly developing field of polymer-colloid nanocomposites (PCN) [62]. Here, small colloidal particles are used as additives ("fillers") in polymer melts and rubbers, and they can bring about dramatic changes in the microstructure of the composite, influencing as a result its macroscopic behavior, such as, e.g., its viscoelastic and mechanical properties. Much as in the case of the protein limit, the polymers of the matrix cannot be treated as soft spheres, and a microscopic theoretical approach is required, which is again provided by the PRISM theory [63–65]. Considerable emphasis has been put in determining the miscibility of the two components as well as the structural correlations between the fillers and their dependence on monomer-to-colloid affinity, which is a departure from the strict non-adsorbing case mentioned above. These and related issues have also been addressed experimentally [66–70], and comparisons between experiment and theory have also been performed [71].

A system related to but also distinct from CP-mixtures are star-polymer–colloidal mixtures [39, 72, 73]. Star polymers have a mixed character between polymers and colloids, approaching the latter as their arm number (functionality) f grows [32]. Two special features of multiarm star polymers render them clearly distinct from their linear counterparts: first, the topological constraint in their architecture, namely that f polymer chains be covalently bonded on a single site, gives them an overall compact, spherical shape. This shape, as well as the nature of stars as soft colloidal spheres, is maintained deeply inside the semi-dilute regime [74, 75]. Second, the fact that their effective interaction becomes stiffer as f grows. Accordingly, a wealth of phenomena related to crystallization [34] and the glass transition [76, 77] of star polymers bear striking similarities to those encountered in hard spheres, including polymer-induced melting [75, 76] and a multitude of glass transitions in star-polymer mixtures [78, 79]. When they act as depletants on hard colloids, low-functionality stars bring about depletion effects similar to those seen for CP-mixtures in the colloidal limit, $q < 1$ [39, 72, 73]. However, nothing is known about the behavior of star-polymer–colloid (SPC) mixtures in the protein or, as we prefer to term it, the nanocomposite limit, in which the stars are bigger than the colloids: $q > 1$. The purpose of this work is to lay the foundations for theoretical investigations on such SPC-nanocomposites by performing a coarse-graining of the mixture towards

a mesoscopic description at the level of *effective interactions*. As the star-star and the colloid-colloid effective interactions are readily known [32], the task lying ahead is to derive the cross-interaction between stars and colloids. To this end, we have extended a previous theoretical approach for SPC-mixtures, set forward in the colloid limit [1], to the nanocomposite limit, and we have also performed extensive, monomer-resolved computer simulations. We find remarkable, quantitative, and parameter-free agreement between the two for a large variety of parameters, which allows us to establish the star-colloid effective interactions in simple forms, and to thus complete the coarse-graining of the SPC-nanocomposite. In addition, we show how this effective interaction, together with the ones acting between like species, allows to make quantitative predictions about the miscibility of such nanocomposites.

The rest of this paper is structured as follows: we start by introducing in section 2.2 the model and simulation methods and then describe in section 2.3 the theoretical approach used to derive the effective star-colloid interaction. In section 2.4, we discuss in detail the comparison between the effective potentials obtained with simulations and theoretical approach, the quantitative features of the effective interaction for $q > 1$ as opposed to the same for $q < 1$, and we derive the non-additivity parameter that allows us to make quantitative predictions about the miscibility of star-colloid nanocomposites. Finally, in section 2.5, we summarize and draw our conclusions.

2.2 The model and simulation details

This work is exclusively concerned with the calculation of the star-colloid interaction potential, $V_{SC}(r)$, r being the center-to-center distance of the two particles, because the star-star effective interaction is known [32] and the colloid-colloid interaction is assumed to be of the hard-sphere type. To set the parameters of the problem, we consider a star with functionality f and with radius of gyration $R_{g,S}$, as well as a colloidal particle of radius R_c. The size ratio q is defined as

$$q \equiv \frac{R_{g,S}}{R_c}, \tag{2.1}$$

and, as stated in the introduction, we focus exclusively on the case $q > 1$. We begin our description by introducing the microscopic model used to represent the star polymers on the monomer level and the colloids in our computer simulations, as well as the simulation technique itself.

In the off-lattice simulation, star polymers are made of f arms of N monomers (Kuhn segments) of size σ_{LJ} each, grafted on a central anchoring point. The non-bonded interaction between any two of the Nf monomers in the star at a distance r between their

centers is given by a purely repulsive and truncated Lennard-Jones potential, mimicking athermal solvent conditions:

$$V_{\mathrm{LJ}}(r) = \begin{cases} 4\epsilon \left[\left(\frac{\sigma_{\mathrm{LJ}}}{r} \right)^{12} - \left(\frac{\sigma_{\mathrm{LJ}}}{r} \right)^{6} + \frac{1}{4} \right] & \text{for} \quad r \leq 2^{1/6}\sigma_{\mathrm{LJ}} \\ 0 \quad \text{for} & r > 2^{1/6}\sigma_{\mathrm{LJ}}, \end{cases} \tag{2.2}$$

where $\epsilon = k_{\mathrm{B}}T$, with Boltzmann's constant k_{B} and the absolute temperature T. The backbone of each arm is held together via a FENE (finite extensible nonlinear elastic) potential between neighboring monomers along the chain:

$$V_{\mathrm{FENE}}(r) = \begin{cases} -15\epsilon \left(\frac{R_0}{\sigma_{\mathrm{LJ}}} \right)^{2} \ln \left[1 - \left(\frac{r}{R_0} \right)^{2} \right] & \text{for} \quad r \leq R_0 \\ \infty \quad \text{for} & r > R_0 \end{cases}. \tag{2.3}$$

Here R_0 is the maximum extension of the bond and it is chosen to have the value $R_0 = 1.5\sigma_{\mathrm{LJ}}$. All monomers interact with the colloid via a steeply diverging potential given by the expression:

$$V_C(r) = \begin{cases} 4\epsilon \left[\left(\frac{\sigma_{\mathrm{LJ}} + R_c}{r} \right)^{12} - \left(\frac{\sigma_{\mathrm{LJ}} + R_c}{r} \right)^{6} + \frac{1}{4} \right] & \text{for} \quad r \leq 2^{1/6}(\sigma_{\mathrm{LJ}} + R_c) \\ 0 \quad \text{for} & r > 2^{1/6}(\sigma_{\mathrm{LJ}} + R_c), \end{cases} \tag{2.4}$$

where R_c is the radius of the colloid.

To compute within Monte Carlo simulations the effective pair potentials $V_{SC}(r)$ between star polymers of any functionality f and the colloidal particles, we sample the equilibrium radial distribution functions $g_{SC}(r)$ between a single star and a single colloid in the simulation box, taking advantage of the fact that the two quantities are linked by the relation:

$$V_{SC}(r) = -k_{\mathrm{B}}T \ln g_{SC}(r). \tag{2.5}$$

In the case of big star polymers interacting with colloidal spheres, a direct sampling of the $g_{SC}(r)$ turns out to be an inadequate procedure to efficiently sample the effective interactions, especially for small distances between the centre of the star and the surface of the colloid. Therefore, to obtain effective potentials between star polymers and colloids of different size ratios, virtual move - parallel tempering Monte Carlo (VMPT-MC) simulations were performed. The VMPT-MC [80] is a combination of the adaptive parallel tempering algorithm [81] and the waste recycling method developed by Frenkel [82]; it consists in iteratively building a biasing potential by using the information gathered in the rejected moves during a block of MC steps, to force the system to explore regions of the phase space that would otherwise have a very low probability to be reached. At the end of each block the bias potential is updated to improve the sampling of the next

iteration. Every trial move is considered as a virtual move, whose weight is related to its accepting probability. If we use the symmetric acceptance rule for MC trial moves, then the weights P_O of the original and P_N of the new (trial) state in the sampling of virtual moves are given by

$$
\begin{aligned}
P_O\left(Q,T\right) &= \frac{1}{1 + e^{\beta \Delta E_{O\to N}(Q,T) + \Delta W_{O\to N}(Q,T)}} \\
P_N\left(Q,T\right) &= \frac{e^{\beta \Delta E_{O\to N}(Q,T) + \Delta W_{O\to N}(Q,T)}}{1 + e^{\beta \Delta E_{O\to N}(Q,T) + \Delta W_{O\to N}(Q,T)}} \,.
\end{aligned}
\tag{2.6}
$$

In the latter, $\Delta E_{O\to N}\left(Q,T\right)$ indicates the variation of energy from the old to the new state sampled in the presence of the bias W, T is the temperature and Q a collective variable that will be defined in the following. Further, W is iteratively built using the histograms of the states that have been sampled during the iterations:

$$
W_i(Q,T) = W_{i-1}(Q,T) - \alpha \ln[\mathcal{P}_i(Q,T)].
\tag{2.7}
$$

Here, i is the iteration number, $\alpha \in [0,1]$ is a value that we use to control the rate of convergence of W. The probability $\mathcal{P}_i(\tilde{Q},T)$ of observing at iteration i a configuration with a specific value $Q = \tilde{Q}$ of the order parameter is given by

$$
\mathcal{P}_i\left(\tilde{Q},T\right) = \frac{\sum_{j=1}^{\mathcal{N}} \left[P_O^i(Q,T)\,\delta\left(Q - \tilde{Q}\right) + P_N^i(Q,T)\,\delta\left(Q - \tilde{Q}\right) \right]}{\sum_{j=1}^{\mathcal{N}} \left[P_N^i(Q,T) + P_O^i(Q,T) \right]},
\tag{2.8}
$$

where $\mathcal{N}$ is the number of MC steps per iteration, and $P_O^i(Q,T)$ and $P_N^i(Q,T)$ are defined in Eq. (2.9) below. At the end of every iteration, the probability $\mathcal{P}_i\left(Q,T\right)$ is set to zero. During the iterative steps used to build the bias, Eq. (2.6) appears as

$$
\begin{aligned}
P_O^i(Q,T) &= \frac{1}{1 + e^{\beta \Delta E_{O\to N}^{i-1}(Q,T) + \Delta W_{O\to N}^{i-1}(Q,T)}}, \\
P_N^i(Q,T) &= \frac{e^{\beta \Delta E_{O\to N}^{i-1}(Q,T) + \Delta W_{O\to N}^{i-1}(Q,T)}}{1 + e^{\beta \Delta E_{O\to N}^{i-1}(Q,T) + \Delta W_{O\to N}^{i-1}(Q,T)}} \,.
\end{aligned}
\tag{2.9}
$$

since the energies sampled depend on the the bias W_{i-1} that has been built up to the iteration i.

The collective variable used in the present work to build the biasing potential is the distance r between the anchor point of the star and the center of the colloid. In this work we did not swap configurations of the system obtained at different temperatures, but rather considered a single temperature T. MC simulations were performed for stars with functionality $f \in [18,50]$ and arms made of $N = 50$ monomers, that was proven to
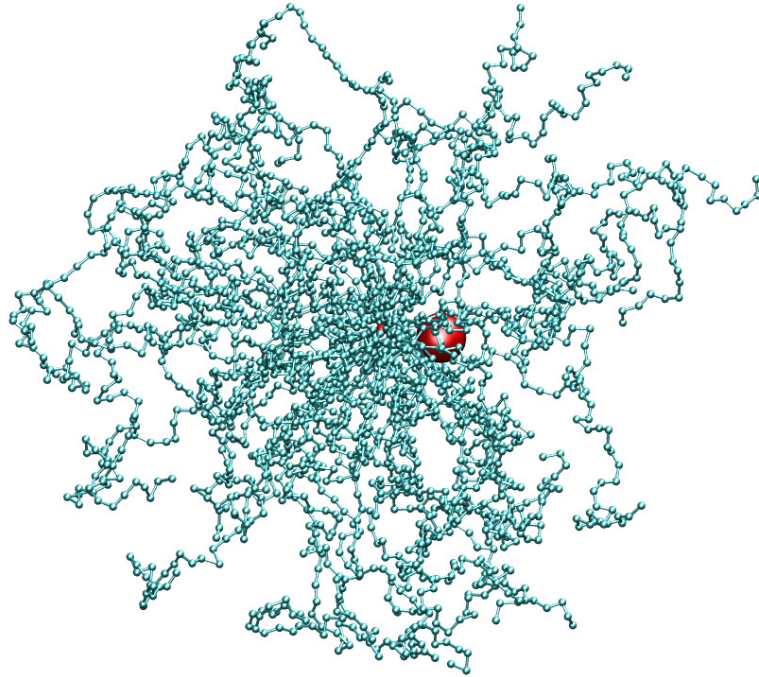
Figure 2.1: Simulation snapshot: a colloidal particle (red) interacting with a star polymer of functionality $f = 50$ (cyan). In this case, the size ratio is $q = 12.48$. The small red dot at the middle represents the center of the star, i.e., the common anchoring point of the f chains.

be in the scaling limit for the potentials and models that we used. We only considered translational single particle moves for both the monomers of the star and the colloid. Each monomer of the star was moved 500 times before attempting a colloidal move, therefore every MC step consisted of $500(fN) + 1$ single particle moves. All simulations ran for at least 10^4 MC steps, where all potentials were found to have converged to their final profiles. A large variety of colloidal sizes was used, all satisfying the constraint $q > 1$, and in what follows we will be showing representative results for selected parameter combinations, in comparison with theory. In Fig. 2.1, a simulation snapshot of a big star polymer and a small colloid for a case in which the latter is placed close to the center of the former is shown.

2.3   Theoretical approach

In this section, we provide a generalization of the theoretical results of Ref. [1], where effective potentials were derived for the case $q < 1$. The theory is hereby extended to arbitrary size ratios and in particular to the case $q \geq 1$. The starting point of our considerations lies in considering the local osmotic pressure $\Pi(s)$ in the interior of a multiarm star polymer, where s denotes the radial distance from the anchoring point of

f	2	5	10	15	18	30	40	50	65	80	100
$\pi\Lambda$	0.46	0.35	0.30	0.28	0.27	0.24	0.24	0.23	0.23	0.22	0.22
κR_S	0.58	0.68	0.74	0.76	0.77	0.83	0.85	0.86	0.87	0.88	0.89

Table 2.1: The values of the parameters used in the theory of the effective star-polymer – colloid interaction potential.

the chains to an arbitrary point in the star. Scaling considerations within the Daoud-Cotton model [31] lead to the result that there exists a length scale R_S in the star, within which the macromolecule can be described as a semi-dilute polymer solution with a local segment concentration $c(s)$ given by:

$$c(s) \sim a^{-3} \left(\frac{s}{a}\right)^{-4/3} \bar{v}^{-1/3} f^{2/3}. \tag{2.10}$$

Here, a stands for the segment/bond length and $\bar{v} \equiv v/a^3$ for the dimensionless excluded volume parameter. The length scale R_S, called the corona radius, has been found in a number of investigations [1, 32] to fulfill with high accuracy the relationship:

$$R_S/R_{g,S} = 2/3. \tag{2.11}$$

For $s > R_S$, the monomer density $c(s)$ remains, of course, inhomogeneous but it is sufficiently low, so that there the theory of dilute polymer solutions can be applied [83].
The above considerations allow us to write down a closed expression for the local osmotic pressure $\Pi(s)$ at an arbitrary distance s from the star center. For $s \leq R_S$, the known scaling law $\Pi(c) \sim c^{-9/4}$, valid for semi-dilute polymer solutions, leads to a $\Pi(s) \sim s^{-3}$ scaling, whereas for $s > R_S$ the form of the osmotic pressure has been derived in Ref. [1]. Putting things together, $\Pi(s)$ is given by the following equations in the two differing regions [1]:

$$\Pi(s) = \Lambda f^{3/2} k_{\mathrm{B}} T \begin{cases} s^{-3} & \text{for } s \leq R_S; \\ \left(\frac{1}{s^2} + 2\kappa^2\right) \frac{\xi}{R_S} e^{-\kappa^2(s^2 - R_S^2)} & \text{for } s > R_S, \end{cases} \tag{2.12}$$

with the two free parameters Λ and κ, which have been previously determined for a number of functionalities [1], and whose numerical values are summarized in Table 2.1. Note that $\lim_{f \to \infty} \Lambda(f) = 5/(36\pi)$. The parameter ξ in Eq. (2.12) above is determined by the requirement that the pressure $\Pi(s)$ be continuous at $s = R_S$:

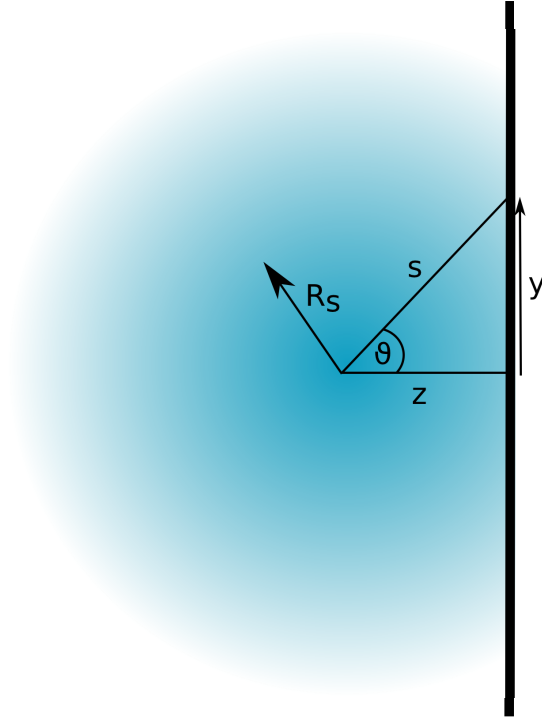$$\xi = \frac{1}{1 + 2\kappa^2 R_S^2}. \tag{2.13}$$

Figure 2.2: A sketch of a star polymer (diffuse blue sphere) interacting with a flat wall.

The pioneering idea for obtaining the force between a star polymer and a hard object has been set forth by Pincus [84], who considered the force acting between a star polymer and a hard, flat wall, as depicted in Fig. 2.2. It has been proposed that the star-wall force, $F_{SW}(z)$, be obtained by integration of the *normal component* of the osmotic pressure, $\Pi_n(s)$, over the symmetry plane, $F_{SW}(z) = \int \Pi_n(s) \mathrm{d}A$ or, equivalently:

$$F_{SW}(z) = 2\pi \int_0^\infty \Pi(s) \cos\vartheta\, y \mathrm{d}y = 2\pi z \int_z^\infty \Pi(s) \mathrm{d}s, \qquad (2.14)$$

where $z = s\cos\vartheta$ and $y = z\tan\vartheta$ have been used to transform the y-integral into an integration over s in Eq. (2.14) above. This approach leads to the correct scaling behavior, $F_{SW}(z) \sim f^{3/2}/z$ for small star-wall separations z and the validity of the approximation has been established via comparisons with extensive simulations [1]. Nevertheless, the approach requires some further interpretation, in particular as far as the notion of the normal component of the pressure is concerned. The pressure of an inhomogeneous fluid, such as the star interior, is of course a tensorial quantity, expressing both the normal and the shear forces that act on some arbitrarily oriented elementary surface $\mathrm{d}A$ in the interior

of the fluid. Evidently, the entries of the tensor depend on the orientation of the surface and only in the special case of a homogeneous and isotropic fluid is this pressure tensor diagonal and has all its non vanishing entries equal to one another for any orientation of the surface. Accordingly, an *exact* calculation of the elementary force $dF_{\mathrm{ring}}(z)$ acting on the area element $dA_{\mathrm{ring}} = 2\pi y dy$ of a ring of radius y on the wall [see Fig. 2.2 and Eq. (2.14)], would require knowledge of the whole pressure tensor inside the star. What Eq. (2.14) instead suggests, is an approximation of a different nature: it states that on the surface element $dA = y dy d\phi$ there is a force acting in the *radial* direction from the star center, whose magnitude is equal to $\Pi(s)dA$ i.e.:

$$\begin{aligned}
d\mathbf{F}_{SW}(z) &= \Pi(s)y dy d\phi \hat{\mathbf{s}} \\
&= \Pi(s)y \cos\vartheta dy d\phi \hat{\mathbf{z}} + d\mathbf{F}_{\perp},
\end{aligned} \tag{2.15}$$

where $\hat{\mathbf{s}}$ and $\hat{\mathbf{z}}$ are the unit vectors along the s- and z-directions, ϕ is the azimuthal angle and $d\mathbf{F}_{\perp}$ is the elementary force perpendicular to the z-direction. Performing the ϕ-integration of Eq. (2.15) along a ring of radius y results into a vanishing perpendicular component by virtue of symmetry, yielding a force $dF_{\mathrm{ring}}(z) = 2\pi\Pi(s)\cos\vartheta y dy$ that acts on this ring, and which is pointing along the z-direction. The total force $F_{SW}(z)$ follows then trivially by integrating $dF_{\mathrm{ring}}(z)$ over y, Eq. (2.14).

This ansatz has been successfully generalized in Ref. [1] to slightly curved surfaces, i.e., to the case $q < 1$, in the spirit of the Derjaguin approximation. Here, we make the assumption that it can be employed for *arbitrary* curvatures of the colloids, i.e., also in the case $q > 1$ or even $q \gg 1$. Though there is no *a priori* reason to expect that this is a valid assumption, we employ it as a working hypothesis and comparison with the simulation results will provide an *a posteriori* justification for it. The pertinent geometry is shown in Fig. 2.3. As the colloidal particle is now smaller than the star, an insertion of it inside the star polymer means that the line pointing radially from the star center towards the colloid intersects the latter at *two* points, whose distance from the star center are s and $s + t$. Referring to Fig. 2.3 and using standard trigonometric identities, we obtain:

$$\begin{aligned}
R_c^2 &= (s+t)^2 + (z+R_c)^2 - 2(s+t)(z+R_c)\cos\vartheta; \tag{2.16} \\
R_c^2 &= s^2 + (z+R_c)^2 - 2s(z+R_c)\cos\vartheta, \tag{2.17}
\end{aligned}$$

which can be used to express the dependence of t on z, R_c and s:
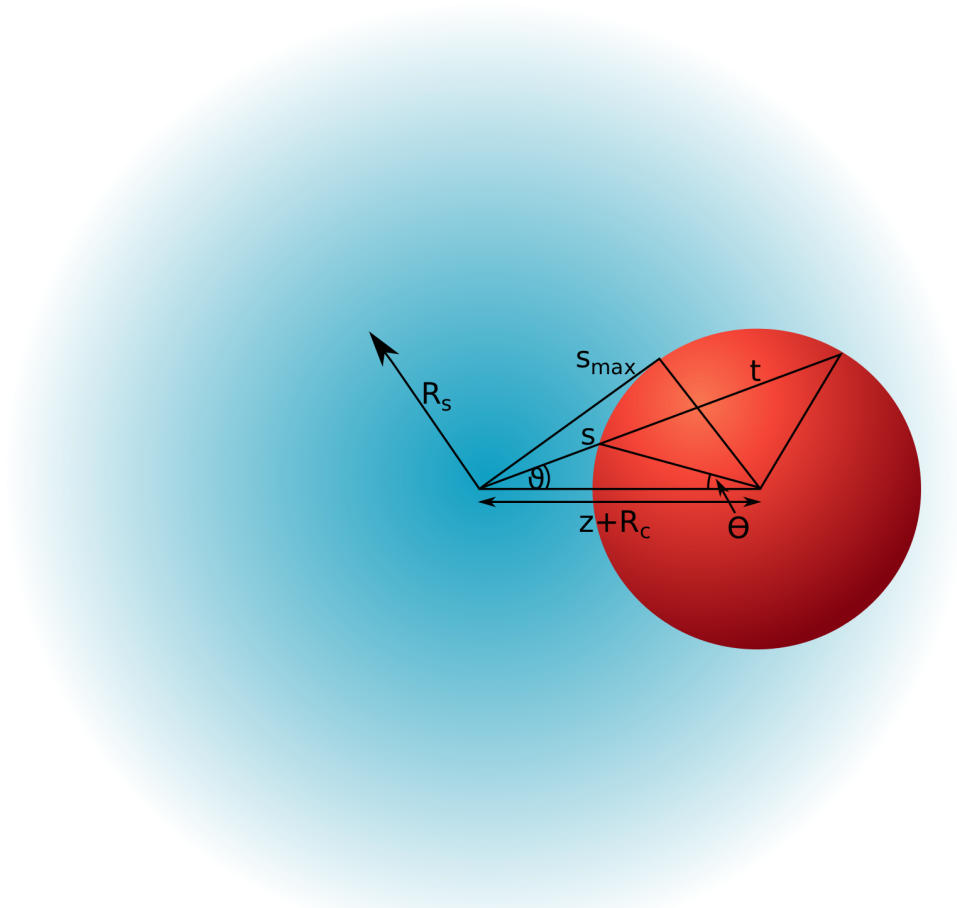
$$t(s) = \frac{z(2R_c + z) - s^2}{s}. \tag{2.18}$$

Figure 2.3: A sketch of a star polymer (diffuse blue sphere) interacting with a colloidal particle (red sphere), also showing the geometry and the quantities entering into the calculation of the effective force.

In calculating now the effective star-colloid force $\mathbf{F}_{SC}(z) = F_{SC}(z)\hat{\mathbf{z}}$, according to the ansatz discussed above, we must take into account that the radial forces always act from the region where there the polymer lies, towards to the interior of the colloidal volume. As such, contributions from the regions for which the radial distance from the star center to the colloidal surface exceed $s_{\max}$ in Fig. 2.3 will have a projection pointing towards the negative z-axis. Accordingly, the force $F_{SC}(z)$ takes the form:

$$F_{\mathrm{SC}}(z) = 2\pi R_c^2 \int\limits_0^\pi \mathrm{d}\theta [\Pi(s) - \Pi(s+t)] \sin\theta \cos\vartheta. \qquad (2.19)$$

Eq. (2.19) can be simplified by making use of the geometrical relations

$$s \sin \vartheta = R_c \sin \theta; \tag{2.20}$$

$$s \cos \vartheta = z + R_c - R_c \cos \theta, \tag{2.21}$$

to eliminate the variables θ and ϑ in favor of s. The result reads as:

$$
\begin{aligned}
F_{SC}(z) &\equiv F_1(z) + F_2(z) \\
&= \frac{\pi R_c}{(z + R_c)^2} \int\limits_z^{s_{\max}} \mathrm{d}s \left[(z + R_c)^2 - R_c^2 + s^2 \right] \left[\Pi(s) - \Pi(s + t) \right],
\end{aligned}
\tag{2.22}
$$

where we have defined the repulsive and attractive contributions to the force, $F_1(z)$ and $F_2(z)$ respectively, as the forces arising from the integration of $\Pi(s)$ and of $\Pi(s + t)$ in Eq. (2.22) above. Finally, $s_{\max}$ is the distance between the center of the star and the tangential point to the surface of the colloid when the star is at a distance z from the colloid, and it is expressed as:

$$s_{\max} = \sqrt{z(z + 2R_c)}. \tag{2.23}$$

The integral of Eq. (2.22), together with the expression for the osmotic pressure, Eq. (2.12), and with Eq. (2.18) form a complete set for the theoretical determination of the star-colloid effective force. The integrations have been performed numerically, although in Sec. 2.4 we will also discuss some simple, analytical results that can be obtained in certain cases. The comparison with simulation results will also be presented there. In Fig. 2.4 we show some generic results on the dependence of the force on the center-to-surface separation between the star and the colloid for different size ratios $q > 1$, which allow us to obtain a preliminary understanding of its salient features. The forces are soft, they diverge as $z \to 0$ and their range grows with colloidal size. Moreover, we see that the intuitive expectation of the behavior of the force as q grows is confirmed: it is easier for smaller colloids to penetrate within the star region, so that the effective force remains very low as q grows, until one reaches close approaches to the star center. The asymptotic behavior of the force with z and with q as $z \to 0$ will be discussed in detail in the following section.

2.4   Discussion and Comparison to Simulation

The theoretical effective force between a star polymer and a colloid, obtained by integrating the osmotic pressure exerted by the polymer star on the surface of the colloid, as
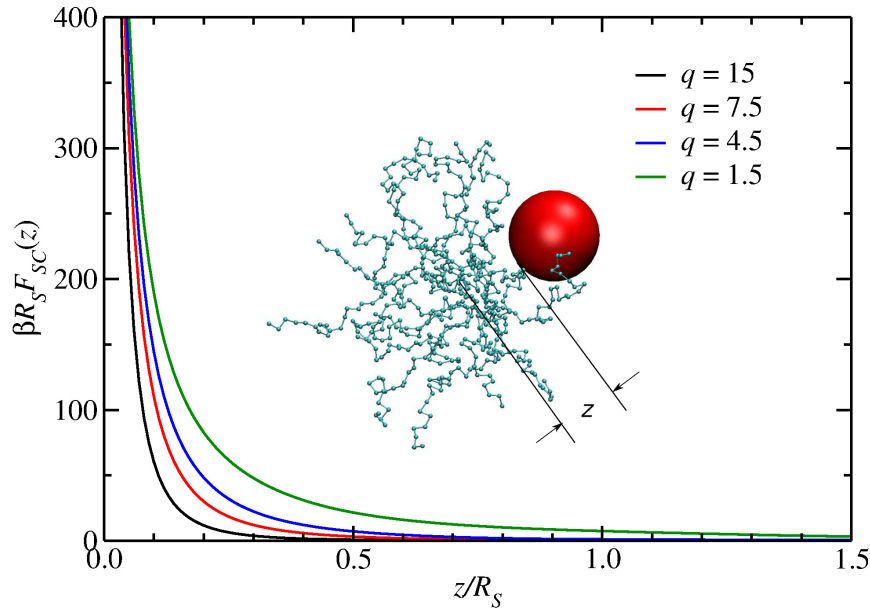
Figure 2.4: The effective force between a star polymer and a colloid for $f = 18$ and various q-values as indicated in the legend, calculated according to Eq. (2.22). The inset shows a sketch of the two particles and the distance z between the star-center and the colloidal surface.

explained in Sec. 2.3 above, can be readily integrated to yield the theoretical prediction for the effective potential $V_{SC}(z)$ between the two. This theoretical pair potential, can be compared to the one obtained by means of VMPT-MC simulations, to assess the validity of the theoretical approach over a wide range of values of functionality of the star and of size ratio between the star and the colloid. We have performed simulations for different functionalities $f = 18, 30, 50$ and various size ratios q, employing degrees of polymerization per arm $N = 30$ and $N = 50$, and we calculated the corresponding theoretical effective interactions to provide a comparison. Results are shown Figs. 2.5 - 2.7 below.

A comparison between the simulation and the theoretical results must take into account two important factors. First and foremost, the theory has been worked out in the scaling limit, in which the monomer number of the arms, N, is very large, so that any microscopic details of the star become irrelevant. In the simulation, although already in the scaling regime, this is not the case, since we work with moderate degrees of polymerization, $N = 50$ and $N = 30$. Accordingly, the core region of the star, in which the chains are stretched instead of having the statistics of a semi-dilute polymer solution, is
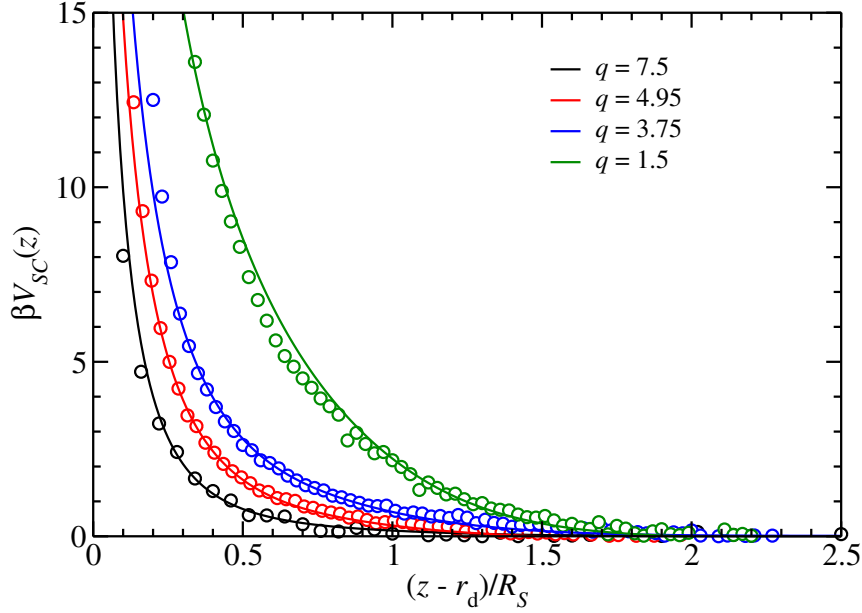
Figure 2.5: The effective interaction potential $V_{SC}(z)$ between $f = 18$ star polymers and smaller colloids, for size ratios q as indicated in the legend. Symbols represent the values of the effective potential obtained via VMPT-MC simulations, the number of monomers per arm being $N = 50$; solid lines are the theoretical predictions of the same. The effective interaction is plotted against the distance z between the center of the star and the surface of the colloidal particle, shifted by a microscopic distance r_d (see the text), and scaled with the star corona radius R_S.

comparable in size with the overall star size. This core region extends over distances of the order $R_{core} \sim a\sqrt{f}$ from the star center [31], where a is the monomer size. When $N \gg 1$, the gyration radius $R_{g,S} \sim af^{1/5}N^{3/5}$ dominates, since $R_{core}/R_{g,S} \sim f^{0.3}N^{-3/5}$ but for $N = 50$, an estimate $R_{core}/R_{g,S} \cong 0.2$ is obtained for the values of f used in this work. Accordingly, and in agreement with previous work [1], in the simulation data, the center-to-surface separation z has to be shifted by an amount r_d for a comparison with theory to be made. We found that a choice $r_d/R_S \cong 0.15 - 0.25$ (depending on f and growing with it), in full agreement with the above estimate of the core size, is sufficient to bring excellent agreement between the simulation and the theoretical results. Second, it should be noted that the corona radius R_S is not directly measured in a simulation but rather the star gyration radius $R_{g,S}$. Here, the relation of Eq. (2.11) has been used to rescale the simulation data.

The results shown in Figs. 2.5, 2.6, and 2.7 for $f = 18$, $f = 30$, and $f = 50$, respectively, show remarkable agreement between theory and simulation for a variety of size ratios q. The excellent agreement between theory and simulation obtained for a degree of poly-
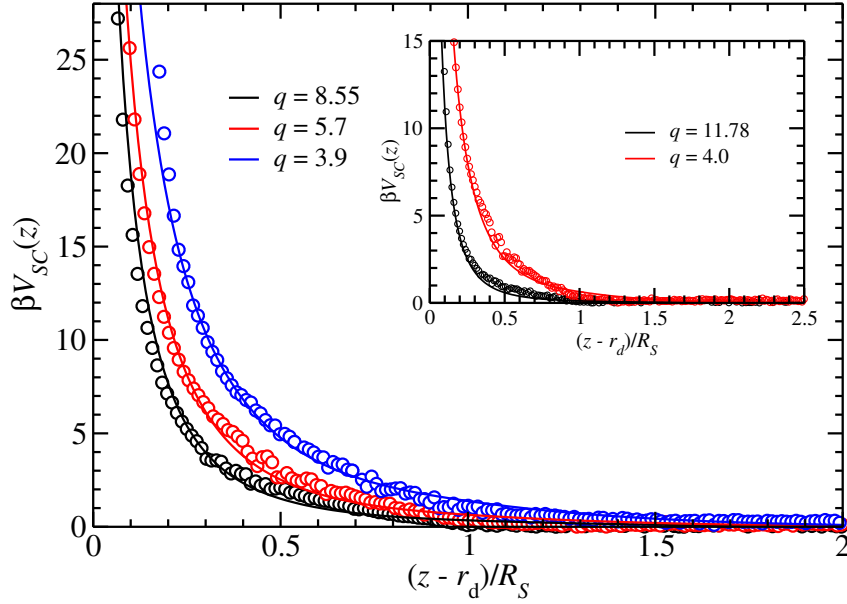
Figure 2.6:   Same as in Fig. 2.5 but for a star of functionality $f = 30$. The inset shows the comparison between the effective potentials obtained via the theoretical approach and VMPT-MC employing a star of $f = 30$ arms and $N = 30$ monomers per arm.

merization $N = 30$ (see inset of Fig. 2.6), smaller than the one used for the rest of the simulations in this work, stresses that the simulation model star polymers with $N = 50$ monomers (Kuhn segments) per arm indeed lie in the scaling regim. Since the core size r_{d} is not arbitrary but rather determined by scaling considerations of the star, it can be stated that the agreement between theory and simulation is parameter-free. In this sense, the theoretical approach is fully justified and it can be trusted to by true also for cases for which a simulation is computationally prohibitively expensive, i.e., $N \gg 1$ and $f \gg 1$. The effective force is soft and it becomes more and more reduced as q grows, which is a manifestation of the fact that small colloidal particles can penetrate more easily the interior of the star than large ones. Similar behavior has been found in Ref. [85], where it was shown that spherical-brush colloidal particles with a sizeable hard core can deform and wrap around smaller colloids, the mutual repulsion increasing with f and decreasing with size ratio. The effect of decreasing colloid size for a given star size is twofold: on the one hand, the surface area of the colloid that is exposed to the osmotic pressure $\Pi(s)$ giving rise to the repulsive force $F_1(z)$, Eq. (2.22), diminishes. On the other hand, the contribution of the attractive force $F_2(z)$ becomes more important. This state of affairs is demonstrated in Fig. 2.8, for the specific case of a star with $f = 18$ interacting with a colloid with size ratio $q = 15$. It can be seen that the contribution from the attractive
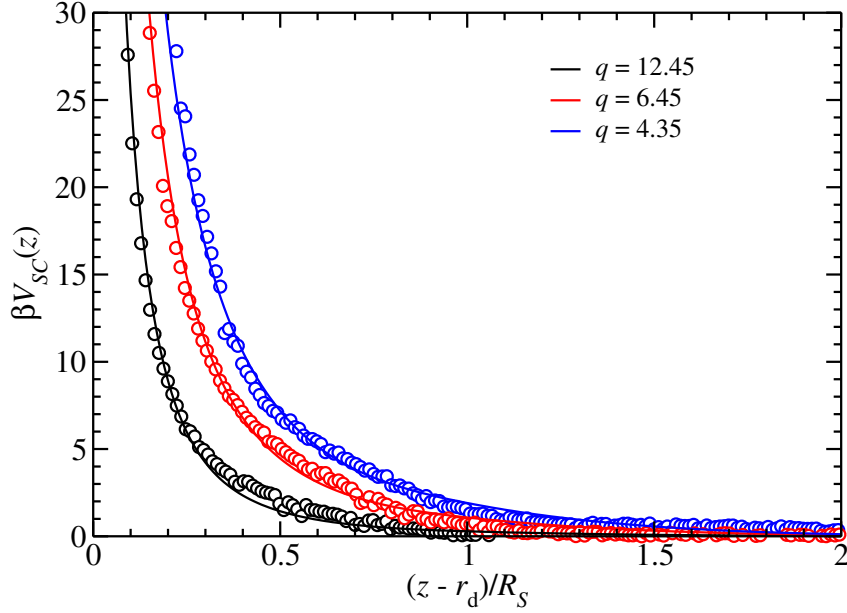
Figure 2.7: Same as in Fig. 2.5 but for a star of functionality $f = 50$.

force is considerably strong and that it brings forward a significant reduction to the overall (net) effective force, in contrast to the case $q < 1$, for which this term is completely absent [1].

Of particular interest is the asymptotic behavior of the effective force $F_{SC}(z)$ for small values of z and the corresponding behavior of the effective potential $V_{SC}(z)$, for which the scaling law $V_{SC}(z) \sim \ln z$ has been established in the case $q < 1$ [1]. We focus here on the case $q \gg 1$ and we consider close approaches between the star center and the colloidal surface. Analytical results are straightforward to obtain for the case in which z is small enough, and q is large enough, so that for *both* terms $F_1(z)$ and $F_2(z)$ in Eq. (2.22), the conditions $s < R_S$ and $s+t < R_S$ hold throughout the domain of integration $z \le s \le s_{\max}$. It is easy to show that these two conditions can be satisfied if the inequalities

$$z \;\le\; R_S - 2R_c, \tag{2.24}$$

$$q \;\ge\; 3 \tag{2.25}$$

are simultaneously fulfilled. In this case, the pressures $\Pi(s)$ and $\Pi(s + t)$ in Eq. (2.22)
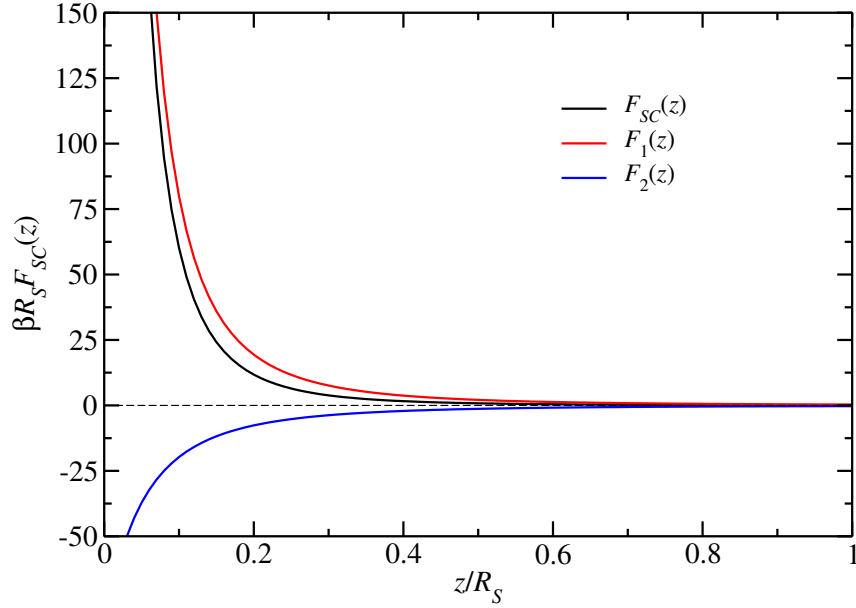
Figure 2.8: The total center-to-surface effective force $F_{SC}(z)$ acting between a star polymer of functionality $f = 18$ and a smaller colloid, as well as the individual contributions $F_1(z)$ and $F_2(z)$ to it, according to Eq. (2.22). Here, the size ratio between the star and the colloid is $q = 15$.

take simple, power-law forms, namely:

$$\Pi(s) \quad = \quad k_{\mathrm{B}}Tf^{3/2}\Lambda(f)s^{-3}; \tag{2.26}$$

$$\Pi(s+t) \quad \equiv \quad \tilde{\Pi}(s) = k_{\mathrm{B}}Tf^{3/2}\Lambda(f)\frac{s^3}{z^3(z+2R_c)^3}, \tag{2.27}$$

throughout the domain of integration of Eq. (2.22). Accordingly, the integral can be carried out analytically, yielding for the star-colloid force the expression:

$$F_{SC}(z) \quad = \quad k_{\mathrm{B}}Tf^{3/2}\frac{\pi\Lambda(f)R_c}{(z+R_c)^2}$$

$$\times \quad \left[\frac{R_c}{z} + \frac{1}{2}\ln\left(1 + \frac{2R_c}{z}\right) - \frac{5}{12} + \frac{z^2}{4(z+2R_c)^2} + \frac{z^3}{6(z+2R_c)^3}\right]. \tag{2.28}$$

Fig. 2.9 shows representative results of the effective star-colloid force for parameter combinations such that Eq. (2.28) holds; for completeness, both the analytical and the numerical result, which fully coincide, are shown there. As Eq. (2.28) readily establishes,
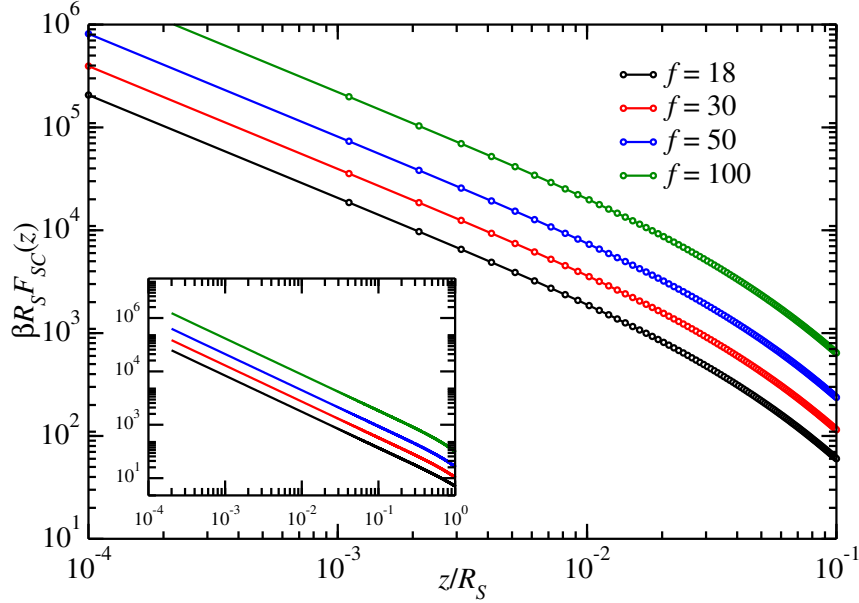
Figure 2.9: Double-logarithmic plot of the dependence of the effective star-colloid force on the center-to-surface separation for size ratio $q = 15$ and for distances z such that Eq. (2.24) is fulfilled, for various functionalities f as indicated in the legend. The solid lines are the analytical result of Eq. (2.28), whereas the open points are results from the numerical integration of Eq. (2.22), and they fully coincide. Inset: Same as the main plot but the lines are now the results of the numerical integration for a much more symmetric mixture, with size ratio $q = 1.5$.

the asymptotic form of the effective force for $z \to 0$ is an inverse-power, $F_{SC}(z) \sim 1/z$, giving thus rise to a logarithmically diverging effective potential $V_{SC}(z)$ as the star center approaches the colloidal surface. It is worth mentioning that the contribution from the "rear side" of the colloid to the force, $F_2(z)$, is given by the last three terms in the brackets of Eq. (2.28); as can be seen there, this contribution remains finite even as $z \to 0$ and thus it has the overall effect of reducing the effective force by a constant. Therefore, the logarithmic divergence of the potential is brought about by the strong repulsions between the inner part of the star and the colloidal surface at the 'front side" of the colloid, which faces the star center. The logarithmic form of $V_{SC}(z)$ as $z \to 0$ thus arises as a *universal* characteristic of the same, irrespective of the colloidal size, since in Ref. [1] it was shown that it also holds for the opposite case, $q < 1$, including the flat wall ($q \to 0$). The inset of Fig. 2.9 shows the numerical result for a symmetric case, $q = 1.5$. Also there, the scaling $F_{SC}(z) \sim 1/z$ can be seen. However, the *range* of validity of this asymptotic form is much broader there, as it can be readily established by comparing the abscissas of the
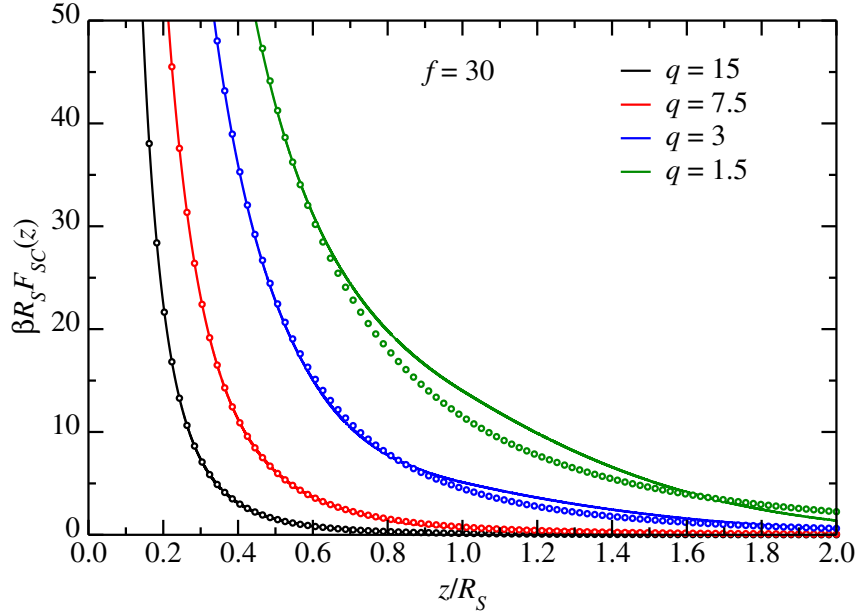
Figure 2.10: Comparison of the results of the analytical expression, Eq. (2.28), (lines) and the numerical integration, Eq. (2.22), (points) for the effective star-colloid force. Here, the star functionality is fixed at $f = 30$ and the size ratio q varies as indicated in the legends. Note that the conditions of validity of Eq. (2.28), i.e., the inequalities (2.24) and (2.25) are either partially or fully violated here, so that deviations between the two results become visible.

main plot and the inset. Indeed, as Eq. (2.28) shows, the asymptotic behavior sets in for distances $z \lesssim R_c$ or $z/R_S \lesssim q^{-1}$. Accordingly, one has to go to very close approaches to see the logarithmic divergence of the effective potential as q grows. Finally, in Fig. 2.10 we show a comparison of the analytical expression, Eq. (2.28), with the exact result, Eq. (2.22), also for parameter combinations for which Eq. (2.28) does *not* hold, either because condition (2.24) or because condition (2.25) is violated, or both. It can be seen that for sufficiently large values of q the analytical expression works quite well for all values of z, whereas discrepancies between the two become clearly visible as q diminishes. Even in that case, however, the asymptotic behavior $F_{SC}(z) \sim 1/z$ as $z \to 0$ maintains its validity.

The center-to-center effective cross-interaction potential $V_{SC}(r)$ is, evidently, infinite for $r < R_c$ and it is obtained from the center-to-surface interaction discussed above via the formal substitution $z \to r - R_c$ for $r \geq R_c$. With all three effective potentials readily available, it is advantageous to perform a second mapping to effective hard-sphere interactions with hard-sphere diameters σ_{ij}, $i, j = S, C$ obtained with the help of the
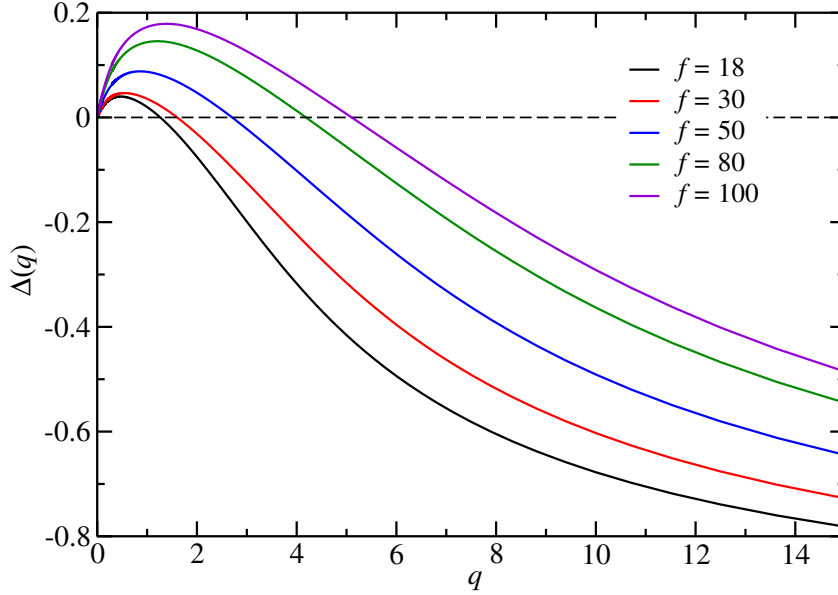
Figure 2.11: Dependence of the non-additivity paramater Δ on the size ratio q for various values of f, as indicated in the legend.

Barker-Henderson approximation [86], i.e.:

$$\sigma_{ij} = \int_0^\infty \mathrm{d}r \left[1 - \exp\{-\beta V_{ij}(r)\}\right]. \tag{2.29}$$

Evidently, $\sigma_{CC}/2 = R_c$, independently of star functionality and size ratio, whereas σ_{SS} is an f-dependent quantity [32] and σ_{SC} depends on both f and the size ratio q. With the help of the effective hard sphere diameters, we can define the *non-additivity parameter* $\Delta = \Delta(q, f)$ of the mixture via the relation [87]:

$$\sigma_{SC} = (1 + \Delta)\frac{\sigma_{SS} + \sigma_{CC}}{2}. \tag{2.30}$$

Results for $\Delta(q)$ for various different functionalities are shown in Fig. 2.11. The non-additivity parameter displays, for fixed f, a non-monotonic behavior as a function of the size ratio, which stems from the dependence of σ_{SC} on the size ratio and can be understood as follows. As $q \to 0$, the colloids are much bigger than the stars and the latter become 'point particles', whose interaction can be ignored, since the physics is dominated by the hard-core repulsions. Accordingly, $\sigma_{SC} \to R_c$ because the range of the tail of the star-colloid interaction has a vanishingly short range compared to the colloidal radius; on the
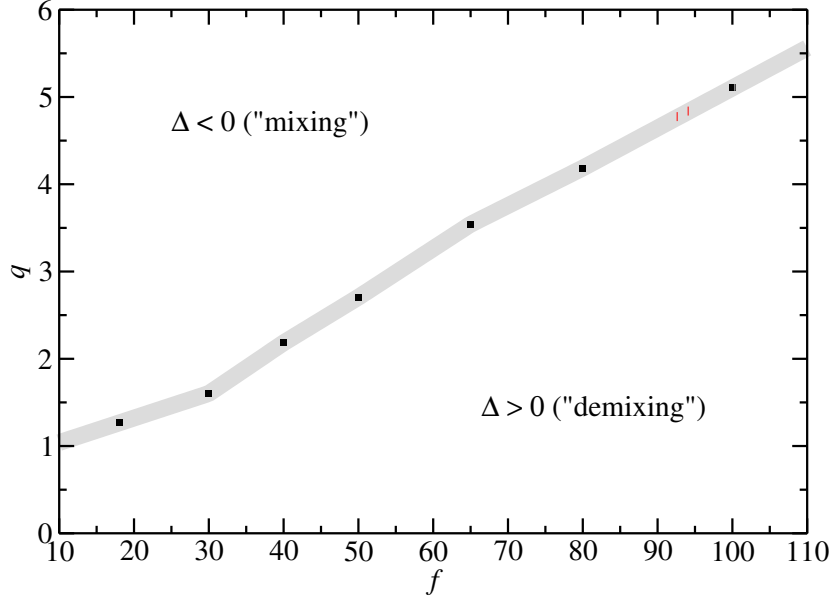
Figure 2.12: The "state diagram" of star-polymer – colloid mixtures, in the functionality-size ratio plane showing a prediction of the mixing and demixing regions of the system. The points denote numerical solutions of the equation $\Delta(q; f) = 0$ and can be read-off from Fig. 2.11. The thick gray line passes through all these points and it serves as a guide to the eye. Above this line, $\Delta < 0$ holds and we expect the mixture to be stable against demixing, whereas below the line $\Delta > 0$. Thus, mixtures in this region have the propensity of becoming unstable with respect to demixing at sufficiently high overall concentrations.

same grounds, $\sigma_{SS} \to 0$ and Eq. (2.30), together with $\sigma_{CC}/2 = R_c$ leads to $\Delta \to 0$ in this limit. As the stars start growing in size, the cross interaction, which is stiffer than the star-star interaction in this range, leads to positive values of Δ. On the other hand, at the opposite limit, $q \gg 1$, the colloidal size becomes negligible and the hard spheres can penetrate arbitrarily closely to the star center, so that $\sigma_{CC}, \sigma_{SC} \to 0$ whilst σ_{SS} remains finite. Accordingly, $\Delta(q) \to -1$ in this limit. It follows that the non-additivity parameter crosses over from positive to negative values at some f-dependent value q_* as q grows, for any given f. For fixed q, on the other hand, $\Delta(f)$ is a monotonically increasing function of f.

The non-additivity parameter is a very useful tool to make reliable predictions on the stability of the system against demixing, because it is known that even small, negative values of Δ strongly suppress macrophase separation, whereas positive ones strongly enhance it [48, 87–89]. Motivated by this fact, we draw in Fig. 2.12 a rough-and-ready

"state diagram" of the mixture by plotting, on the (f, q)-plane, the locus of points for which $\Delta = 0$. Above this line, $\Delta < 0$ and the mixture is expected to be stable against phase separation at all concentrations: well-mixed star-colloid nanocomposites are thus expected as the size ratio of stars to colloids grows, and the threshold value of q becomes bigger with functionality of the stars. On the other hand, for $\Delta > 0$, macro phase separation is expected at sufficiently high overall densities, with the value of the consolute density becoming lower as Δ grows. This is supported by previous experimental and theoretical results obtained in the colloidal limit, $0.18 \leq q \leq 0.49$, for which macrophase separation has been observed [39], in full agreement with the results in Fig. 2.12, in which the $q \leq 0.5$-region lies well inside the demixing part for all f-values. Nevertheless, we emphasize that the separation into mixing and demixing region according to the sign of the non-additivity parameter mostly serves as an orientation, i.e., it is not an exact result. Accordingly, the gray line of Fig. 2.12 is intentionally drawn as a broad strip and it should not be understood as a strict border between the two regimes.

2.5 Conclusions

In this work we have presented a comprehensive derivation of the effective potentials acting between star polymers and colloids for various size ratios q, and for arbitrary star functionalities f, obtained both via analytical calculations and full monomer Monte Carlo simulations. Within the theoretical approach the potentials were derived by integrating the functional form of the osmotic pressure generated by a colloid onto a star polymer. Excellent agreement between the simulation results and the analytical approach was shown, thus allowing to use the theoretical framework to predict the functional form of the effective potentials between stars and colloids for ranges of functionality f that could not be easily reached via numerical methods, but are of great experimental interest. Being able to reliably determine effective potentials between star polymers and colloids provides thus for a full and realistic coarse-graining of the complex mixture also in the nanocomposite limit, in which the size of the stars significantly exceeds that of the dispersed colloidal particles. It also allows us to make quantitative predictions on the miscibility and thermodynamic stability of these composites, leading to the result that colloids of size much smaller than the stars will mix well with the latter, at least in the absence of enthalpic interactions between the two.

With the coarse-grained picture readily available, a number of questions regarding the behavior of concentrated star-colloid mixtures becomes tractable by means of theoretical and simulation approaches, and it allows for direct contact with experimentally accessible information. In particular, the way is now open for the investigation, by means of integral equations and simulation, of the full structure of the mixture. Of major importance is

the influence that the small colloids have on the star-star partial correlation functions, depending on their size and the star functionality. We expect that for very high values of q this effect will not be important, since the colloids can easily penetrate in the star interior. However, for high star functionalities, colloids of size ratios even as large as $q = 10$ will have significant impact on the structure of a high functionality star matrix, as witnessed by the fact that the value of Δ there is close to the borderline case $\Delta = 0$. It is thus anticipated that a small amount of colloids will influence the properties of the arrested star polymer glass [77]. Three- and higher-body effective interactions play a significant role when analyzing properties of systems at density considerably higher than the overlap density of star polymers [74, 90] However, glass formation and re-melting take place at densities around the overlap star-polymer concentration, where the physics is dominated by pair effective potentials. Access to the full pair structure of the system, in combination with the Mode Coupling Theory of the glass transition will allow us to shed light into this experimentally relevant question. It will also be quite interesting to consider now the smaller colloids as depletants of the stars and analyze the impact they have on the star-star effective interaction. These topics will be the subject of future work.

Acknowledgements

Chapter 3

Glassy States in Asymmetric Mixtures of Soft and Hard Colloids [1]

Suspensions of colloidal particles are ubiquitous in nature and represent an ever stimulating and technologically challenging field of research [19]. The majority of the work relating to the dynamics and rheology of colloids has been performed with the simplest hard sphere systems, both experimentally and theoretically [91, 92]. Indeed, in a breakthrough study [93] it was demonstrated that added non-adsorbing polymers, smaller than the colloids, control the rich morphology diagram of colloid-polymer mixtures and its rheological consequences primarily via depletion. In general, colloidal mixtures exhibit a variety of phases and kinetic states from colloidal gas to liquid, crystal, repulsive and attractive glass and gel [94].

These important developments prompted the question of the effects of soft interactions on the macroscopic properties of the colloids [5, 95]. Star polymers have been explored in detail, since they exemplify stable, long hairy particles. At high concentrations, they deform but also interpenetrate via their grafted arms, as reflected by their effective interactions: their tunability at the molecular level allows repulsive pair potentials ranging from ultrasoft to hard as their functionality (number of arms), f_S, changes from typically below 30 to above 400 [32]. The very same deformability also determines their purely entropic interactions with planar or curved hard walls [2]. Stars with functionalities $f_S \gtrsim 50$ form glassy states at large volume fractions [77, 95]. Mixtures of star polymers and smaller, linear polymers have shown great richness in metastable states, controlled by the osmotic pressure of the latter, and leading to star shrinkage and depletion [37, 76]. Star polymers with $f_S \leq 32$ were also mixed with larger hard spheres and the phase behavior of the

---

mixtures was examined experimentally and theoretically [39]. However, the inverse case, in which hard spheres are used as depletants for deformable, glass-forming stars has not been addressed to-date.

In this Letter, we address the formation of multiple glassy states in soft-hard colloidal mixtures composed of large stars and small hard sphere-like depletants. To ensure purely entropic interactions, we used stars of the same chemistry and drastically different functionalities. The hard colloids were stars with very short chains, expected to be fully stretched in the core portion [31], so that they act as hard spheres (HS). Using rheology, Mode-Coupling Theory (MCT) and Molecular Dynamics (MD) simulations, we observe vitrification of the soft star glass, melting upon the addition of colloidal spheres and subsequent arrested phase separation as the repulsive glass line crosses the binodal.

Polybutadiene star polymers (1,4-addition) of $f_S = 214$ (soft sphere) and $f_C = 1109$ (hard sphere), and respective arm molar masses 67000 and 1270 g/mol, were synthesized anionically. The polydispersity indexes (PDI) and the molar fraction of contaminants (MFC) have been measured via size exclusion chromatography (SEC): PDI=1.07 and MFC=0.12 for the soft spheres, whereas PDI=1.11 and MFC=0.036 for the hard spheres. Details are given in refs. [29, 96] and in the Supplemental Material 3.1. To express the concentrations in terms of the number densities of the star- and colloid-components (ρ_S and ρ_C, respectively), we employ the effective corona diameter of the stars, σ_S, as the unit of length. The star-to-HS hydrodynamic size ratio is $\xi = 4$ and the nominal glass transition concentrations for the stars and HS are $\rho_S \sigma_S^3 = 0.339 \pm 0.002$ and $\rho_C \sigma_S^3 = 10.75 \pm 0.7$. Accordingly, the pure star solutions were investigated at number densities $\rho_S \sigma_S^3 = 0.342, 0.347, 0.368$, and 0.421, in which the samples are glassy, and colloidal spheres of various concentrations have been added to analyze the ensuing rheology of the mixture. Here, we focus on the effects of adding HS to stars at $\rho_S \sigma_S^3 = 0.342$, where more than one glassy state as well as melting of the mixture can be unambiguously distinguished.

In the absence of HS, the concentrated star solution with $\rho_S \sigma_S^3 = 0.342$ exhibits features typical of glassy behavior [Fig. 3.1(a)]: both the storage (G') and loss (G'') moduli are only weakly frequency-dependent, with G'' exhibiting a broad minimum, $G'(\omega) > G''(\omega)$ over four decades of frequency, while being also time dependent due to aging 3.1, [95].

While maintaining the star density fixed at $\rho_S \sigma_S^3 = 0.342$, the addition of HS colloids induces remarkable softening of the initial glassy suspension, and eventually a transition to the ergodic liquid state above a certain HS volume fraction ($\rho_C \sigma_S^3 > 0.029$) is observed, Fig. 3.1(b). This is also confirmed by the absence of aging 3.1, [95]. For even higher HS fractions ($\rho_C \sigma_S^3 \geq 1.0311$), shown in Fig. 3.1(c), the mixture undergoes a reentrant transition to another solid-like state which, with the help of MCT, is attributed to arrested phase separation; the latter is corroborated by two facts: (i) at the reentrance the plateau modulus G_p is nearly identical to that of the original repulsive glass (see Fig. 3.2), and (ii)

there is no visual evidence of this dense sample becoming turbid. This suggests a scenario of a purely repulsive glass regime up to the reentrant line, an interpretation supported by the theoretical analysis. Note that if the reentrant state were an attractive glass, its storage modulus would have been much higher as compared to that of the repulsive glass [97]. We also observe in Fig. 3.2, that upon further increasing the concentration of HS colloids in the reentrant regime, the modulus eventually increases by more that one decade. It is tempting to interpret this increase as a third transition, but this requires additional experimental and theoretical work, which are currently underway. Turning to the intermediate ergodic regime, the characteristic time of the liquid (extracted from the terminal crossover of the moduli) varies by several decades: it first decreases with ρ_C as we move away from the repulsive glass due to depletion, and then goes through a minimum and increases as the reentrance is approached (Fig. 3.2). The rheological yielding transition was examined with dynamic strain sweeps at different frequencies (here the 10 rad/s results are discussed). While a single yield point could be identified in the initial repulsive glassy phase [Fig. 3.1(a), inset] and no yielding was observed in the liquid state [Fig. 3.1(b), inset], the re-entrant state exhibited a two-step yield process [Fig. 3.1(c), inset] for $\rho_C\sigma_S^3 < 3.53$. Beyond this value the single yielding behavior was recovered along with an increase in the modulus. Double yielding is thought of as reflecting two constraining length scales (say bonds and cages) which occur in attractive glasses [97] or arrested phase separating systems alike. It is tempting to interpret the observed increase of the modulus as a third transition but this requires additional experimental and theoretical work, which is currently underway.   Fig. 3.3(a) assembles all experimental data in the form of a morphology diagram where the different rheological states are indicated for varying fractions of star and the added HS depletant particles. The vertical arrow indicates the onset of the glassy star regime at $\rho_C = 0$. Thereafter, for $\rho_S\sigma_S^3 = 0.342$, which is the most extensively studied mixture, we observe the transformation from a repulsive glass to a liquid and eventually to a reentrant arrested state, as a result of the depletion effect of the added HS. Finally, for larger ρ_S we find glasses and glass-glass transitions with the glass at larger ρ_C having larger moduli, consistently with the presence of attraction in the system cages.

The theoretical analysis was based upon a coarse-grained picture of the binary mixture. Thereby effective interaction potentials $V_{ij}(r)$, $i, j = S, C$, acting between the centers of two particles separated by distance r could be employed. For the star-star interaction, $V_{SS}(r)$, the potential introduced in Ref. [32] was employed, which features a crossover from a logarithmic divergence at small r into a Yukawa form for large r at the corona diameter σ_S. Comparisons with experiments [32, 76, 79, 98] have shown that $\sigma_S \cong R_h^S \cong 4R_g/3$,
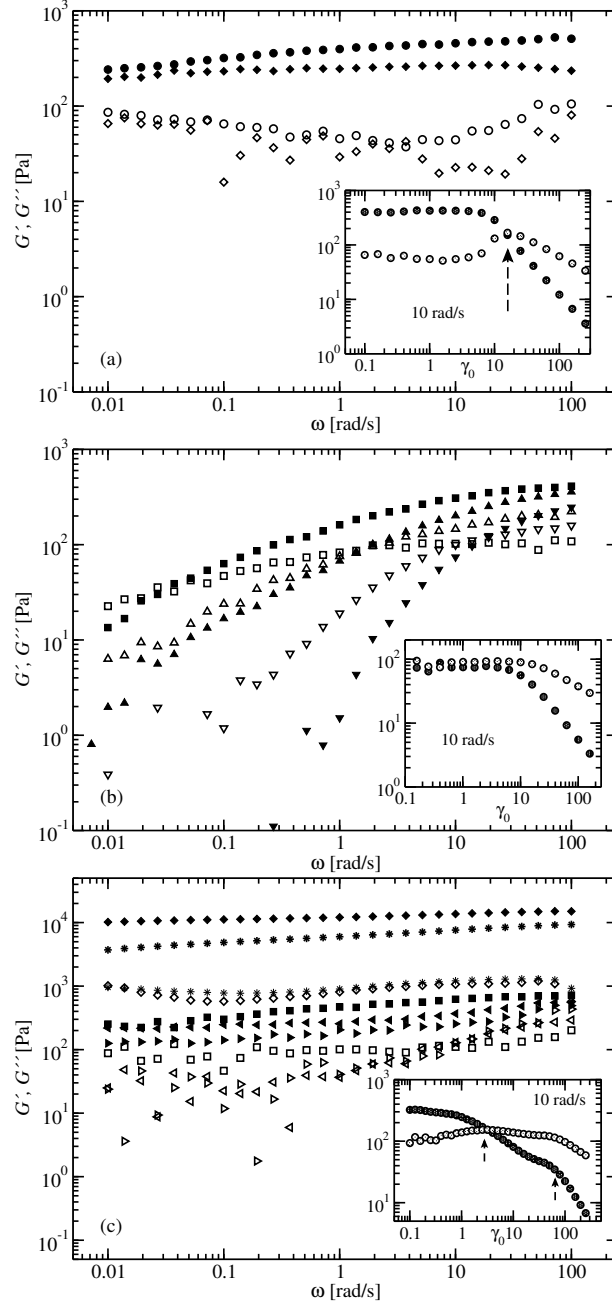
Figure 3.1: Linear viscoelastic spectra for HS-star mixtures at $\Phi_S = 1.625$ ($\rho_S \sigma_S^3 = 0.342$). G' and G'' are shown with full and empty symbols respectively. (a) Repulsive Glass: $\rho_C \sigma_S^3 = 0$ (circles) and $\rho_C \sigma_S^3 = 0.0147$ (diamonds). Inset: Dynamic strain sweep for $\rho_C \sigma_S^3 = 0$ at $10\,\mathrm{rad/s}$. The arrow indicates the yield point. (b) Liquid: $\rho_C \sigma_S^3 = 0.1473$ (squares); $\rho_C \sigma_S^3 = 0.2946$ (up triangles); $\rho_C \sigma_S^3 = 0.4419$ (down triangles). Inset: Dynamic strain sweep for $\rho_C \sigma_S^3 = 0.4419$ at $10\,\mathrm{rad/s}$. (c) Reentrant glass: $\rho_C \sigma_S^3 = 1.1784$ (squares); $\rho_C \sigma_S^3 = 1.7676$ (left triangles); $\rho_C \sigma_S^3 = 3.5352$ (right triangles); $\rho_C \sigma_S^3 = 5.892$ (stars); $\rho_C \sigma_S^3 = 7.070$ (diamonds). Inset: Dynamic strain sweeps for $\rho_C \sigma_S^3 = 1.7676$, showing G' (dark circles) and G'' (light circles). The arrows mark the yield points: two-step yielding occurs in the arrested phase separated mixtures.
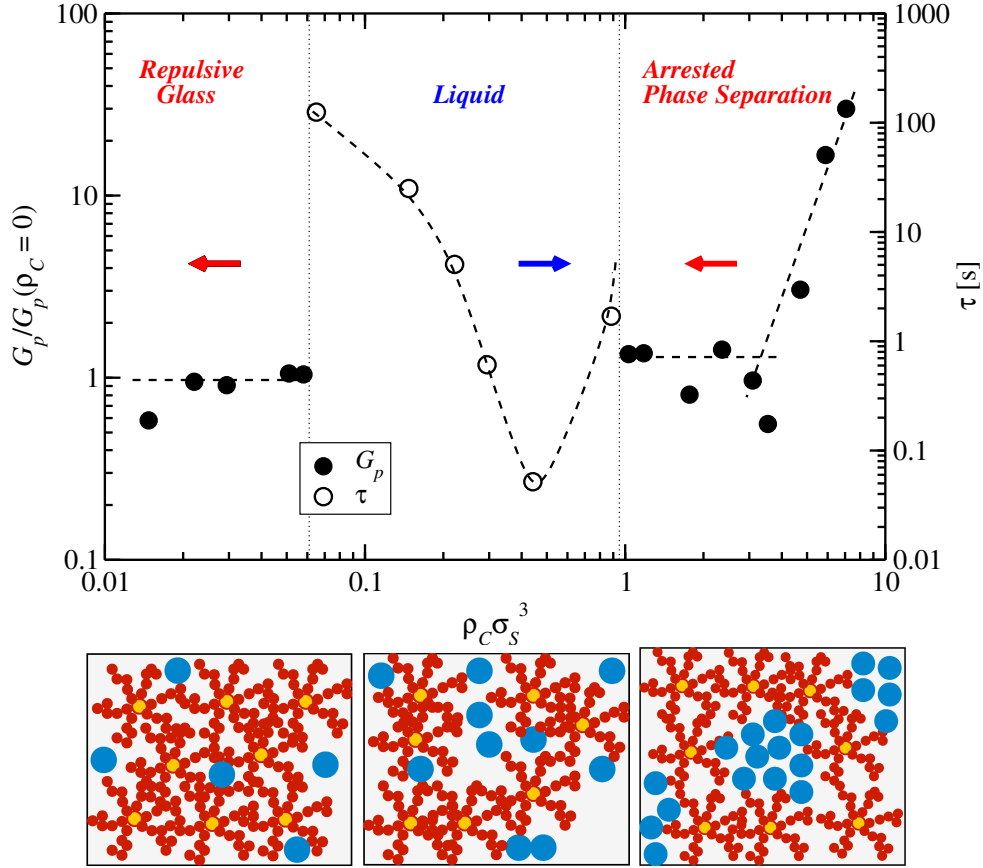
Figure 3.2: The plateau moduli of the arrested states (closed circles, left vertical axis) and the relaxation times of the ergodic phases (open circles, right vertical axis) observed for star polymer density $\rho_S\sigma_S^3 = 0.342$ as a function of the colloid density $\rho_C\sigma_S^3$. The three cartoons show, from left to right, sketches of the repulsive glass, the liquid and the arrested phase separation-state.

R_g being the radius of gyration of the stars [99]. $V_{CC}(r)$ was modeled as a hard sphere potential for a diameter $\sigma_C = 2R_C$, a choice justified by the ultra-high functionality of the hard-like stars. For $V_{SC}(r)$ we employed the recently developed corresponding potentials [2] for star functionality $f_S = 214$, as in the experiments. We used two-component integral equation theories with the Rogers-Young closure [100] to calculate the partial structure factors for mixtures with arbitrary density and composition. Their validity was confirmed by the excellent agreement with Monte Carlo simulations for the coarse-grained mixtures at selected points.

The locus of ideal glass transition points on the (ρ_S, ρ_C)-plane was determined by employing the one-component version of the MCT [98, 101], in which the structure factor $S(k)$ of the stars is the input for the determination of their non-ergodicity factor $f(k)$. The latter vanishes for an ergodic liquid and it is nonzero for a glass. Inherent in this one-component approach is the assumption that within the glassy state of the stars, the small colloidal particles remain ergodic; were this not to be the case, then the full, two-
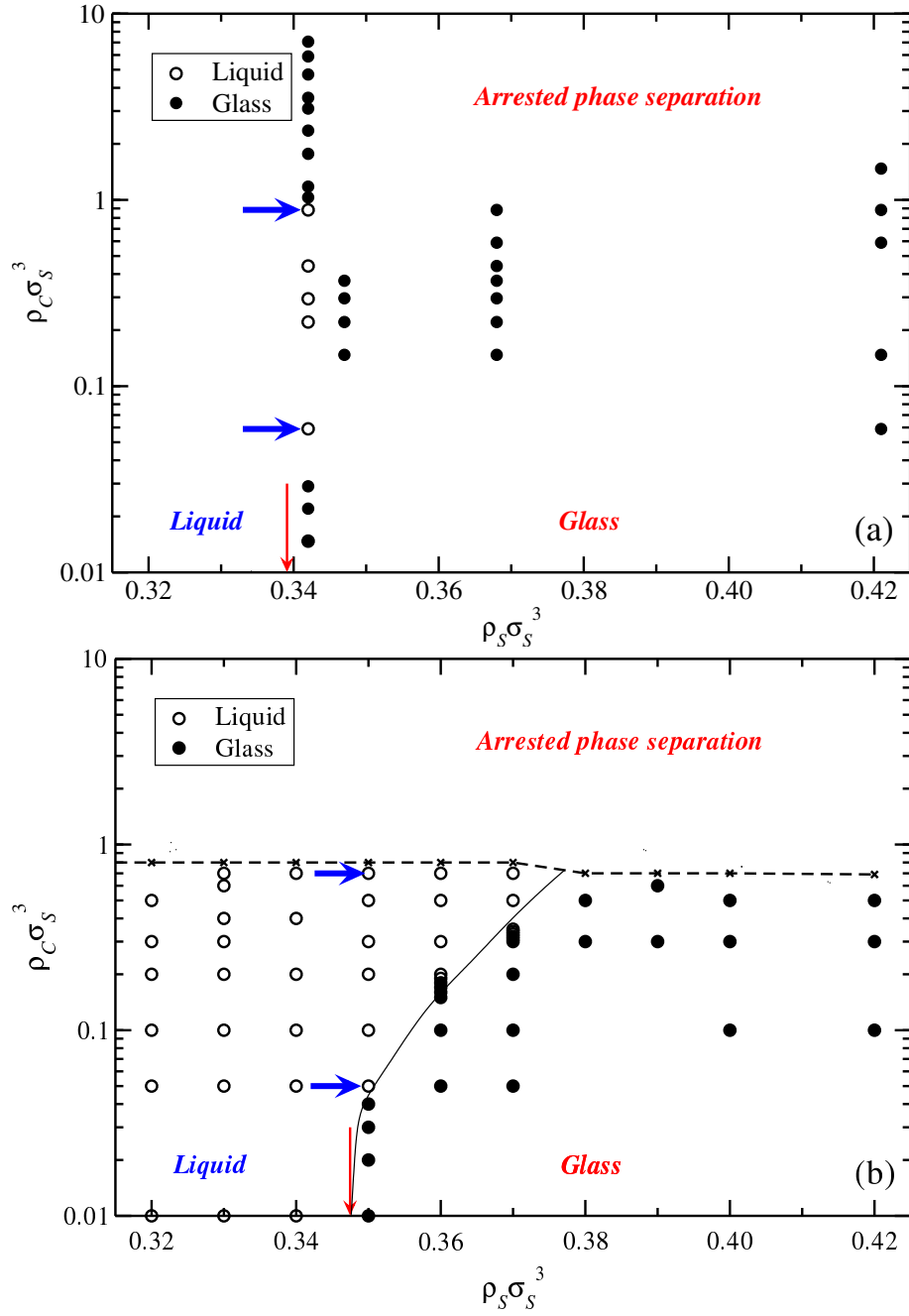
Figure 3.3: (a) The experimental state diagram of star polymer–colloidal mixtures with $\xi = 4$ and star functionality $f_S = 214$. The vertical arrow denotes the star polymer density at which a star solution arrests in the experiment in the absence of colloids and the horizontal arrows denote the points where the system melts and revitrifies. (b) The MCT-phase diagram of the same system. The dashed line denotes the locus of points for which integral equations fail to converge due to a demixing phase transition, whereas the hand-drawn solid line separates the region of the liquid and the repulsive glass. Arrows and circles as in panel (a).

component version of the MCT should be employed [79, 101]. This assumption was fully confirmed by our MD simulations 3.1.

Fig. 3.4 shows the dependence of the non-ergodicity factor for a star solution at density $\rho_S \sigma_S^3 = 0.36$, for which the pure system is glassy, on the density of the added colloids. Upon addition of a sufficient amount of HS-particles ($\rho_C \sigma_S^3 \geq 0.5$), the glass melts. The physical mechanism responsible for this transition lies in the fact that the small colloids act as depletants for the large stars – a situation specular to the usual colloid/polymer case, in which the small polymers deplete the big colloids [39, 93, 102–104]. In contrast to the latter case, in which the depletion attraction takes the form of an Asakura-Oosawa or square-well potential [102], for the system at hand the colloid-induced depletion is superimposed on a soft repulsion between the stars. Thus, at moderate colloid concentrations, it has initially the effect of reducing the repulsions, leading to melting of the glass [76, 79]. Upon further addition of colloid, net attractions between the stars appear 3.1, which drive the system towards a demixing phase separation into a star- and a colloid-rich phase, as already predicted in Refs. [2, 105]. This manifests itself in the integral equation approach by the fact that all structure factors develop increasingly high peaks at $k = 0$, and convergence of the integral equations can no longer be achieved. The locus of points for which the solution is lost, which can be loosely identified with the demixing line of the system, is denoted in Fig. 3.3(b) by the dashed line. This figure presents a compilation of the MCT-results and it should be directly compared to its experimental counterpart, Fig. 3.3(a). Quantitative and parameter-free agreement can be seen between experiment and theory by comparing Fig. 3.3(a) with Fig. 3.3(b) regarding the glass-to-liquid transition for the value of ρ_S lying most closely to the glass transition in the absence of colloids, denoted by the horizontal arrows there.

For higher star densities, theory predicts gradual shrinkage of the liquid regime, which forms an intruding pocket into the glassy region. The extent of this intrusion is overestimated by theory. The reentrant glass observed in experiments can arise from the intervention of the demixing binodal, thus rendering the high-ρ_C glass as the result of an arrested phase separation. The latter has been extensively discussed in the literature in conjunction with gelation, and in all cases within the context of colloid-polymer mixtures with very sharp and short-range attractions caused by the polymers depleting the colloids [103, 104, 106–110]. In that case, it has been shown [107, 110] that the attractive glass line intersects the binodal on the high-density side of the glass former. Here, it is the *repulsive glass* line that meets the binodal on the high-density side of the star-polymer glass former. However, as the binodal is crossed, the ensuing phase separation becomes arrested in the continuation of the glass line within the demixed region and the system arrests into a high-star concentration glass. This increase in concentration compensates for the reduced repulsions and leads to a glass whose modulus is essentially the same as that of the original one. Deeply inside the binodal, i.e., for even higher values of ρ_C, depletion attractions are strong and can lead to arrest into an attractive glass with much

higher values of the modulus (Fig. 3.2). The high-ρ_S-region above the demixing line in Fig. 3.3(b) thus corresponds to arrested states, consistently with the experimental findings for reentrant glasses. It is not amenable to MCT-analysis, though, since no structural data are available there, due to the loss of solutions of the integral equations.

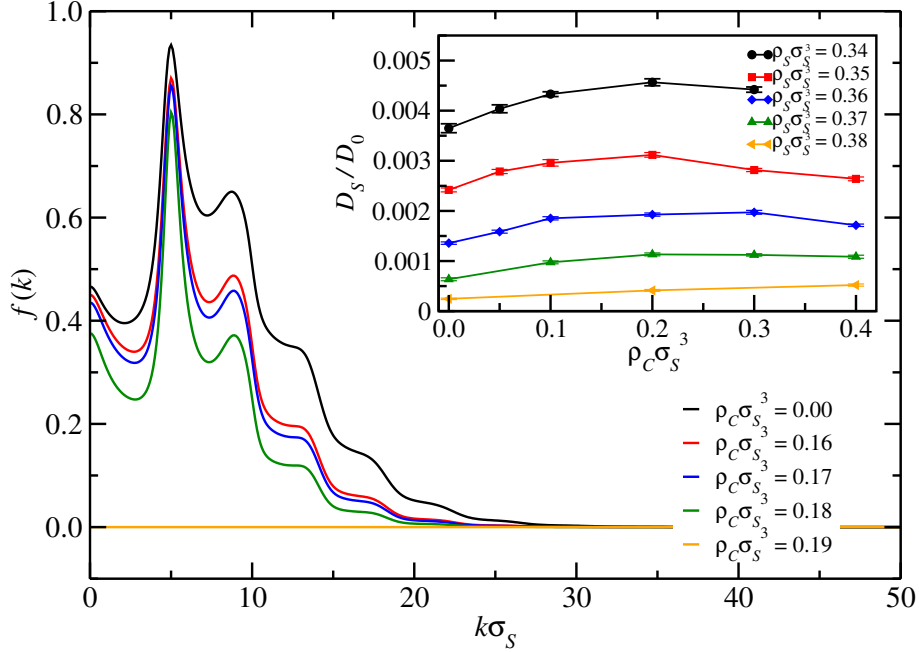We have assumed in our MCT analysis that the colloidal additives remain ergodic within

Figure 3.4: The dependence of the star non-ergodicity factor $f(k)$ for a star polymer solution at density $\rho_S\sigma_S^3 = 0.36$ on the density of added colloids, as indicated in the legend. Between $\rho_C\sigma_S^3 = 0.18$ and $\rho_C\sigma_S^3 = 0.19$, $f(k)$ drops abruptly to zero, indicating an ideal glass-to-liquid transition. Inset: the long-time diffusion constant D_S of the stars, normalized with $D_0 = \sqrt{k_BT\sigma_S^2/m_S}$, as a function of the density of the colloidal additives and for various star densities as indicated in the legend.

the star glass; it is not obvious whether this assumption is correct, hence its validity has to be proven. Zaccarelli *et al.* [101] have shown that in a binary mixture the long-time dynamics are determined by the short-time mobility ratio α between the large and the small components. For Brownian particles, as for the case at hand, this is set by the hydrodynamic size ratio: $\alpha = \xi^{-1} = 0.25$. The assumption of colloidal ergodicity has been validated via MD simulations 3.1. Indeed, the mean-square displacements (MSD) of the colloids showed typical diffusive behavior. On the contrary, the MSD curves for the stars displayed a clear plateau at the crossover from the ballistic to the diffusive regime, which shrunk upon the addition of colloids 3.1. The measured long-time diffusion constants D_S for the stars are summarized in the inset of Fig. 3.4. Consistently with the MCT results, the addition of colloids first accelerates the star dynamics and then slows them down again as the colloidal concentration is increased, whereas phase separation sets in at even higher

colloidal densities. This non-monotonic behavior is consistent with glass reentrance and with that of the relaxation time of the fluid shown in Fig. 3.2, middle panel.

In conclusion, we have shown by combining experiments, theory and simulation that the addition of small, hard colloidal additives to a structural glass formed by large, soft colloids brings forward a wealth of novel, tunable rheological states, including a melting to an ergodic liquid and new states that appear due to an interplay between the structural arrest line of the repulsive glass and macroscopic demixing. The star functionality and the size ratio represent the natural, physical parameters to adjust in order to steer the rheology of the mixtures. The quantitative, parameter-free agreement between the experiments, simulations and theory shown in this work offers a strong basis for the extension of our investigations to other functionalities and size ratios in the future.

3.1 Supplementary Material

We give details of the stars used in the rheological experiments, the preparation and the characterization of the samples and the aging of the mixtures. Further, we rationalize the demixing transition by means of a colloid-mediated star polymer potential and we show results on the mean-square displacements of stars and colloids from the MD simulations.

Characterization of the samples and rheology:

In the experiments, we employed multiarm 1,4-polybutadiene (PBD) stars with a weight-average functionality $f_S = 214$ and a weight-average molar mass $M_w^S = 14\,500\,\text{kg/mol}$, whose synthesis is described elsewhere [29, 96]. The effective hard-sphere systems consisted of PBD stars with $f_C = 1109$ and $M_w^C = 1600\,\text{kg/mol}$. The size exclusion chromatography (SEC) traces of both the soft and hard sphere-like star polymers are shown in Figures 3.5 and 3.6 and they are compared with the traces of the linear chains which are grafted to the cores. The SEC traces were obtained using a Viscotek GPC max unit equipped with a VE 2001 GPC Solvent/sample Module, a Viscotek triple detector array equipped with refractive index, viscosity, and dual-angle light scattering (7° and 90°, $\lambda = 670$ nm) detectors, and an external Viscotek UV 2600 detector. A polystyrene standard with a peak molecular weight $M_p = 99,500$ and $M_w/M_n = 1.03$ (Viscotek) was used to calibrate the instrument. The reported dn/dc value and intrinsic viscosity for this standard in THF were 0.185 ml/g and 0.477 dl/g, respectively. Three PolyAnalytik mixed bed columns, PAS-103-L, PAS-104-L, PAS-105-L, each 8 mm (ID) × 300 mm (L), with an overall linear polystyrene molecular weight range of 103 - 107, were employed with THF as the mobile phase at a flow rate of 1.0 ml/min and a column temperature of 30 °C. The results were analyzed using the Viscotek OmniSEC software package.

The SEC traces shown in Figures 3.5 and 3.6 prove that both soft and HS-like star polymers are without free chains left. Nonetheless, a small shoulder in the molar mass distribution of the HS-like stars ($f_C = 1109$) can be detected with high hydrodynamic volume. We fitted the molar mass distribution with two Lorenz functions and calculated the relative heights of the distributions to estimate the fraction of high molecular weight contaminant (Figure 3.7). We find that the molar fraction of contaminant is 0.036. We performed the same analysis of the SEC traces also in the case of the soft stars ($f_S = 214$) to estimate the fraction of low molecular weight contaminant that is possibly due, in this case, to the presence of stars with smaller functionality. From the relative height of the distributions (Figure 3.8) we find that the molar fraction of contaminant is 0.12. SEC analysis served to determine also the polydispersity index (PDI $= M_w/M_n$) values for the branched polymers: PDI=1.07 for the soft stars and PDI=1.11 for the HS-like stars.

As additional information we report here the intensity correlation functions obtained via Dynamic light scattering (DLS) experiments performed on a HS-like star polymer solution in the dilute regime at different angles. All the correlation functions are well fitted (Figure 3.9) by a stretched exponential (KWW) function:

$$g_2(t) - 1 = \left\{ K_1 \exp\left[\left(-\frac{t}{\tau} \right)^\beta \right] \right\}^2 + K_2. \tag{3.1}$$

The stretching parameter β is related to the width of the distribution of the relaxation times. We obtained $0.9 < \beta < 1.0$ (inset of Figure 3.9) with no specific dependence of β on the scattering wave vector, i.e., the high molecular weight contaminant detected via the analysis of the SEC trace does not scatter enough to be readily detected via DLS.

The particles were dissolved in squalene, a nearly athermal, non-volatile solvent for PBD. The respective hydrodynamic radii $R_h^S = 45.0$ nm and $R_h^C = 11.5$ nm were determined from dynamic light scattering measurements in dilute solution at $20\,^\circ$C, yielding overlap concentrations $c_S^\star = 44.5$ mg/ml and $c_C^\star = 416$ mg/ml, respectively. We define the ratio of hydrodynamic sizes as $\xi \equiv R_h^S/R_h^C \cong 4$ in the case at hand. The respective nominal effective volume fractions $\Phi_S^g = c_S^g/c_S^\star = 1.6125 \pm 0.0125$ and $\Phi_C^g = c_C^g/c_C^\star = 0.75 \pm 0.05$ for rheological glass transitions were determined via small amplitude oscillatory experiments (SAOS), performed with a strain-controlled ARES rheometer (TA, USA). In Fig. 3.10(a),(b) and (c) we show the time dependence of moduli for the three states described in the paper.

Theory and Simulation:

The added colloids modify the effective potential between the star polymers, bringing about depletion-mediated attractions that lead to phase separation at sufficiently high colloid concentrations. In particular, we determine the effective, colloid-modfied interaction potential between the star polymers, $V_{\mathrm{eff}}(r; \rho_C^r)$ from integral equation theory as

follows:

$$\beta V_{\text{eff}}(r; \rho_C^r) = - \lim_{\rho_S \to 0} \ln \left[g_{SS}(r; \rho_S, \rho_C^r) \right],\tag{3.2}$$

where $g_{SS}(r; \rho_S \to 0, \rho_C^r)$ is the star-star radial distribution function at a reservoir density ρ_C^r of the colloids. The mapping from the reservoir-representation to the system variabes (ρ_S, ρ_C) is performed under the standard way of matching the partial chemical potential μ_C of the colloids of the two [111]. Accordingly, and since the mixture consists of mutually repulsive species, $\rho_C(\rho_S) < \rho_C^r$, the inequality getting stronger as ρ_S grows.

We have derived effective potentials $V_{\text{eff}}(r; \rho_C^r)$ for increasing values of reservoir colloidal densities, confirming the gradual development of attractive, depletion-induced wells that lead to a gas-liquid transition for the stars, which is the one-component representation of the demixing transition in the full, two-component representation. The detailed analysis of these potentials and the mapping between the reservoir and the system variables will be the subject of a future publication.

We performed MD simulations, for which $\alpha = \sqrt{m_C/m_S}$, in terms of the masses m_S and m_C of the stars and the colloids, respectively. To preserve the value of α, we fixed the mass ratio at $m_C : m_S = 1 : 16$ in the MD. Crystallization of the star polymer was hindered by introducing a 20% size polydispersity in the stars in the range $0.70\,\sigma_S - 1.30\,\sigma_S$. A total of 1024 stars were simulated in a cubic box with periodic boundary conditions in the relevant density regions for both stars and colloids, and the equations of motion were integrated using a timestep $\Delta t = 10^{-3} \tau_{\text{MD}}$ with $\tau_{\text{MD}} = \sqrt{m_S \sigma_S^2 / k_B T}$. After 10^6 timesteps for equilibration, the mean-square displacements of both components were measured for a total of 10^7 timesteps.

Mean-square displacement curves for the colloids and the stars from our MD simulations are shown in Fig. 3.11, demonstrating the ergodic nature of the former as well as their influence in accelerating the dynamics of the latter.
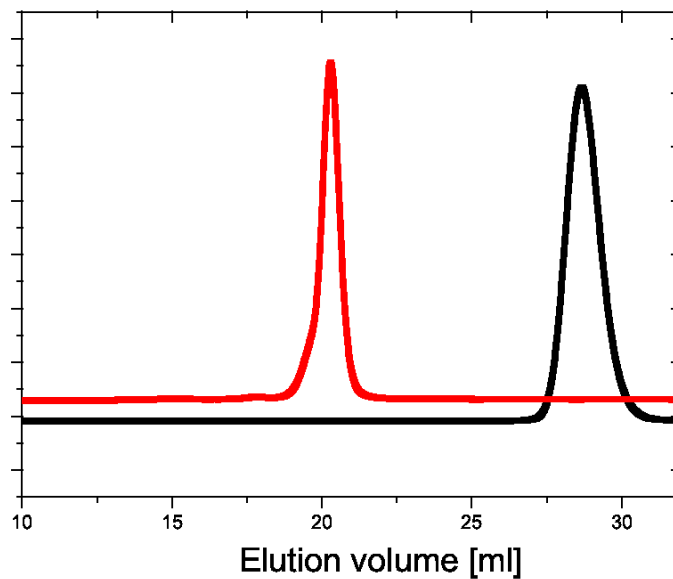
Figure 3.5: In black (rightmost peak): 1.5K linear chains used as arms to generate RS64-PBD1.5 In red (leftmost peak): Purified star (RS64-PBD1.5, $f = 1109$), also called HS in the manuscript.
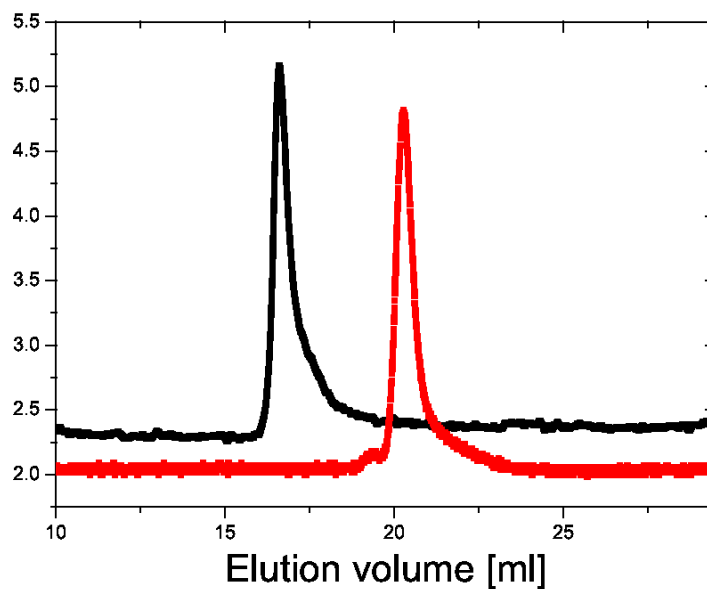

Figure 3.6: In red (rightmost peak): 68K linear chains used as arms to generate the star polymer. In black (leftmost peak): purified star PBD ($f = 214$).
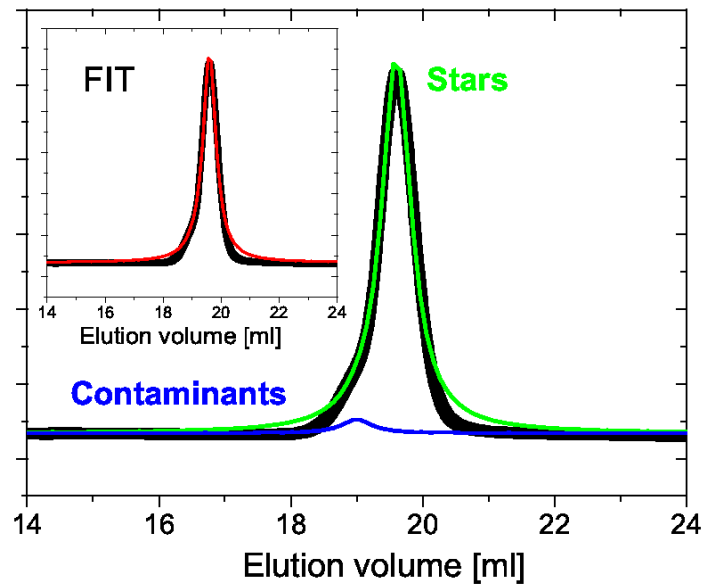
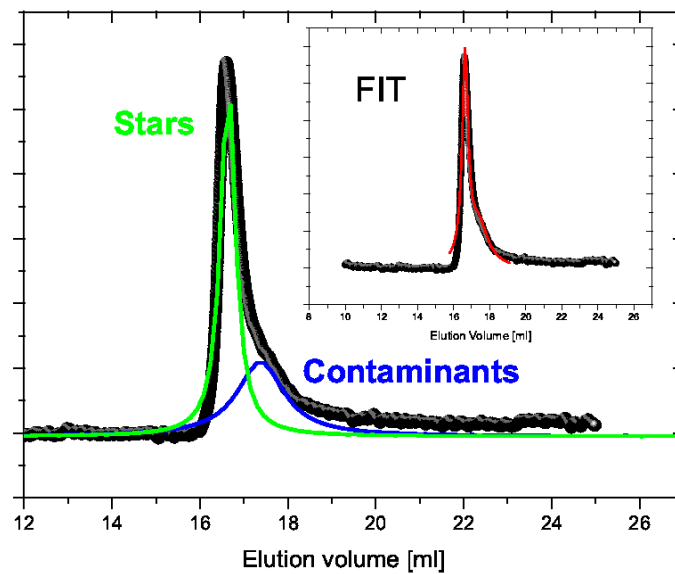Figure 3.7: Fit of the SEC trace of the HS-like stars ($f = 1109$) with two convoluted Lorenz functions. Inset: The resulting total fit is shown by the red curve.

Figure 3.8: Fit of the SEC trace of the stars ($f = 214$) with two convoluted Lorenz functions. Inset: The resulting total fit is shown by the red curve.
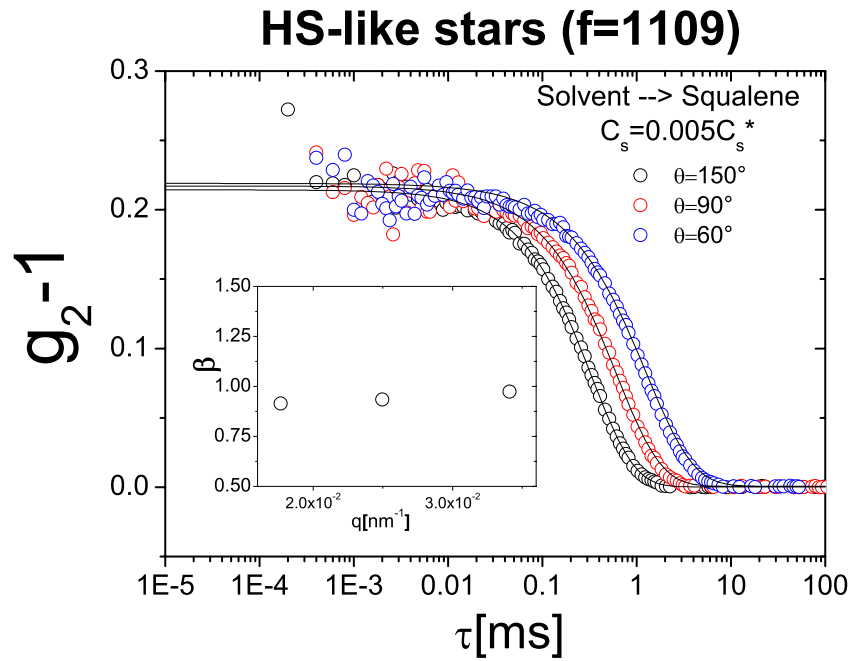
Figure 3.9: Intensity correlation functions of a diluted solution of purified HS-like star (RS64-PBD1.5, $f = 1109$) in squalene at different angles as indicated in the main panel. Inset: Stretching parameter β in function of the scattering wave-vector q.
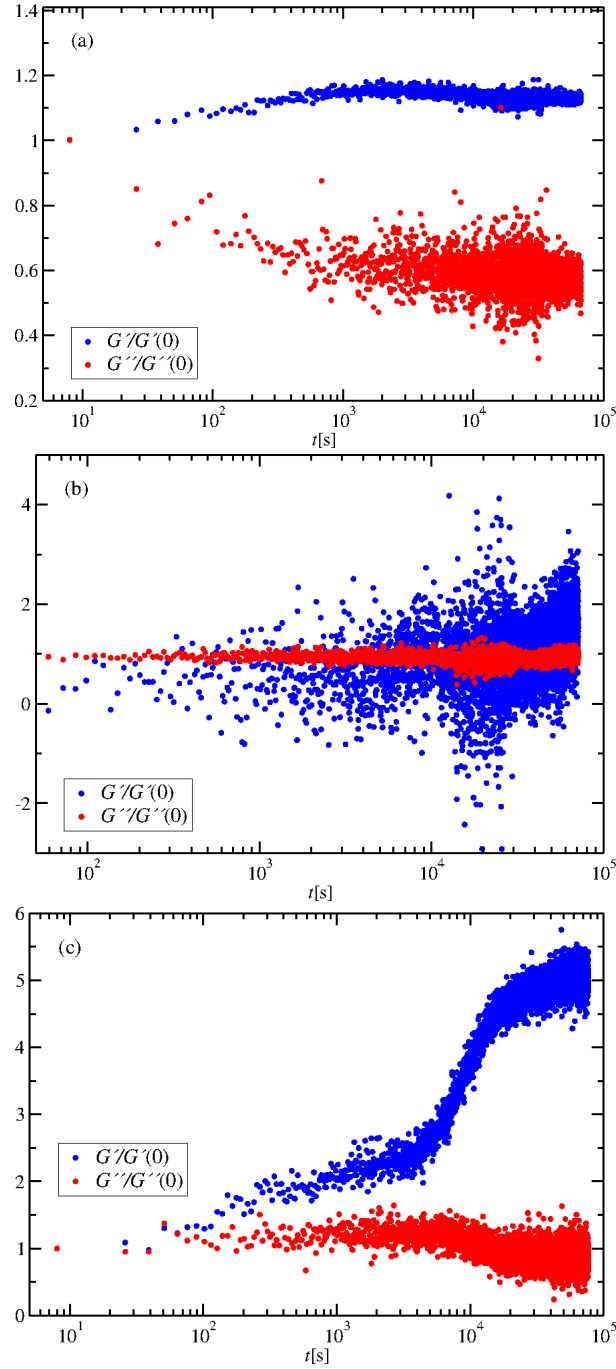
Figure 3.10: Normalized moduli as functions of time after rejuvenation (aging) for fixed star density $\Phi_S = 1.625$ ($\rho_S \sigma_S^3 = 0.342$), $\omega = 1$ rad/s, $\gamma_0 < 1\%$ and for colloid concentrations: (a) $\rho_C \sigma_S^3 = 0$; (b) $\rho_C \sigma_S^3 = 0.44$, and (c) $\rho_C \sigma_S^3 = 1.17$.
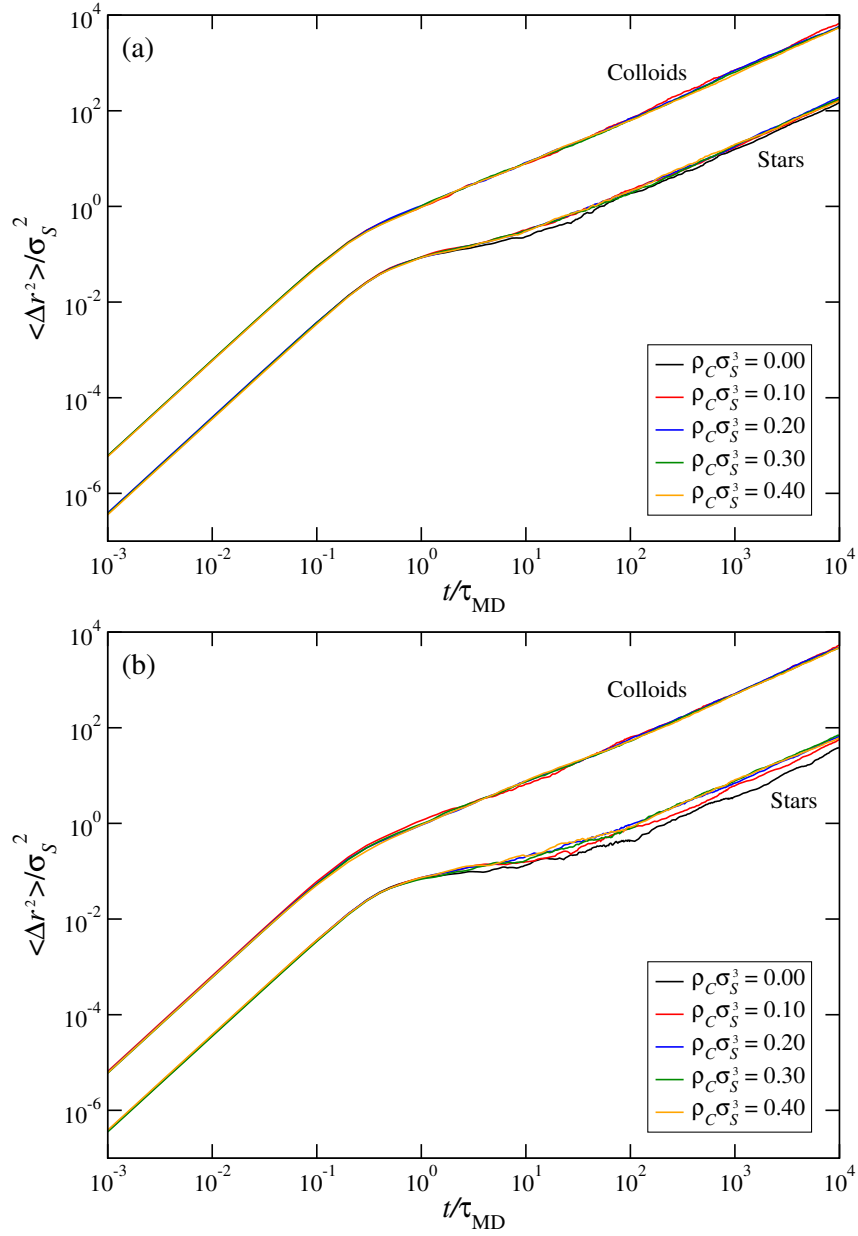
Figure 3.11: The mean-square displacement $\langle \Delta r^2 \rangle$ against MD time for the colloids (upper curves) and the stars (lower curves), at two different star polymer densities: (a) $\rho_S \sigma_S^3 = 0.35$; (b) $\rho_S \sigma_S^3 = 0.37$, and for various densities of the added colloids, $\rho_C \sigma_S^3$ as indicated in the legends.

Chapter 4

Glassy states and melting in polymer star - colloid mixtures

Presumably the first glass was produced in ancient Egypt several thousand years ago and since then many *amorphous materials* have found their way into our everyday life: Window glass, plastics, rubber, porous materials, etc. Despite being present in daily life, there is still lack of a coherent theoretical description, although from an experimental and simulation point of view, glasses have become an important field of research. Widely studied is the effect that one can cool own many liquids below their melting temperature and then let them solidify in an amorphous structure, the so called *glass-transition*. Amorphous materials and liquids are known for their short range order but lack of long range order as it is found in crystals, a property which makes theories for crystals so much easier than those for glassy materials. One theory that offers a quantitative description of the structural relaxation and is able not only to reproduce experimental results, but also to predict phenomena is the concept of the *mode-coupling theory of the glass transition (MCT)*. We give an overview over the concept and resulting equations in Appendix B.

In principle, disordered materials can be divided into several groups: Spin glasses, dipolar or orientational glasses and "mixed-crystal"-glasses are systems we are not going to investigate in this work, but we rather concentrate on so-called structural glasses (i.e. liquids, polymers, colloids), which are from a theoretical point of view much harder to handle, because the disorder in the material is "self-generated" and not influenced by an underlying crystal lattice. Additionally, also the degrees of freedom that one might want to treat within the concepts of thermodynamics are strongly connected with the positions of the particles. More information on spin glasses, an interesting group of glasses for which mode-coupling theory is an exact theory, can be found in [112].

Structural glasses built of of colloids and non-absorbing polymers have been studied extensively in the last decades [44–47]. Since colloidal glasses allow for tailoring the properties

of glasses, there has been a lot of research, starting from simple hard sphere systems [91, 92] over the so called *colloidal limit* (i.e. $q = R_{g,S}/R_C < 1$, with $R_{g,S}$ being the radius of gyration of the star and R_C the hard sphere radius of the colloids). In the case of the colloidal limit the polymers can be replaced by effective soft spheres [1, 48, 51, 52, 111]. Research continued to the PRISM theory [113], a microscopic theory for polymer solutions based on "off-lattice Polymer Reference Interaction Site Model integral equation methods", and led to recent investigations in the *protein limit* ($q = R_{g,S}/R_C > 1$), e.g. the binary mixture of polymeric stars and small, hard additives [2, 5, 43, 95]. Reasons for the importance of understanding colloid polymer mixtures are on one hand the possibility of tuning the interaction and on the other hand observing various states of the system from liquids to gels over glasses to crystals [79, 114].

Extensive investigations have been carried out on systems of big colloids and (polymeric) additives, since this so-called *colloidal limit* can be studied within the well-known depletion picture and computer simulations are able to explain several properties: For example, in colloidal systems, effects like higher-order glass transitions, dynamical heterogeneity or gelation have been observed and a wide range of attractive interactions have been employed [93, 102–104]. Even after decades os research in the field of depletion interactions, the approach by Asakura and Oosawa [20] is still the prototype and forms the guiding paradigm.

The formation of attractive glasses has important ramifications to the related issues of gelation and the relationship between the gel formation and arrested phase separation. A large number of gel forming systems and systems that form several distinct glasses have been investigated, presenting also the distinction of gels and attractive/repulsive glasses. [22, 78, 107, 108, 110, 115]. These studies have introduced several mechanisms of how gels are formed: kinetic/dynamic arrest, phase separation, percolation, etc. The variety of gel formation gives an idea of how dramatically the properties of materials can change under the influence of colloidal particles. Later investigations have questioned and investigated the validity of the depletion picture [101] and specified sufficient asymmetry in size and short-time mobilities as circumstances under which reentrant glass scenarios can be found in binary mixtures. In these investigations, the lack of validity of the commonly used depletion picture has been explained as an inadequacy in the description of the dynamical behavior. The particular importance of this description for hard/hard mixtures was presented in Ref. [116] and further related investigations considered also soft/soft mixtures [117–122]. Similarities in the dynamical behavior have been found for confined colloids, e.g. in porous media [123–127], where a colloidal fluid is confined in a disordered porous matrix and some of the particles are trapped while others can move relatively free, leading to interesting effects in the occurrence of glass transitions due to single-particle and collective dynamics. Important results have been obtained also for soft-soft binary

mixtures in [79, 98, 128] and finally soft polymers were investigated within the depletion picture [75]. With this work we extend the investigations on binary mixtures by exploring the effects of soft polymers and hard colloids of different size ratios $q = R_{g,S}/R_C$, where the softness of the stars can be changed by varying the number of arms f.

Star polymers can be seen as a model system for a wide range of soft and even hard particles, stemming from the property that changing the number of arms, i.e., the functionality f, can model a system of linear chains with ($f = 2$), a wide range of soft colloidal systems and even hard spheres ($f \to \infty$) [32]. Star polymer mixtures of different functionalities and/or size ratios have also been investigated, showing the existence of multiple glassy states [79, 98, 129]. Glassy states of colloidal glasses can vary from repulsive glasses at low additive densities to attractive (reentrant) glasses for high additive concentrations [24], which has been seen in experiments [93], computer simulations [130] and theoretical investigations [131]. Star polymers are one model system, for which several glassy states can be observed. Additionally, an additive induced melting effect has also been seen in mixtures of star polymers and linear chains [76, 83].

The theoretical and experimental findings demonstrate the variety of phases of colloid - polymer mixtures leading from liquid to glassy and crystal states.

4.1 Theoretical model for the structure and phase diagram of the binary mixture

Recently, it was shown that small, hard sphere like colloidal additives with $q = R_{g,S}/R_C > 1$ to a star polymer glass with stars of functionality f act as depletants and lead to a melting of the glass [43]. In the previous Chapter 3 we have shown results for the comparison of our theoretical approach consisting of Rogers Young integral equation theory calculations and MCT with experiments and coarse-grained Monte-Carlo and Molecular Dynamics simulations. The agreement of experiments, theory and simulations was quantitative and parameter-free for a certain parameter choice ($f = 214, q = 3$). In this Chapter we extend the preceeding results to arbitrary combinations of parameter choices for q and f.

The theoretical approach we employ in this Chapter is based on the coarse grained model introduced for the binary mixture, where $q > 1$, in Ref. [2]. The introduced effective interaction $V_{SC}(r)$ between the colloids and stars was employed for functionalities $f \in \{214, 250, 300\}$ and size ratios $q \in \{3, 4, 8\}$. Additionally, for $f = 214$ also the parameter choice of $q = 2$ is presented. The effective colloidal interaction $V_{CC}(r)$ was modeled as a hard sphere potential with the colloid diameter $\sigma_C = 2R_C$, whereas for $V_{SS}(r)$ we have made use of the effective interaction introduced in Ref. [32].

The structure of the star polymer - colloid mixture can either be described in real space with the help of partial radial distribution functions $g_{ij}(r)$ with $i,j = $ C(olloid)/S(tar), or, equivalently in reciprocal space, by the partial structure factors $S_{ij}(k)$. Both the partial radial distribution functions and the partial structure factors can be obtained by using two-component Rogers Young integral equation theory (RY) [100]. We have concentrated on the calculation of structure factors, since the partial structure factor $S_{SS}(k)$ can be used as an input quantity for the one-component Mode Coupling Theory calculations (see Appendix B).

The partial structure factors are defined as

$$S_{ij}(k) = \delta_{ij} + \sqrt{\rho_i \rho_j}\, \tilde{h}_{ij}(k), \tag{4.1}$$

where i,j corresponds to colloid or stars, ρ_i is the density of species i and $\tilde{h}_{ij}(k)$ is the Fourier transform of the pair distribution function $h_{ij}(r) = g_{ij}(r) - 1$. We have also employed Monte Carlo simulations using the coarse-grained effective interactions for the binary mixture and calculated the partial structure factors for certain parameters. The excellent agreement (see Figs. 4.8, 4.9 and 4.10) proves the validity of the used theory. It is important to use valid $S(k)$ since they are the input variable for the one component mode coupling theory of the glass transition (MCT). We have derived non-ergodicity factors stemming from the one-component MCT which we explain in Appendix B: To identify if our system is in a liquid state, forms a glass or has melted already, non ergodicity factors $f(k)$ were calculated [132]. The non-ergodicty factor $f(k)$ is given by the long time limit of the density autocorrelation function $F_k(t)$:

$$f(k) = \lim_{t \to \infty} F_k(t), \text{where} \tag{4.2}$$

$$F_k(t) = \frac{\langle \rho_k^*(0) \rho_k(t) \rangle}{N S(k)}. \tag{4.3}$$

In Eq. (4.3) $\rho_k(t) = \sum_{j=1}^{N} \exp(i\mathbf{k} \cdot \mathbf{r}_j(t))$ is the Fourier transform of the one-particle density

$$\rho(\mathbf{r}, t) = \sum_{j=1}^{N} \delta(\mathbf{r} - \mathbf{r}_j(t)), \tag{4.4}$$

where $\mathbf{r}_j(t)$ is the position vector of particle j at time t, N is the number of particles and $S(k)$ the static structure factor (which we have obtained by RY).

In the fluid state the non-ergodicity parameter $f(k)$ is always zero, which results in remaining ergodicity. For arrested states, the non-ergodicity parameter has a finite value different from zero, meaning that particles are trapped in cages formed by their nearest neighbors and the system is arrested in a non-ergodic state [132].
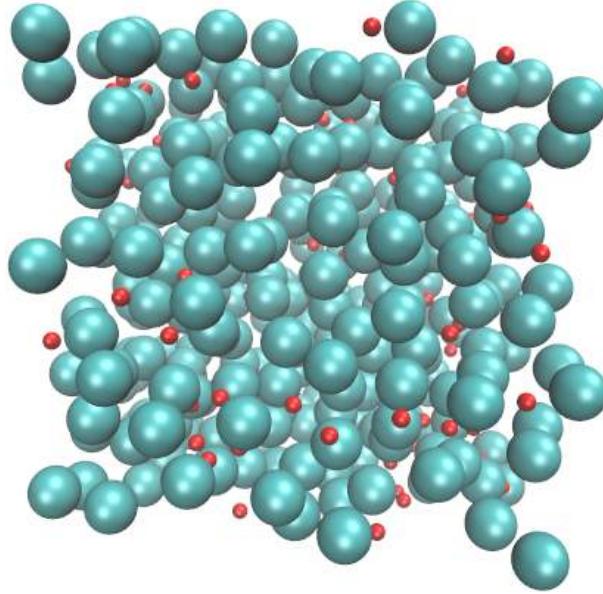
Figure 4.1: Simulation snapshot for a mixture consisting of stars (light blue) with functionality $f = 30$ and colloids (red). The size ratio is $q = 3$ and densities are $\rho_S \sigma_S^3 = 0.3$ and $\rho_C \sigma_S^3 = 0.1$.

4.2 Comparison of structure from theory and simulation

Using the two component Rogers-Young integral equation theory, one can obtain partial radial distribution functions and structure factors. The obtained data for $g(r)$ and $S(k)$ have been compared with the results from coarse-grained Monte Carlo simulations.

For the comparison of the theoretical calculations and simulations, we have concentrated on stars of functionality $f = 30$ and $f = 250$, representing relatively soft and hard star polymers. Typical simulation snapshots are shown for $f = 30$, $q = 3$, $\rho_S \sigma_S^3 = 0.3$ and $\rho_C \sigma_S^3 = 0.1$ in Fig. 4.1 and 4.2. These snapshots show, which advantages the coarse-grained Monte Carlo simulation has in comparison with a full-monomer simulation: Due to the theoretic coarse-graining, which we have presented in Chapter 2, each star is represented by a single sphere, so that a large number of star polymers in the mixture with colloids can be simulated.

Figures 4.3 and 4.4 show the partial radial distribution functions for stars with a relatively low functionality of $f = 30$, a size ratio $q = 3$, a star density of $\rho_S \sigma_S^3 = 0.3$ and an increasing colloid density from $\rho_C \sigma_S^3 = 0.1$ in Fig. 4.3 to $\rho_C \sigma_S^3 = 1$ in Fig. 4.4. In Figure 4.5 the functionality is increased to $f = 250$ and Figs. 4.8 - 4.10 show the corresponding partial structure factors.
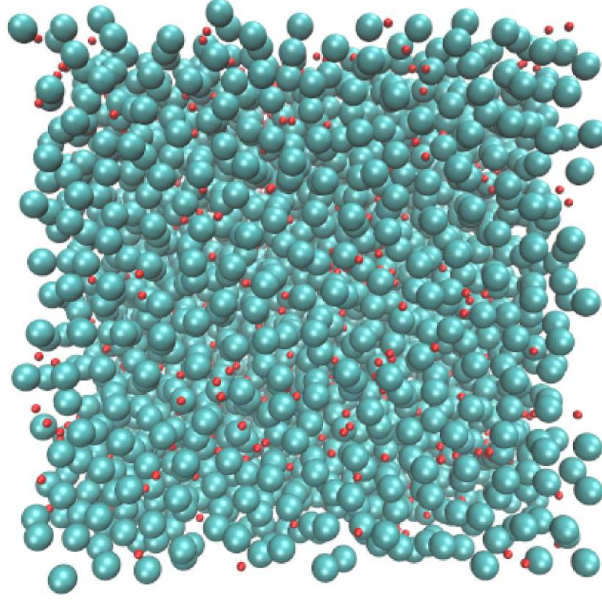
Figure 4.2: Simulation snapshot for a mixture consisting of colloids (red) and stars (light blue) with functionality $f = 250$, size ratio $q = 3$ and densities $\rho_S \sigma_S^3 = 0.3$ and $\rho_C \sigma_S^3 = 0.1$
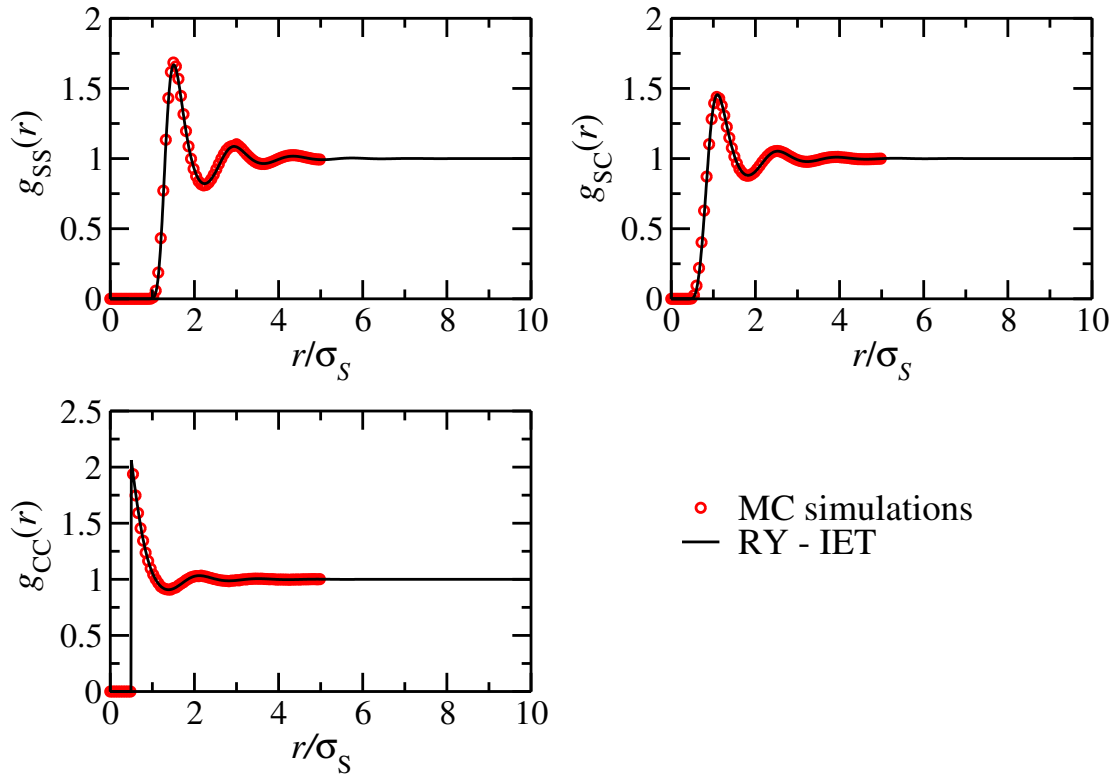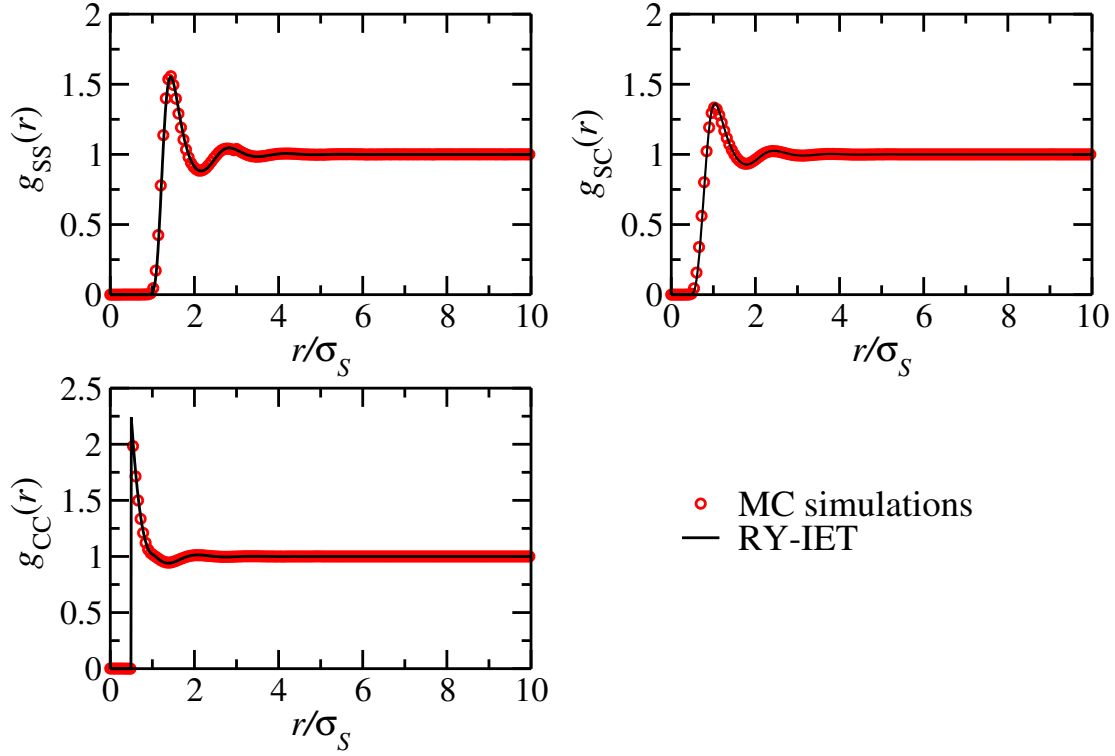

Figure 4.3: Partial radial distribution functions for a mixture consisting of stars with functionality $f = 30$, size ratio $q = 3$ and densities $\rho_S \sigma_S^3 = 0.3$ and $\rho_C \sigma_S^3 = 0.1$ from MC simulations (red circles) and RY integral equations (black lines). Note that due to a limited simulation box size of a length $L = 10\sigma_S$, only simulation data up to $L/2 = 5\sigma_S$ were obtained.
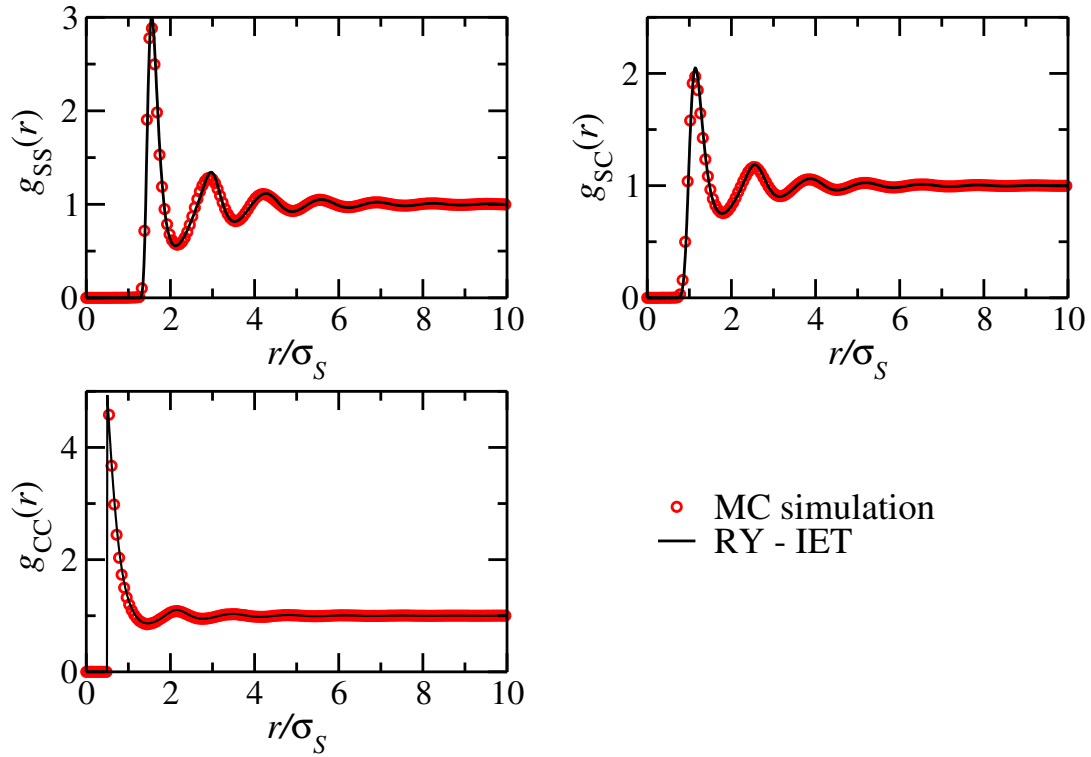
Figure 4.4: Partial radial distribution functions for a mixture consisting of stars with functionality $f = 30$, size ratio $q = 3$ and densities $\rho_S \sigma_S^3 = 0.3$ and $\rho_C \sigma_S^3 = 1.0$ from MC simulations (red circles) and RY integral equations (black lines).

Let us consider first an increase in the colloidal density ρ_C (4.3 and 4.4). While the height of the nearest neighbor peak for the star-star radial distribution function $g_{SS}(r)$ and for the mixed distribution function $g_{SC}(r)$ decrease for a larger amount of additives, the peak of $g_{CC}(r)$ slightly increases and gets more narrow. Although the effects are very small, it is a first hint, that the colloidal particles find space between the stars, meaning that the colloids come relatively close together (the first peak of $g_{CC}(r)$ gets more narrow) pushing the stars slightly further away from each other (less pronounced structure in the $g_{SS}(r)$). The effect is very small though, which can be explained by the softness of polymer stars with a functionality of $f = 30$: Even for higher colloidal densities, colloids find always a space between stars or between the arms of a star. The less pronounced structure in all three radial distribution functions, meaning, that the height of second- and third-neighbor peaks decrease, shows, that the two components mix well with each other.

The differences for all three partial distribution functions become much stronger, if instead f is increased (compare Fig. 4.3 with 4.5). Although the colloidal density is very

Figure 4.5: Partial radial distribution functions for a mixture consisting of stars with functionality $f = 250$, size ratio $q = 3$ and densities $\rho_S \sigma_S^3 = 0.3$ and $\rho_C \sigma_S^3 = 0.1$ from MC simulations (red circles) and RY integral equations (black lines).

small ($\rho_C \sigma_S^3 = 0.1$, where we measure ρ_C in units of the star diameter), the peaks are much more pronounced. Changing the functionality of the star results in a more stiff particle, which is less penetrable for colloidal additives and so their space is much more limited (see Fig. 4.6). Here, we have visualised how penetrable a star of small f is in comparison to a star with many arms. An increasing number of arms leads to a hard particle, in the limit of $f \to \infty$, it is a hard sphere-like particle, which is not penetrable. A star with less arms offers for the colloid more space (only the small inner circle marked by the dashed line is not penetrable for the colloids), leading to a easier mixing of stars and colloids.

The enormous increase for the nearest neighbor-peak both in $g_{SS}(r)$ and $g_{CC}(r)$ from Figure 4.3 to Fig. 4.5, which is provoked by the increase of f, shows that colloids and polymer stars tend to "cluster". The mixed partial radial distribution function $g_{SC}(r)$ increases as well, but less than $g_{SS}(r)$ and $g_{CC}(r)$. Still, the increase can be explained by looking at the dependence of the interaction potential $V_{SC}(r)$, which we visualize in Fig. 4.7. For smaller functionalities the effective pair interaction becomes more stiff. On the other hand, stars and colloids can approach each other much closer than for higher functionalities, since the colloids find space in the arms of the polymer stars. This confirms what we show in the schematic graphic 4.6. Higher functionalities force the colloids to stay out of the arms of the star, leading to some kind of "caging" effect, which at the end leads to a clustering of colloids (and makes a demixing more probable). All the observations in the radial distribution functions for increasing f give an idea, why for star polymers with less arms it is easier to add colloids without facing a phase separation.

Figures 4.8 and 4.9 show the partial static structure factors for a system of star polymers with $f = 30$, a star density of $\rho_S \sigma_S^3 = 0.3$ and a colloid density of $\rho_C \sigma_S^3 = 0.1$ and $\rho_C \sigma_S^3 = 1.0$, respectively, Fig. 4.10 the partial structure factors for $f = 250$, $\rho_S \sigma_S^3 = 0.3$ and $\rho_C \sigma_S^3 = 0.1$. All densities are in units of σ_S, the star polymer diameter.

The above mentioned observations in the radial distribution functions also hold for the reciprocal space. A very interesting first hint for phase separation is the colloid-colloid structure factor $S_{CC}(k)$ for $f = 250$ in Fig. 4.10, which strongly differs in its appearance for the $k \to 0$ limit from the two other examples. For $f = 250$, the structure factor develops a high peak for $k \to 0$. And indeed, for this case we have observed a phase separation for relatively low colloidal densities, which is visible in Fig. 4.12a. The increase of this peak for high functionalities and also for very high colloid densities in some cases of our studies, lead, if the peak is high enough, to a numeric breakdown of the integral equation theories. In our state diagrams (see Figs. 4.11a - 4.13c) we
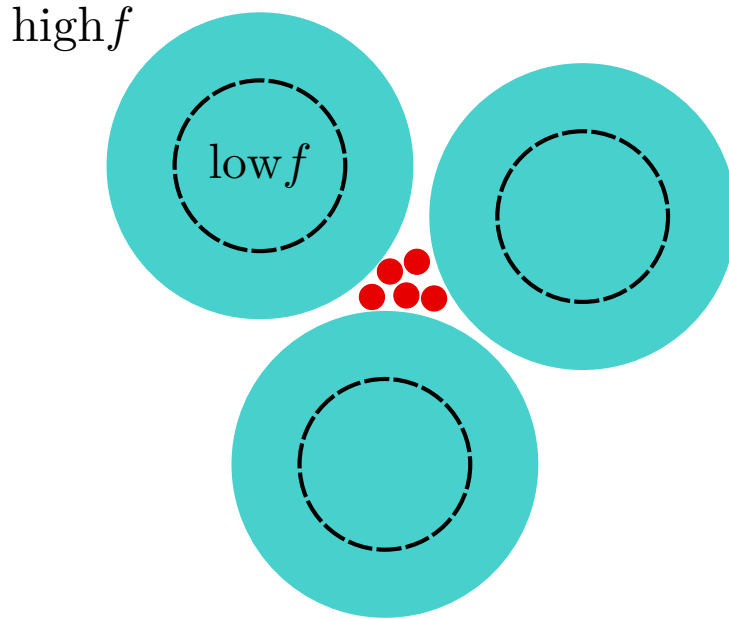
high f

low f

Figure 4.6: The small colloidal particles (red spheres) find easier free space, if the polymer star (turquoise spheres) has less arms (dashed lines), i.e. f is small. Less arms does not mean, that the star polymer is actually smaller in size, it just means, that the colloids can penetrate easier into the stars by finding space between the arms.

have visualised this effect with a green line and in a first approximation it represents the binodal demixing line. We have specified the binodal demixing lines for the system at hand in Chapter 5. The agreement between theoretical calculations coming from the inversion of the Ornstein-Zernike equation and the coarse-grained Monte Carlo Simulations, where the effective interactions presented in Chapter 2 have been employed, are excellent and therefore we use the partial structure factor of the star polymers $S_{SS}(k)$ in the following MCT calculations for $f \in \{214, 250, 300\}$.

4.3   Results and Discussion

The state diagrams were calculated in the following way: First, static structure factors had to be obtained by using two component Rogers Young integral equation theory (see e.g. Appendix A), yielding partial radial distribution functions and static structure factors for different star polymer densities, first for a pure star polymer system. Then the star-star structure factor $S_{SS}(k)$ was used in the one-component Mode Coupling Theory (see e.g. Appendix B) to calculate the non-ergodicity factor $f(k)$. If a solution $f(k) \neq 0$ was found, so that the system is non-ergodic, we identified this state to be glassy. This way, the onset of structural arrest for pure stars was determined at a density $\rho_S(f)$.
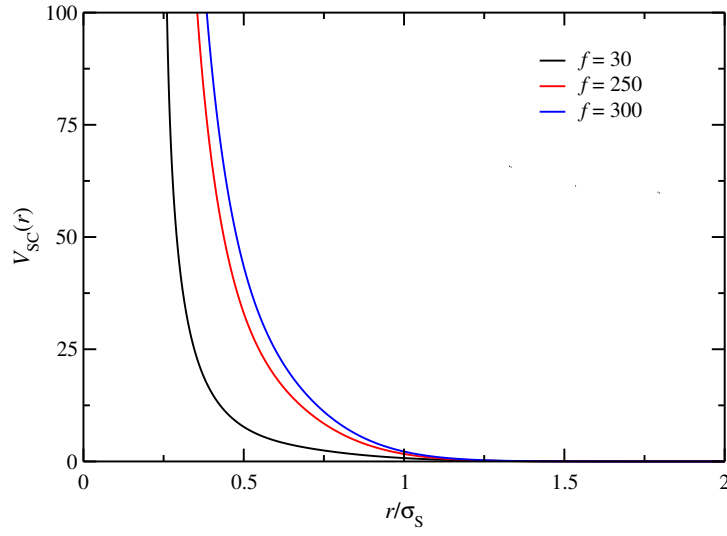
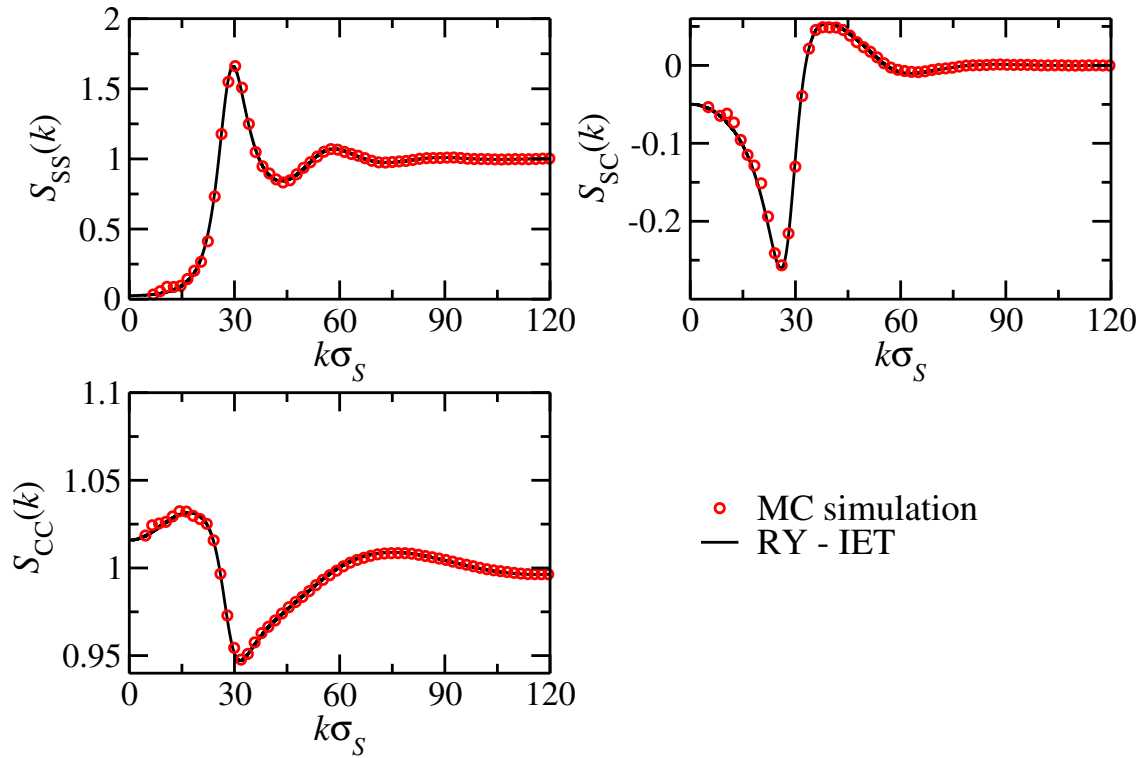Figure 4.7: The effective star-colloid potential for $q = 3$.

Figure 4.8: Partial structure factors for a mixture consisting of stars with $f = 30$, $q = 3$ and densities $\rho_S \sigma_S^3 = 0.3$ and $\rho_C \sigma_S^3 = 0.1$ from MC simulations (red circles) and RY integral equations (black lines).
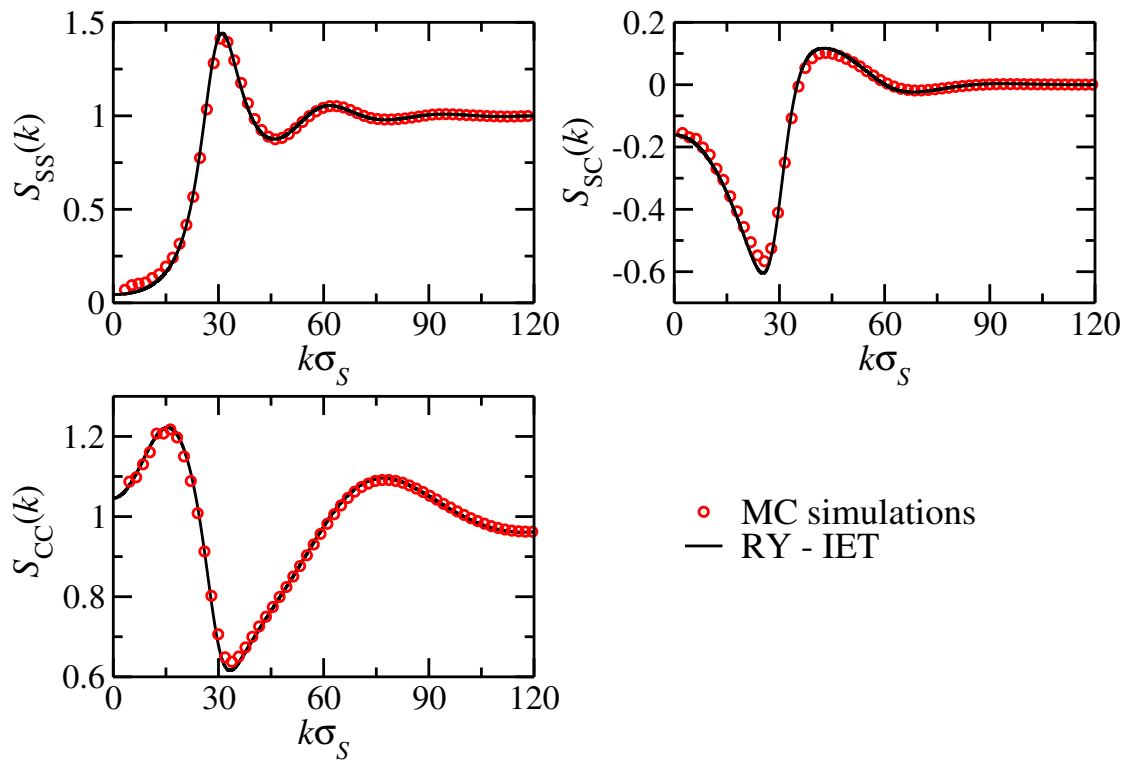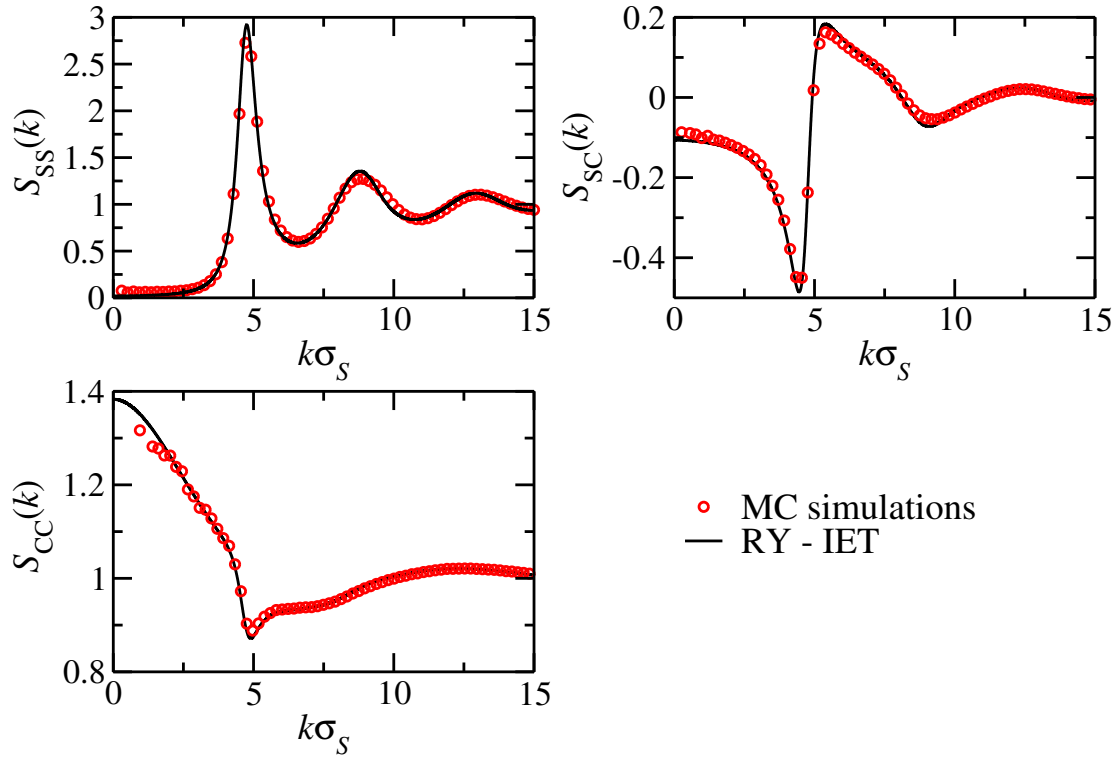
Figure 4.9: Partial structure factors for a mixture consisting of stars with $f = 30$, $q = 3$ and densities $\rho_S \sigma_S^3 = 0.3$ and $\rho_C \sigma_S^3 = 1.0$ from MC simulations (red circles) and RY integral equations.

Figure 4.10: Partial structure factors for a mixture consisting of stars with $f = 250$, $q = 3$ and densities $\rho_S \sigma_S^3 = 0.3$ and $\rho_C \sigma_S^3 = 0.1$ from MC simulations (red circles) and RY integral equations. (black lines)

The colloid density ρ_C was increased and the static structure factors were calculated and the $f(k)$ obtained. For star densities, which were identified as glassy in a pure star polymer system, it is interesting to check if there still exists a solution $f(k) \neq 0$ (so that it is still non-ergodic), or if the star polymer glass has melted. This procedure was repeated for a broad range of colloid densities.

From a certain ρ_C, no convergence in the integral equation routine could be achieved, due to the fact, that for $k = 0$ in the structure factors develop very high peaks (cf. Fig. 4.10). On the spinodal, the $S(k)$ is known to diverge and here we encounter the numerical problems of this phenomenon. The line where this effect happens is a first guess of where the demixing line of the system is. Its location is very similar to the "real" binodal, which we have calculated in the next chapter via a perturbation theoretical approach (Chapter 5).

Figures 4.11a - 4.11d show the states of the binary colloid-polymer mixtures for different densities ρ_S and ρ_C in units of σ_S^3. In Figures 4.11a - 4.11c it is visible, how for a star of $f = 214$ arms the addition of hard, spherical particles leads to a melting of the glassy state. The region where the glassy states can be melted by the addition of colloids is mostly pronounced for size ratios $q = 3$ and $q = 4$. The smaller the additives, i.e. the higher q, the more the concentration of colloids $\rho_C \sigma_S^3$ can be increased, before an effect becomes visible (see Figs. 4.11a - 4.11d). If the colloidal densities get very high, one might get into the region, where the integral equation routines fail to converge. This region we have identified with an arrested phase separation, an assumption that is supported by experimental results [43].
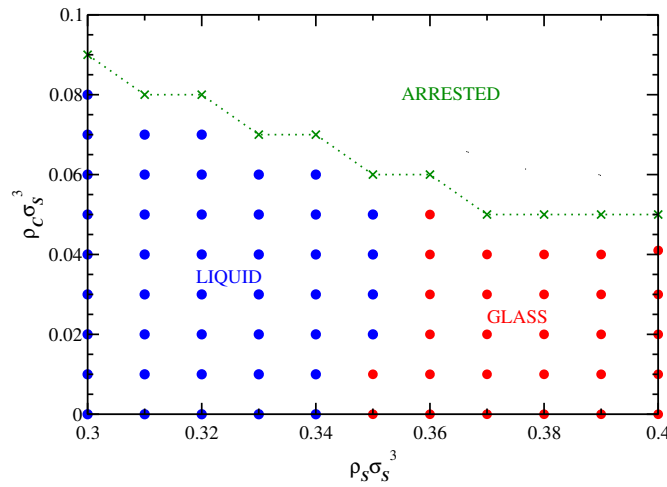
(a) $f = 214$, $q = 2$

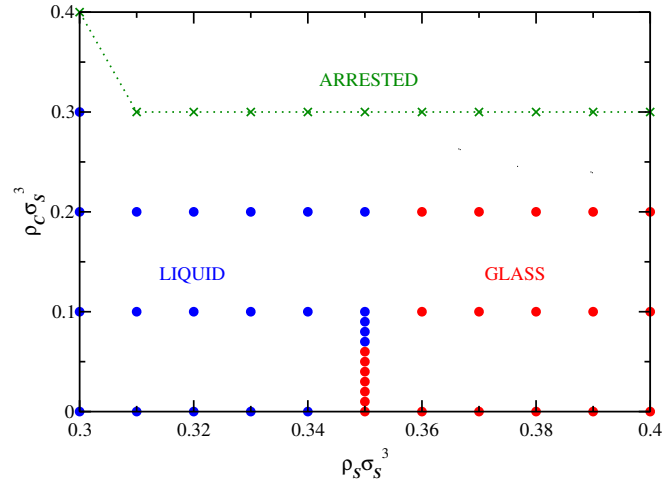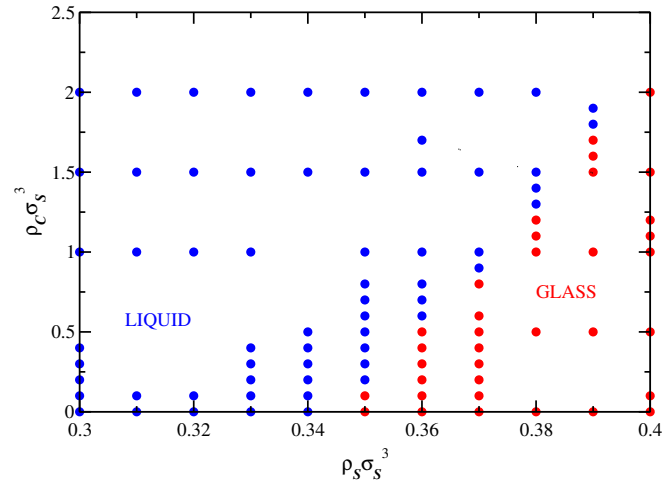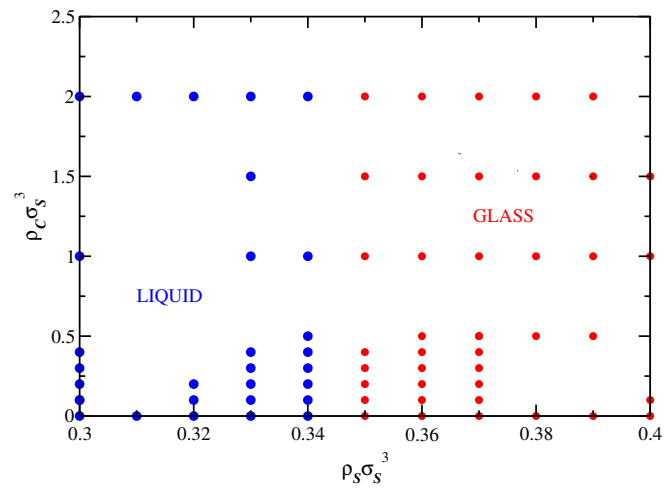Figure 4.11: State diagram for functionality $f = 214$ and size ratio $q = 2$
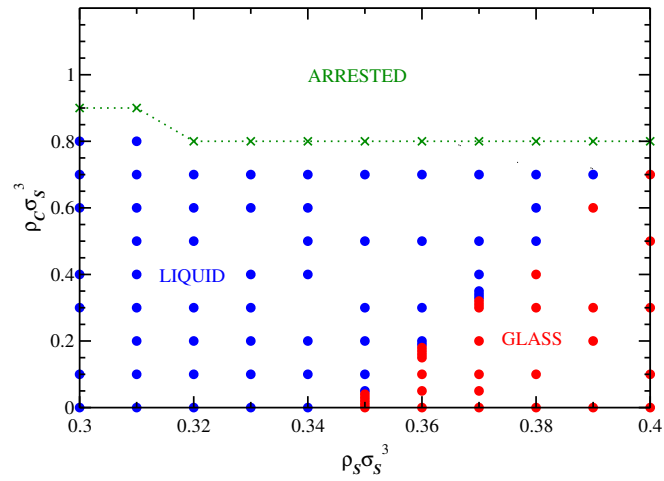
(b) $f = 214$, $q = 3$
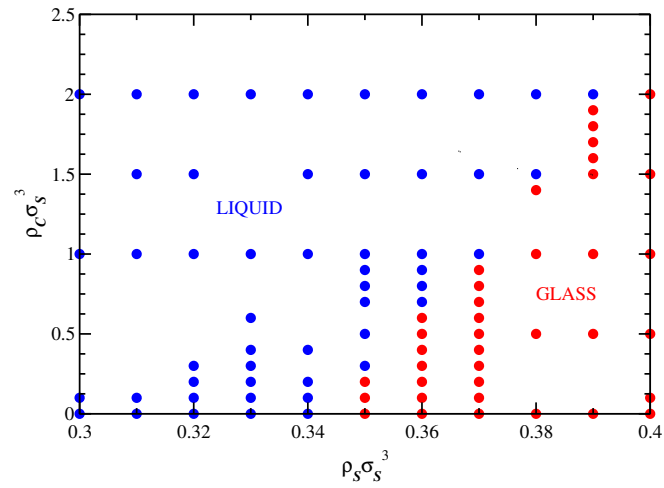
(c) $f = 214$, $q = 4$
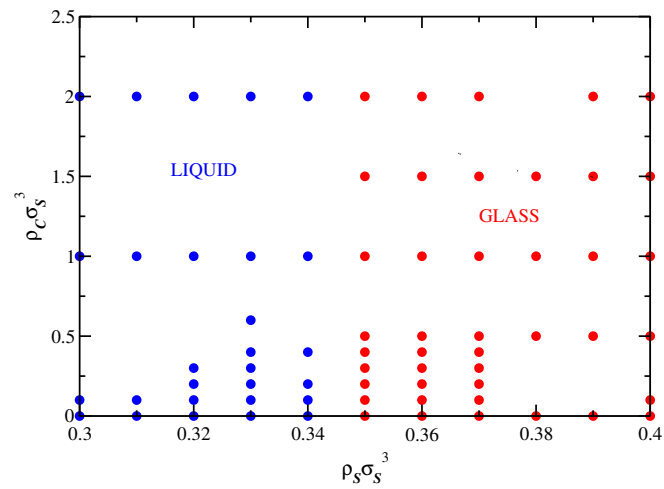
(d) $f = 214$, $q = 8$

Figure 4.11: State diagrams for functionality $f = 214$ and size ratios $q = 3, 4, 8$

For even high densities of $\rho_C \sigma_S^3 = 2.0$ the mixture of $f = 214$ stars (Figs. 4.11c and 4.11d) remained still stable for $q = 4$ and $q = 8$ and did not show any demixing effect, with one difference between the two systems: For $q = 4$ a melting of the glass is visible for high colloid concentrations, while for $q = 8$ (see Fig. 4.11d) we could not obtain any change in the states, which leads to the conclusion that such mixtures of big star polymers and very small, hard additives form a stable binary nanocomposite.

For the second system of $f = 250$ Figures 4.12a - 4.12c give a similar picture, with one major difference: The density range of ρ_C is much lower than for a star system with $f = 214$, which can be explained by the number of arms of the polymers. If the particle is soft, i.e. f is small, it is easier for the colloidal particles to penetrate the star, which is in agreement with our previous observation of the non-additivity parameter [2]. It can be spotted that, the smaller f, the more the colloid density ρ_C can be increased before the integral equation routine fails to converge. Also the amount of colloids that can be added, before the glass of polymers, which was obtained for a pure system, melts. Compare, for example Figures 4.11b, 4.12a and 4.13a, where, for the same size ratio $q = 3$ the demixing line occurs for lower densities, if f is increased. Also the region, in which just an addition of colloids leads to a melting of the polymer glass becomes more narrow. This effect stems from the amount of arms of the polymer stars: the more arms a star has, the more difficult it is for a polymer to go in between those arms. The space the colloids can occupy therefore gets smaller, the higher the number of arms of the stars is. This is also visible from the effective interaction potential between the star polymers and colloids $V_{SC}(r)$ in Fig. 4.7. A star of $f = 30$ arms is much easier to penetrate than a star with $f = 300$. This again reinforces our predictions from calculating the non-additivity parameter in Ref. [2] (see Chapter 2).

The second effect comes from the size ratio q. The smaller a colloid is (q big), the easier it is for a colloidal particle to find a space in between the star polymer arms, so that at the end there is no effect visible. This is also supported by the mixed partial radial distribution function $g_{SC}(r)$ for a fixed functionality f (see Fig. 4.14): The increase in height of the nearest neighbor peak for decreasing size ratios is enormous, showing the strong effect of q in the mixture. The peak also moves to higher values of the distance r: Small colloids will just penetrate into the stars and the mixture will be well-mixed and no phase separation can be observed.

In our system, the size ratios of $q = 3$ and $q = 4$ are the interesting ones, where a star polymer glass can be melted by increasing the amount of colloidal particles in the mixture. If the hard spheres are big enough, a phase separation can be observed even for a small amount of colloidal additives. Also this can be explained by imagining a big, colloidal

(a) $f = 250$, $q = 3$

(b) $f = 250$, $q = 4$

(c) $f = 250$, $q = 8$

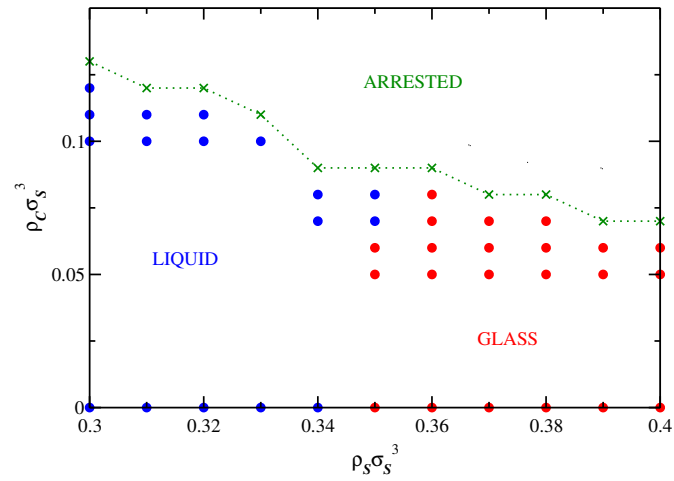Figure 4.12: State diagrams for functionality $f = 250$ and size ratios $q = 3, 4, 8$
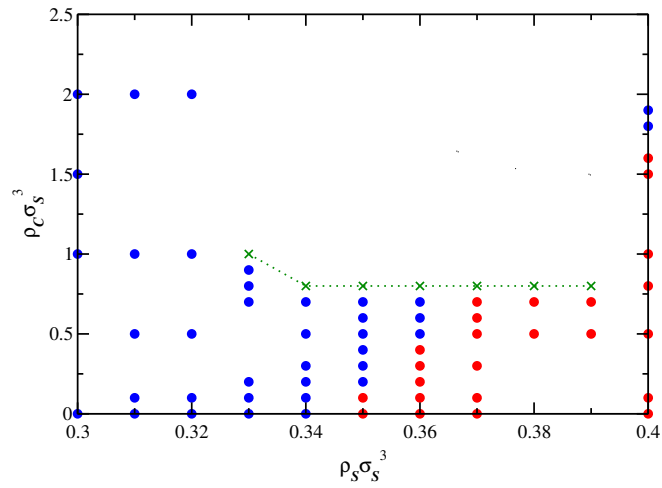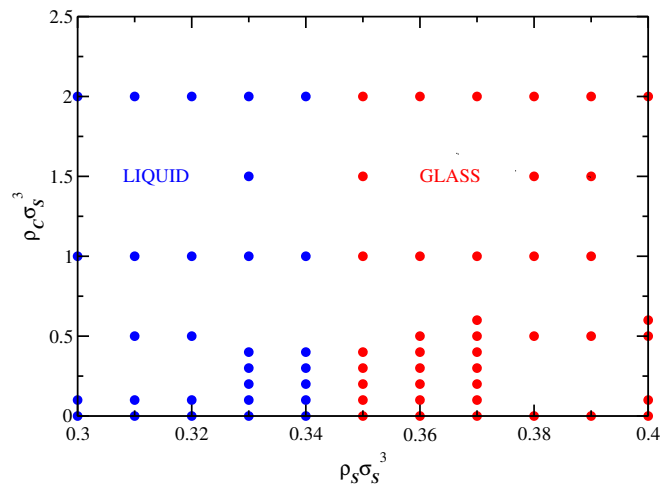
(a) $f = 300$, $q = 3$

(b) $f = 300$, $q = 4$

(c) $f = 300$, $q = 8$

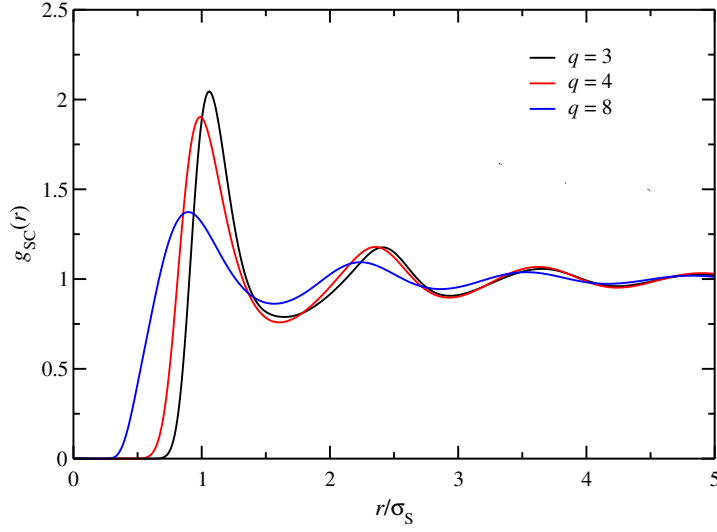Figure 4.13: State diagrams for functionality $f = 300$ and size ratios $q = 3, 4, 8$

Figure 4.14: Comparison for the partial star-colloid radial distribution function with parameters $f = 214$, $\rho_S \sigma_S^3 = 0.34$, $\rho_C \sigma_S^3 = 0.4$ and varying q.

sphere trying to find a space between the arms of a polymer star - here also again the number of arms f of the stars play an important role. These effects are the reason, why we can show a state diagram for $q = 2$ only for the case of a functionality $f = 214$. In all other cases, the system demixes immediately, when colloidal particles are added. The demixing line is in agreement with earlier results that were predicting the demixing/mixing in a "state diagram" in the functionality-size ratio plane [2]: The prediction shows that for very high q the star-colloid mixture is expected to be stable for even high concentrations of hard colloids, which is in agreement with our results for $q = 8$. For $q \gtrsim 1$, we are very clearly in the demixing regime, which explains the immediate macrophase separation for $q = 2$ and high functionalities.

4.4 Conclusions and Outlook

The results obtained with the help of Rogers Young integral equations and the non-ergodicity factor of the one-component MCT have shown the strong influence of the size ratio q on binary colloid-polymer mixtures. While very small colloidal additives tend not to affect the glassy behavior of a certain polymer star glass, some mid-sized colloids are able to weaken the attractions between the polymer stars and cause a melting of the glass. Colloidal particles that are even bigger ($q = 2$ and $q = 3$) tend to force the system into a phase separation, which can be seen in the presented phase diagrams (see Figs. 4.11a, 4.11b, 4.12a, 4.13a and 4.13b).

The second parameter that was investigated is the functionality f of the polymeric stars, showing that for smaller f, it is possible to add much more colloidal particles before either a melting of the glass or a demixing occurs. We explain this effect by the softness of the star and the possibility for small additives to penetrate it. Smaller stars seem to build very stable mixtures, that can be tuned by adjusting the amount and the size ratio of the colloidal additive, leading to a glass softening and melting.

One possible outlook is the comparison with experiments. While a first comparison for one specific parameter choice of $f = 214$ and $q = 3$ [43] has shown very promising results, it will be interesting to consider different parameter combinations. The results that mostly show interesting effects for intermediate size ratios of $q = 3, 4$, where either a polymer glass melting and/or a phase separation can be observed, can guide the parameter search in experiments to which combinations are promising for further research.

The results are motivating to investigate depletion potentials and classify the effect of short range attractions in the binary mixture, which will help to understand the equilibrium and flow behavior of a wide range of mixtures consisting of soft and hard spheres. The calculation of the *exact* binodal line is a topic of further research. The presented line here is a first approach, that already gives a good estimation, where the binary mixture tends to demix. The presented results are very promising for offering mixtures that are very easy to be tuned by just changing the size ratio or the amount of colloidal additives inside which is an interesting starting point for further research.

Chapter 5

Depletion interactions in binary polymer star - colloid mixtures

One characteristic feature of soft matter systems is the possibility of tuning the interactions between the components from short-range repulsions to long-range attractions, which leads to a wide spectrum of phases and interesting observations. Usually these interparticle interactions are effective interactions from coarse-grained approaches [5], for example the introduction of the depletion potential by Asakura and Oosawa [20], in which the size ratio and polymer concentration can be used to tune the range and strength of the interaction. These one-component depletion picture has been helpful in understanding the equilibrium phase behavior of polymer-colloid mixtures [42] and still serves as a guide for developing new models.

Depletion interactions have a long history of extensive investigations, starting from colloid-colloid systems [87, 111, 133–141] over colloid-polymer mixtures [38, 46, 142–150] and the of colloids interaction with walls [151–157]. While in these studies there has been a focus on hard colloidal particles, the research moved on to non-hard-sphere-colloids [158, 159], and anisotropy [160, 161]. Our model system combines small hard and big soft colloids, namely star polymers, in a binary mixture.

Star polymers are a valuable model system for studying soft matter, since their softness can easily be tuned by changes in the functionality f, i.e. the number of arms of the star polymer, and so they are an ideal combination of polymeric and colloidal characteristics [95]. Star polymers have been employed to study glass transitions and have shown multiple glassy states and the effect of star polymer glass melting as a depletion mechanism induced by colloidal additives [41, 43, 76, 98]. They were used to describe the formation of star clusters due to osmotic forces and provide explanations for a wide range of soft particle mixtures. The depletion mechanism used in the study of particles that interact via soft potentials can also explain the disordering of ordered microstructures [162] and

quantify how short range attractions act on soft particles [143, 163].

In this Chapter, our strategy is to trace out most parameters of freedom and capture all effects in the depletion interaction, as it was shown many times in previous work on different systems [5, 21, 42, 46, 51]. The small colloidal additives induce a depletion interaction on the stars, stemming from the repulsion between the two species In what follows, f is the star polymer functionality and $q = R_{g,S}/R_C$ the size ratio between star polymers and hard colloids, where $R_{g,S}$ is the radius of gyration of the star polymers and R_C the hard sphere radius of the colloids. Increasing the amount of additives therefore leads to an overlap of two soft depletion regions and an effective interaction is induced.

We use coarse-grained effective interactions (star-star, star-colloid and colloid-colloid) as an input for an integral equation theory with the help of the Rogers-Young closure and calculate structural information of the binary system which is then used to calculate a depletion potential, the colloid-modified star-star potential and with the help of this, finally the binodal lines for completing a recently investigated phase diagram for the mixture [43].

5.1   The coarse-grained model system

In this Chapter we employ the previously-developed coarse-grained description of the star-polymer mixture, which was recently developed by calculating the effective interaction potential $V_{SC}(r)$ between star polymers and colloids in good solvent conditions [2]. The star-star effective interaction $V_{SS}(r)$ of Ref. [32] was used. It features a crossover from a Yukawa to a logarithmic behavior as the star-star separation diminishes. Finally, the colloid-colloid interaction $V_{CC}(r)$ was modeled by the simple hard sphere interaction.

Fig. 5.1 shows examples for the effective interactions. The red and violet curves show the effective star-star potential and it is clearly visible, how the potential becomes more steep and tends towards a hard sphere potential for higher functionalities f. The more arms a star has, the less interpenetrable it becomes for the colloidal additives, an observation that at the end leads for high f to a phase separation already for small amounts of colloidal additives, which we have found in earlier work (Chapter 4). From

$$q = \frac{R_{g,S}}{R_C} \tag{5.1}$$

and

$$R_{g,S} = \frac{3}{4}\sigma_S \tag{5.2}$$

one can see that, as expected, the hard sphere potential (black lines) shows a divergence at the colloid diameter σ_C. The recently introduced [2] star-colloid interaction (blue and
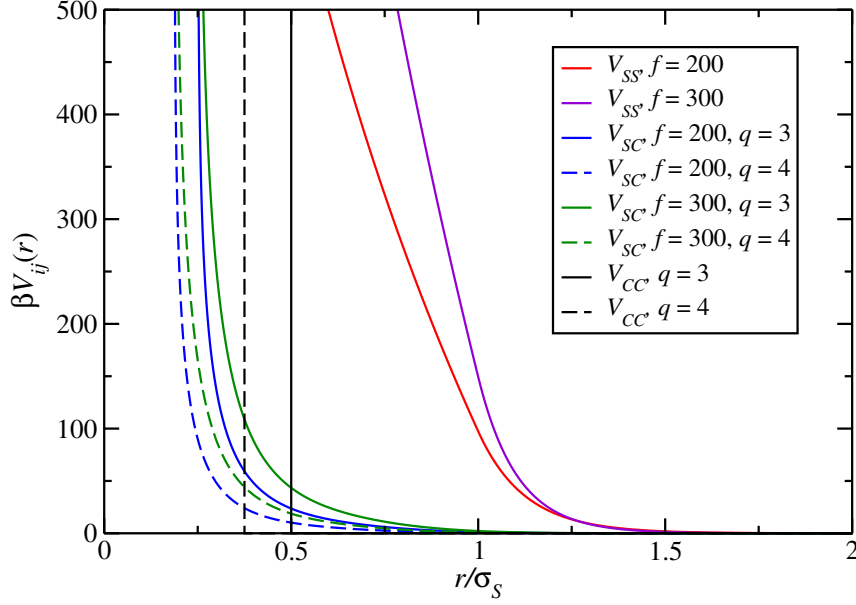
Figure 5.1: Examples for effective star-star (SS), star-colloid (SC) and colloid-colloid (CC) interactions V_{ij} for star functionalities $f = 200, 300$ and size ratios $q = \frac{R_{g,S}}{R_C} = 3, 4$.

green curves) diverges at R_S. For higher q, it also tends to look more and more similar to a hard sphere potential and diverges for higher q at smaller distances r, meaning, that small colloids can penetrate the star much more than bigger particles.

These interactions are now the input to solve the two-component Ornstein-Zernike Equation (OZ) with the help of the Rogers-Young closure (RY), which reads in Fourier space:

$$\hat{\mathbf{H}}(k) = \hat{\mathbf{C}}(k) + \hat{\mathbf{C}}(k) \cdot \hat{\mathbf{D}} \cdot \hat{\mathbf{H}}(k), \tag{5.3}$$

with $\left[\hat{\mathbf{H}}(k)\right]_{ij} = \hat{h}_{ij}(k)$ being a matrix consisting if the pair correlation function in Fourier space, $\left[\hat{\mathbf{C}}(k)\right]_{ij} = \hat{c}_{ij}(k)$ with the Fourier transformed direct correlation function as matrix elements and $\left[\hat{\mathbf{D}}\right]_{ij} = \rho_i \delta_{ij}$. $i, j = C, S$ are the colloids or polymer stars, respectively.

For a solution of Eq. (5.3) it is necessary to make use of additional closure relations. In this work, we have chosen the two-component Rogers-Young (RY) closure, which is known to give thermodynamically consistent results for mixtures of star polymers and hard colloidal particles [72], which represents exactly the situation we are dealing with.

The RY closure relation is given by

$$g_{ij}(r) = \exp[-\beta V_{ij}(r)] \left(1 + \frac{\exp[f(r)(h_{ij}(r) - c_{ij}(r))] - 1}{f(r)}\right), \qquad (5.4)$$

where $g_{ij}(r) = h_{ij}(r) + 1$ is the radial distribution function for pairs $i, j = S, C$ for stars and colloids, respectively and $V_{ij}(r)$ the pair interaction potential, as mentioned above. The tuning of the parameter α in the mixing function $f(r) = 1 - \exp[-\alpha r]$ enforces thermodynamic consistency of the compressibility and virial route [164].

In this paragraph we repeat for convenience some important results of the last chapter (see partial structure factors in Chapter 5), showing again the good agreement of theoretical considerations and simulations: With the help of the Rogers-Young integral equation routine (see Appendix A), we have calculated radial pair distribution functions $g_{ij}(r)$ and static structure factors $S_{ij}(k) = \delta_{ij} + \sqrt{\rho_i \rho_j} \hat{h}_{ij}(k)$ for various functionalities f, size ratios q and densities ρ_C and ρ_S, and have compared the results to those from Monte Carlo simulations to prove their validity (see Figs. 5.2 and 5.3). Note, that all densities $\rho_C \sigma_S^3$ and $\rho_S \sigma_S^3$ are, as all quantities, expressed in units of σ_S.

The comparison of the theoretical Rogers-Young integral equation theory calculations and the coarse-grained Monte-Carlo simulations, where the effective interactions mentioned in [2] have been employed, shows the good agreement both for the partial radial distribution functions (Fig. 5.2) as well as the static structure factors (Figs. 5.3). In Chapter 4 we have presented this comparison for several parameters, showing an excellent agreement for the radial distribution functions and structure factors over a wide range of parameter choices of f and q.

5.2   The depletion interaction

The total colloid-modified effective star-star interaction is given by the relation:

$$V_{\text{tot}}(r) = V_{SS}(r) + V_{\text{depl}}(r), \qquad (5.5)$$

where $V_{SS}(r)$ is the interaction potential without any colloidal additive. Since Equation (5.5) is defined for the limit $\rho_S \to 0$, it holds:

$$V_{\text{tot}}(r) = -k_{\text{B}}T \ln g_{SS}(r; \rho_C^r) \text{ and} \qquad (5.6)$$

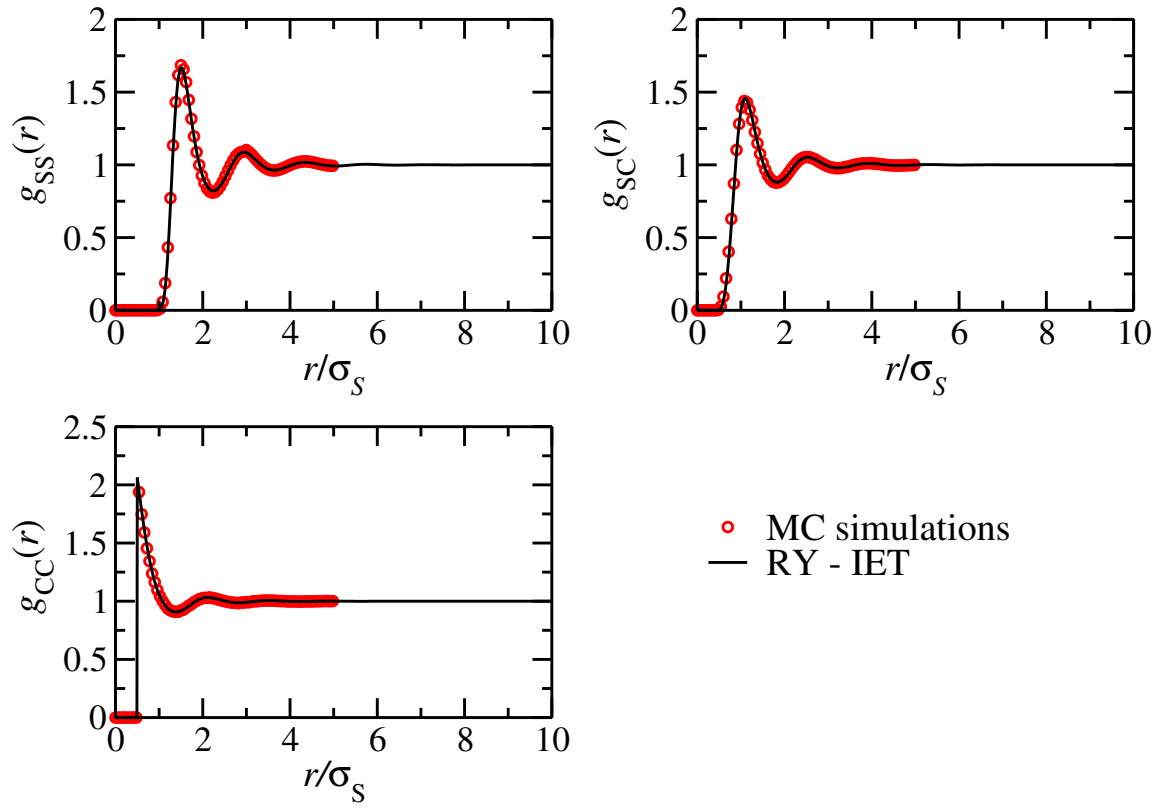$$V_{SS}(r) = -k_{\text{B}}T \ln g_{SS}(r; 0). \qquad (5.7)$$

Figure 5.2: Radial distribution functions from the inversion of the Ornstein Zernike equation (Rogers Young integral equations RY-IET) and from Monte Carlo simulations (MC) $f = 30$, $q = \frac{R_{g,S}}{R_C} = 3$, $\rho_S \sigma_S^3 = 0.3$, $\rho_C \sigma_S^3 = 0.1$.
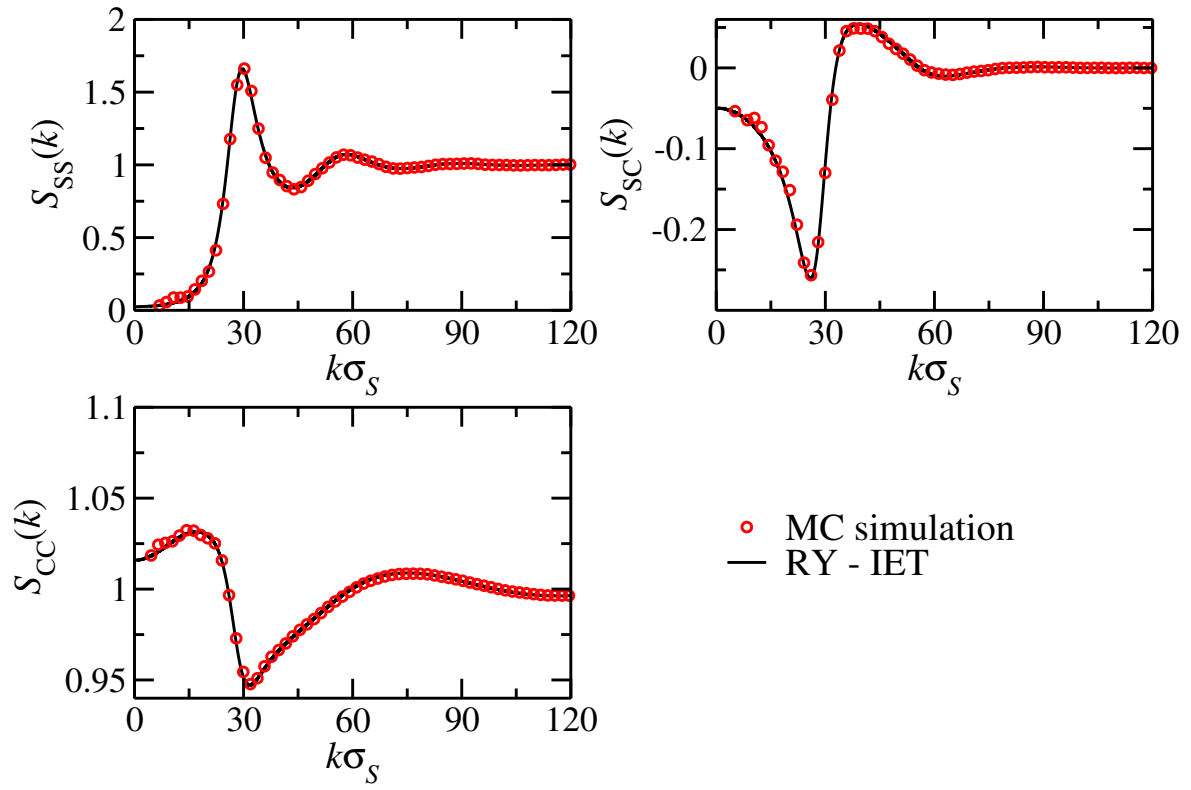
Figure 5.3: Static structure factors from the inversion of the Ornstein Zernike equation (Rogers Young integral equations RY-IET) and from Monte Carlo simulations (MC) $f = 30$, $q = \frac{R_{g,S}}{R_C} = 3$, $\rho_S \sigma_S^3 = 0.3$, $\rho_C \sigma_S^3 = 0.1$.

With this relations, the depletion potential can be calculated from structural data as:

$$V_{\mathrm{tot}}(r) - V_{SS}(r) = V_{\mathrm{depl}}(r) = -k_{\mathrm{B}}T \ln \left[\frac{g_{SS}(r; f, q, \rho_S \to 0, \rho_C^r)}{g_{SS}(r; f, q, \rho_S \to 0, 0)} \right]. \qquad (5.8)$$

$V_{\mathrm{depl}}(r)$ is determined at fixed chemical potential of the colloidal additives, meaning, that ρ_C^r in equations (5.6, 5.8) is the reservoir density of the colloids in contrast to the colloids density ρ_C, i.e. the density of colloids inside the system.

Figs. 5.4a - 5.4d show the results for the depletion interaction for different f, $q = R_{g,S}/R_C$ and ρ_C^r. The depletion effect is stronger for increasing colloid density, for bigger colloid sizes (i.e., decreasing q) and increasing functionality f of the stars. Decreasing the size ratio q from 4 to 3 leads to an increase of the depletion potential by roughly a factor of two. The effect of f is also clearly visible. Of course, the strongest effect is coming from increasing the colloid density. The higher the density the more difficult it becomes for the colloidal particles to find a free space and by that the osmotic pressure of the colloids is growing, leading to an increasing attraction of the polymer stars. Since we have to divide two radial distribution functions that are zero for small distances and take the logarithm, it causes numeric problems and becomes unpractical, leading to the incomplete appearance of the depletion interaction curves for small values of r.

The depletion potential can be fitted with polynomials of high order, but we found this approach to be physically meaningless. Interesting is that the depletion interaction at small distances r seems almost to be linear. The next paragraph, that presents another method for calculating the depletion interaction, does not suffer from this numeric limitation for small r.

5.2.1 Superposition approximation

To provide an independent check of the preceding results of the depletion interaction we have used the superposition approximation (SA) as a second method to calculate the depletion interaction [165]. A detailed explanation can be found in [73], where our scenario is just reversed and two colloids are depleted by the presence of polymers.

We are looking at the following picture depicted in Fig. 5.5: Two polymer stars of functionality f are at a distance R_{12} from each other. In the superposition approximation method the density of the surrounding colloids $\rho_C(\mathbf{r}_1; \mathbf{R}_1, \mathbf{R}_2)$, where $\mathbf{R}_1, \mathbf{R}_2$ are the fixed positions of the two star polymers, is replaced by the product of the two radial distribution functions of the colloids in the presence of an isolated star times the bulk colloid density:

$$\rho_C(\mathbf{r_1}; \mathbf{R}_1, \mathbf{R}_2) \approx \rho_C^r g_{SC}(|\mathbf{r}_1|) g_{SC}(|\mathbf{r}_1 - \mathbf{R}_{12}|), \qquad (5.9)$$
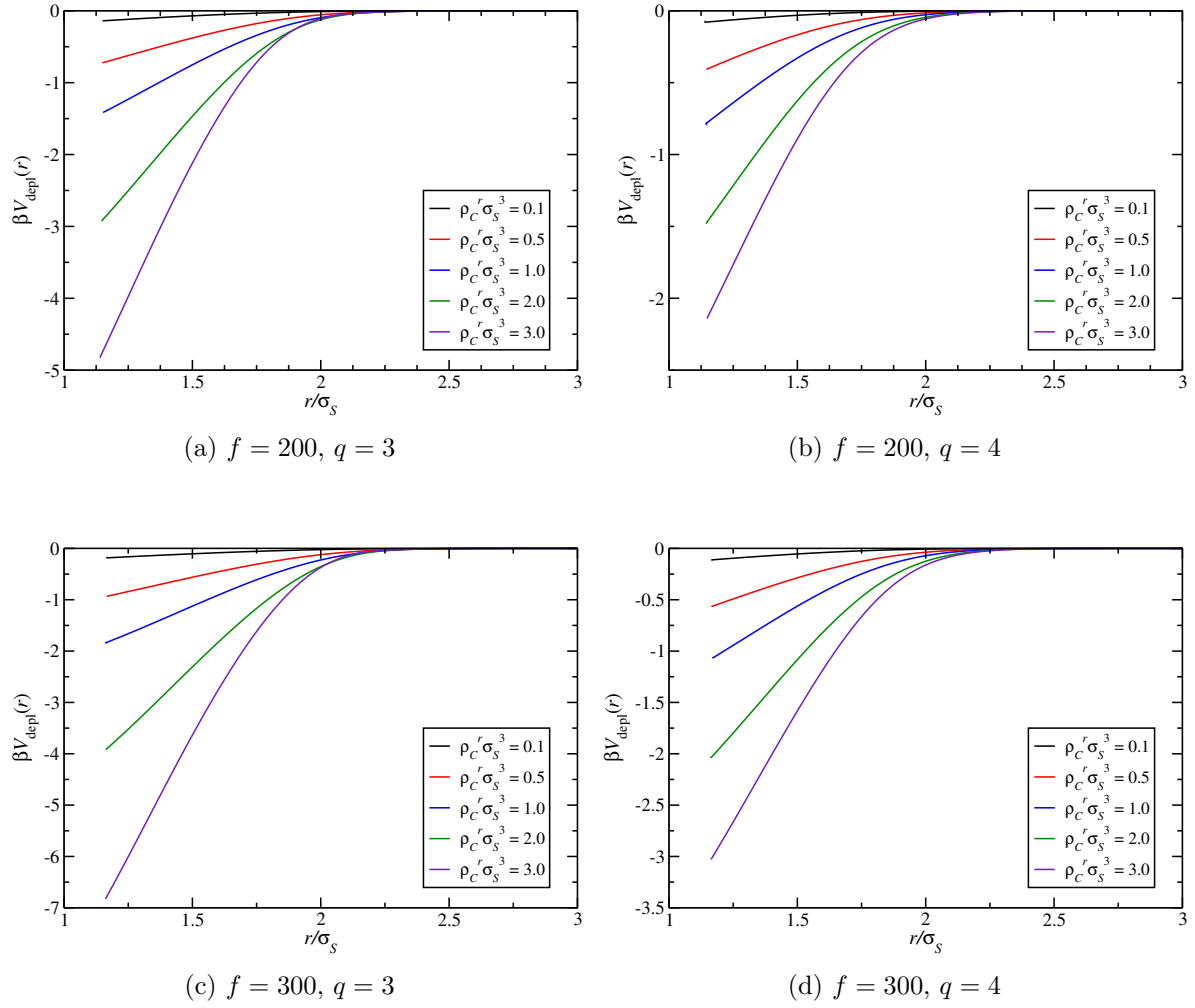
(a) $f = 200$, $q = 3$

(b) $f = 200$, $q = 4$

(c) $f = 300$, $q = 3$

(d) $f = 300$, $q = 4$

Figure 5.4: Depletion interactions for various functionalities f, size ratios q and reservoir colloid densities ρ_C^r.
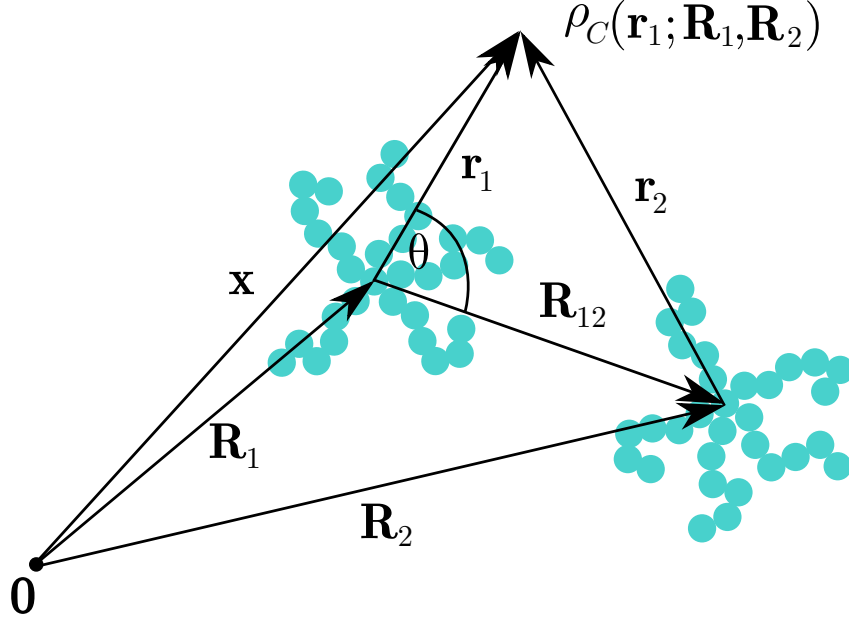
Figure 5.5: Superposition approximation method

where $\mathbf{R}_1, \mathbf{R}_2, \mathbf{R}_{12} = \mathbf{R}_2 - \mathbf{R}_1$ are the positions of the two star polymers and $\rho_C^r = 6\eta_C^r/(\pi\sigma_C^3)$ is the reservoir bulk density.

The radial distribution functions come out as a side product from solving the Ornstein Zernike equation and the depletion force can be calculated. Let us consider the depletion force acting on star one:

$$F_{\text{depl}}^{(1)}(R_{12}) = \int \left(-\frac{\mathrm{d}V_{SC}(r_1)}{\mathrm{d}r_1}\right) \underbrace{\hat{r}_1 \cdot \hat{R}_{12}}_{\cos\theta} \rho_C^{(2)}(r_1;\theta, R_{12})\mathrm{d}^3r_1. \tag{5.10}$$

Due to symmetry all components vanish, except the R_{12} component. Since there is no ϕ-dependence, we get:

$$\begin{aligned} F_{\text{depl}}^{(1)}(R_{12}) &= -2\pi\rho_C^r \int_0^\infty \frac{\mathrm{d}V_{SC}(r_1)}{\mathrm{d}r_1}r_1^2\mathrm{d}r_1 \int_0^\pi \sin\theta\mathrm{d}\theta g_{SC}(r_1)g_{SC}(r_1,\theta, R_{12}) \cdot \cos\theta \\ &= -2\pi\rho_C^r \int_0^\infty \frac{\mathrm{d}V_{SC}(r_1)}{\mathrm{d}r_1}r_1^2\mathrm{d}r_1 \\ &\quad \times \int_{-1}^1 g_{SC}(r_1)g_{SC}\left(\sqrt{r_1^2 + R_{12}^2 - 2r_1 R_{12}\cos\theta}\right)\cos\theta\mathrm{d}\cos\theta. \end{aligned} \tag{5.11}$$

Finally, by setting $\cos\theta \equiv \omega$ and $\mathbf{R}_{12} \equiv \mathbf{r}$, we have derived the explicit equation for the depletion interaction, acting on one polymer star in distance $\mathbf{r}$ from another star polymer:

$$F_{\text{depl}}(r) = -2\pi\rho_C^r \int_0^\infty r_1^2 g_{SC}(r_1)\mathrm{d}r_1 \int_{-1}^1 g_{SC}(\sqrt{r_1^2 + r^2 - 2r_1 r\omega})\omega\mathrm{d}\omega. \tag{5.12}$$

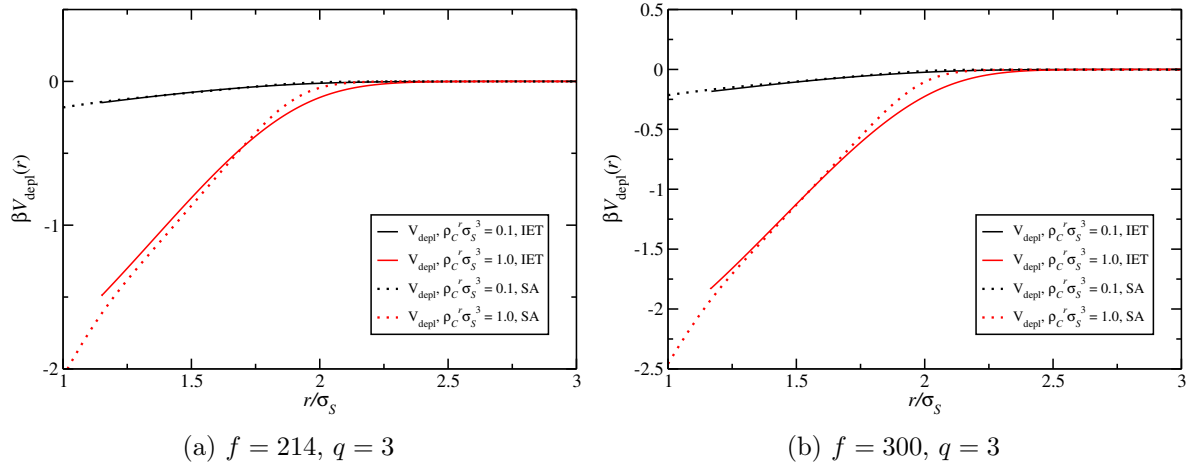(a) $f = 214$, $q = 3$ (b) $f = 300$, $q = 3$

Figure 5.6: Depletion interaction calculated with the two-component Rogers-Young closure (IET) and the superposition approximation (SA) for $q = 3$ and $f = 214, 300$.

In figures 5.6a and 5.6b we show the results of our calculations for the Ornstein-Zernike equation and the superposition approximation for $f = 214, 300$, $q = 3$ and a colloid density of $\rho_C \sigma_S^3 = 0.1, 1.0$.

Especially for a small amount of colloidal additives the agreement between the two methods is excellent, in both cases of the functionality. For higher colloid densities, the agreement becomes less accurate, but the approximation still gives reasonable agreement over a wide range of r.

In the case of the SA, it is possible to calculate the potential also for a distance of $r = 1$, and for $\lim r \to 0$, the depletion force also vanishes, since, if the two stars would fully overlap, there could not be any colloids in between that act as depletants to the stars.

5.3   The colloid-modified star-star potential

The colloid modified star-star effective potential $V_{\text{tot}}(r)$ is a good approximation to an effective one-component representation of the binary mixture. In this picture, the stars are considered to interact with each other not via the above mentioned effective star-star potential, but through a new star-star interaction, which is modified by the colloids, using the relations (5.5) and (5.8) for the depletion interaction. It is calculated by integrating out the degrees of freedom for the colloids and using the two-component solution of the OZ-RY equation in the limit of $\rho_S \to 0$.

The method of how to map a binary mixture to an effective one-component system was put forward by Dijkstra et al [166]: The basic idea is to replace the interaction Hamiltonian
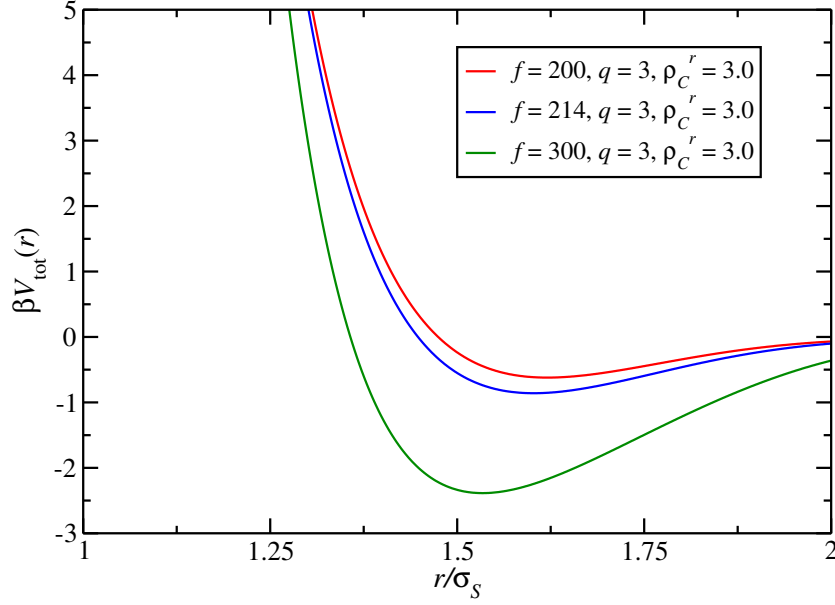
Figure 5.7: The colloid-modified star-star effective potential for various f and $q = 3$, $\rho_C^r \sigma_S^3 = 3$.

$H = H_{11} + H_{12} + H_{22}$ in the total Hamiltonian $\mathcal{H} = K + H$, with K being the kinetic energy, by an effective interaction Hamiltonian $H_{\text{eff}} = H_{11} + \Omega\{(\mathbf{R}; N_1, z_2, V)\}$, that considers the particles of one species in the external field of a fixed configuration of the particles of the other species. Here, N_1 is the number of particles of species 1, $z_2 = \Lambda_2^{-3} \exp \beta \mu_2$ the fugacity and V the macroscopic volume. With the help of a Mayer expansion, Ω is determined and the phase behavior of the mixture is determined with this effective one-component system representation.

The modified star-star interaction of the binary star - colloid mixture is given by:

$$V_{\text{tot}} = -\ln[g_{SS}(r; f, q, \rho_S \to 0, \rho_C)]. \tag{5.13}$$

Figure 5.7 shows the dependence of the colloid-modified star-star potential on the star functionality: The higher f, the more pronounced the depletion effect is. For the colloids it is more difficult to penetrate the space between the arms of a star, the more arms a star has. The effect for different size ratios q one can see in Figs. 5.8a and 5.8b: A higher q, meaning smaller colloids, leads to a much smaller effect, since smaller colloids find much easier a space within a star. For increasing the colloid density ρ_C the system develops an attractive part in the interaction, which is a typical consequence of the depletion mechanism. If the stars get close enough, it becomes more difficult for the colloids to
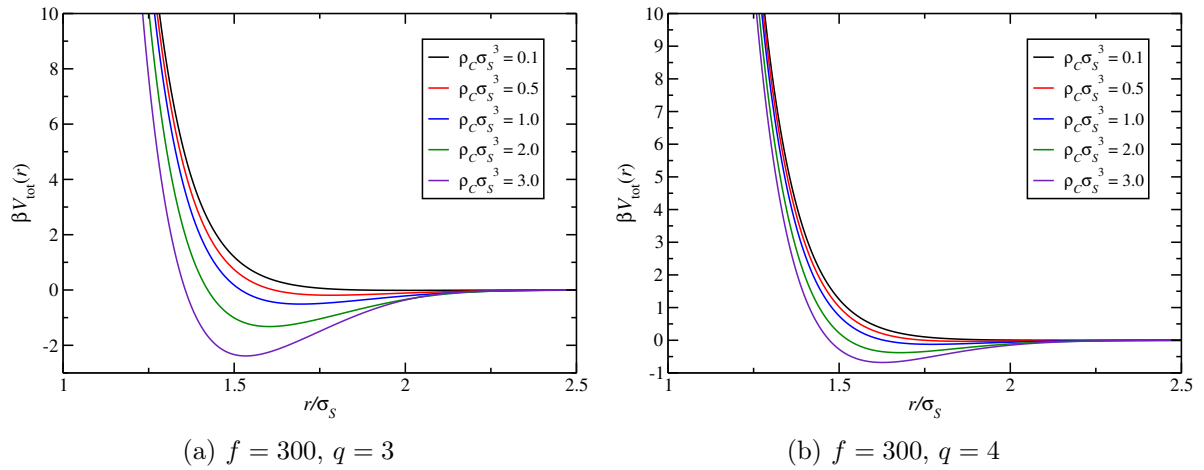
Figure 5.8: The colloid-modified star-star effective potential for different q.

occupy space in between them. A possible consequence is the clustering of stars and also colloids, leading at the end also to phase separation. Our predictions in previous work [2], that high q usually leads to well mixed systems, while for smaller q and large f it is very likely to find phase separations, are in agreement with these observations. The interaction naturally tends to zero for large star-star distances.

5.4   The free energy

As a final step in proceeding to an effective one-component description of the stars, we perform an approximate, mean-field type calculation of the Helmholtz free energy. We then use the free energy curves to calculate binodal demixing lines in the star density - colloid reservoir density plane, which we have predicted, when calculating the non additivity parameter in Chapter 2. If the attractive part in the free energy, stemming from the depletion effect of the colloidal particles on the stars, is strong enough, it will break down the convexity of the free energy curve, leading thereby to a demixing phase transition. We expect that the binodal demixing line will more likely occur for high functionalities of the stars, since in that case the colloidal particles will not find a space in between the arms leading to a clustering of alike particles, which for high densities will result in a phase separation. For the same reason, also a small size ratio, meaning larger colloid size will provoke a demixing.

The calculations in this Section are performed for the pure star system, which will be used as a reference system in the following Section, where the perturbation theory ansatz is presented.

In statistical mechanics, the canonical partition function is defined as [164]:
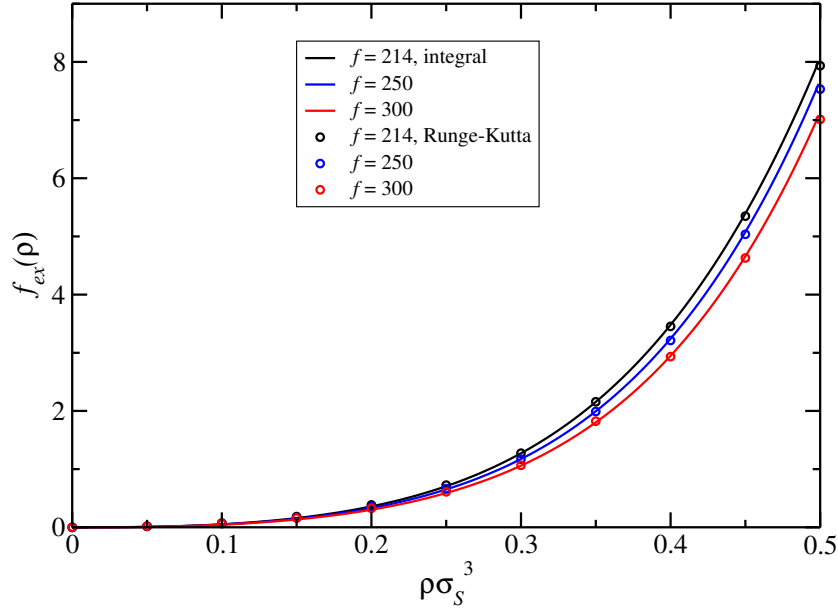
Figure 5.9: The excess free energy. Comparison of the two methods by direct integration and Runge-Kutta.

$$Q_N = \frac{1}{h^{3N} N!} \int \int \exp(-\beta \mathcal{H}) \mathrm{d}\mathbf{r}^N \mathrm{d}\mathbf{p}^N. \tag{5.14}$$

The relation

$$F = -k_{\mathrm{B}} T \ln Q_N \tag{5.15}$$

links the canonical partition function with the thermodynamic potential, the Helmholtz free energy F. By carrying out the integration over momenta in Eq (5.14), the partition function takes the form:

$$Q_N = \frac{1}{N!} \frac{Z_N}{\Lambda^{3N}}, \tag{5.16}$$

where $\Lambda = \sqrt{2\pi\beta h^2/m}$ is the deBroglie thermal wavelength and $Z_N = \int \exp(-\beta V^N) \mathrm{d}\mathbf{r}^N$ is the configurational integral.

The partition function for interacting particles takes the form:

$$Q_N = Q_N^{\mathrm{id}} \frac{Z_N}{V^N}, \tag{5.17}$$

where $Q_N^{\mathrm{id}} = \frac{1}{N!} V^N \Lambda^{3N}$ is the partition function of the ideal gas. Taking the logarithm of equation (5.17) leads to the Helmholtz free energy:

$$F = F^{\mathrm{id}} + F^{\mathrm{ex}}, \tag{5.18}$$

where the ideal part contains the contributions of an ideal gas system, while the excess part is the energy coming from interparticle interactions.

The free energy per volume is given by:

$$f(\rho_S) = \frac{\beta F(\rho_S)\sigma_S^3}{V}. \tag{5.19}$$

and we will use the following relation, splitting the free energy in its ideal and excess part:

$$\underbrace{\frac{\beta F(\rho_S)\sigma_S^3}{V}}_{f(\rho_S)} = \underbrace{\frac{\beta F_{\text{id}}(\rho_S)\sigma_S^3}{V}}_{f_{\text{id}}} + \underbrace{\frac{\beta F_{\text{ex}}(\rho_S)\sigma_S^3}{V}}_{f_{\text{ex}}}, \tag{5.20}$$

where 'id' marks the ideal and 'ex' the excess part of the free energy. With

$$\frac{\beta F_{id}}{N} = \ln(\rho_S \Lambda^3) - 1 \tag{5.21}$$

$$= \ln(\rho_S \sigma_S^3) + \ln\left(\Lambda^3/\sigma_S^3\right) - 1 \tag{5.22}$$

$$= \ln(\rho_S \sigma_S^3) + 3\ln\left(\Lambda/\sigma_S\right) - 1 \tag{5.23}$$

it follows that:

$$f_{\text{id}} = \rho_S \sigma_S^3 (\ln(\rho_S \sigma_S^3) - 1), \tag{5.24}$$

where we have dropped the irrelevant constant from Eq. (5.23). The pressure in the system is given by:

$$\beta P = P_{\text{id}} + P_{\text{ex}} \tag{5.25}$$

$$= \rho_S - \frac{2\pi \rho_S^2}{3} \int_0^\infty \frac{\mathrm{d}\beta V_{SS}(r)}{\mathrm{d}r} g_{SS}(r; \rho_S) r^3 \mathrm{d}r, \tag{5.26}$$

where $g_{SS}^0(r; \rho_S)$ is the radial distribution function of the system consisting only of polymer stars, without any additives. With

$$\beta P = -\frac{\partial \beta F}{\partial V} \tag{5.27}$$

$$= \rho_S f'(\rho_S) - f(\rho_S), \tag{5.28}$$

we can solve the differential equation:

$$\rho_S f'_{ex}(\rho_S) - f_{ex}(\rho_S) = \beta P_{ex}(\rho_S). \tag{5.29}$$

Another method to calculate f_{ex} is to use that $F = V f(\rho_S)$ and $F = N \tilde{f}(\rho_S)$, and therefore

$$f(\rho_S) = \rho_S \tilde{f}(\rho_S). \tag{5.30}$$

With

$$\beta P = -\frac{\partial \beta F}{\partial V} = -\frac{\partial}{\partial V}(N\tilde{f}(\rho_S)) = \rho_S^2 \tilde{f}'(\rho_S), \tag{5.31}$$

we find the relation:

$$\beta \tilde{f}_{ex}(\rho_S) = -\frac{2\pi}{3}\rho_S^2 \int_0^{\rho_S} d\rho' \int_0^\infty \frac{d\beta V_{SS}(r)}{dr} g_{SS}(r; \rho') r^3 dr. \tag{5.32}$$

The results of equations (5.29) and (5.32) are shown in Figure 5.9 and their agreement is undoubtful. The differential equation was used using the Runge-Kutta method and the integral was solved numerically. The excess free energy is a monotonic increasing function.

It should be stated again that the calculations so far have been performed for the pure star system only. The influence of the colloidal additives, seen as a perturbation to the above calculated reference system, are taken into account in the following Section.

5.5 Results: The binodal line for star-colloid mixtures

Without attractions, the star polymer system has no liquid-gas phase transition. In our attempts to calculate a binodal line we have now reached the point, where we should include in our considerations also the attractive part in the free energy $f_{\text{attr}}(r)$, stemming from the depletion interaction. To do so, we will perform a perturbation theory calculation, that will lead us to the calculation of a binodal line in the binary system. We use the following equation for the pair interaction potential, considering $V_{\text{depl}}(r)$ as a perturbation of the reference system $V_{\text{eff}}(r; \rho_C = 0)$:

$$V_{\text{eff}}(r; \rho_C) = V_{\text{eff}}(r; \rho_C = 0) + V_{\text{depl}}(r; \rho_C), \tag{5.33}$$

We make use of the so called λ-expansion [164], that leads to the following description of the free energy:

$$\beta F = \beta F_0 + \beta \langle W_N \rangle_0 - \frac{1}{2}\beta^2 (\langle W_N^2 \rangle_0 - \langle W_N \rangle_0^2) + \mathcal{O}(\beta^3). \tag{5.34}$$
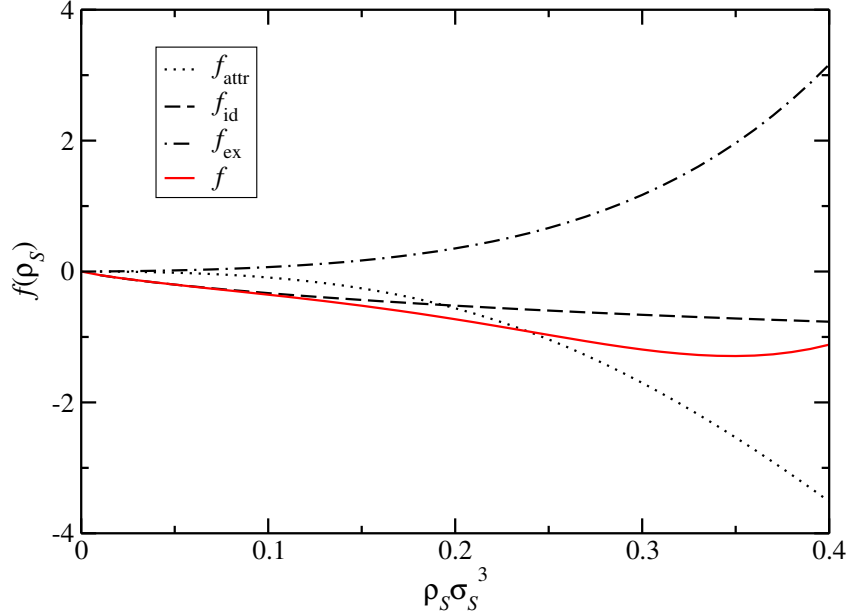
Figure 5.10: The free energy, which is calculated by summing the ideal, excess and attractive part for $f = 250$, $q = 3$ and $\rho_C^r = 1.6\sigma_S^3$.

W_N here is the total perturbation energy $W_N = \sum_{i=1}^{N} \sum_{j>1}^{N} \omega(i,j)$ and F_0 is the excess free energy of the reference system, i.e. the pure star polymer solution, for which F_0 was calculated in Section 5.4. In our calculations, we consider the colloid-induced star-star interaction f_{attr} as a perturbation to the free energy of the pure star system without additives. By assuming pairwise additivity of the potentials and therefore leaving out higher order terms, we get:

$$f(\rho_S) \approx \underbrace{f_{\text{id}}(\rho_S) + f_{\text{ex}}(\rho_S)}_{\text{reference system}} + \underbrace{f_{\text{attr}}(\rho_S)}_{\text{perturbation}} \tag{5.35}$$

$$f(\rho_S) = \rho_S\sigma_S^3 \ln(\rho_S\sigma_S^3) - \rho_S\sigma_S^3 \tag{5.36}$$

$$- \frac{2\pi}{3}\rho_S\sigma_S^3 \int_0^{\rho_S} \mathrm{d}\rho' \int_0^{\infty} \frac{\mathrm{d}\beta V_{SS}(r)}{\mathrm{d}r} g_{SS}^0(r;\rho')r^3\mathrm{d}r \tag{5.37}$$

$$+ 2\pi\rho_S^2\sigma_S^3 \int_0^{\infty} g_{SS}^0(r,\rho_S)\beta V_{\text{depl}}(r,\rho_C^r)r^2\mathrm{d}r. \tag{5.38}$$

In this calculation $g_{SS}^0(r;\rho')$ denotes the radial distribution function for the pure star system. Part of this Equation for the pure star system (5.37) was already presented in Eq. 5.32.

In Fig. 5.10 it can be seen, how the attractive part of the free energy changes the behavior of the total free energy. One can see the typical form that arises, when a binodal
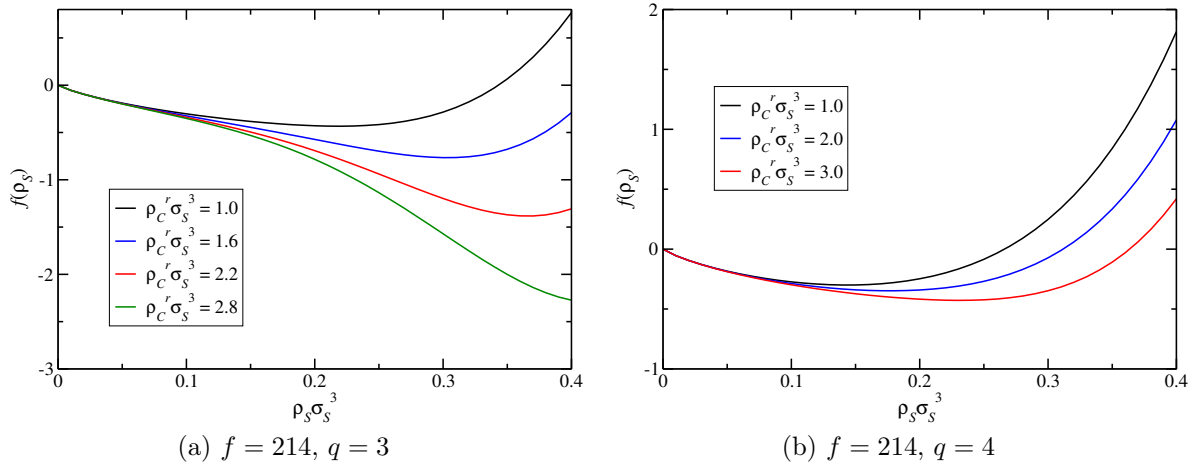
Figure 5.11: The total free energy for fixed f, $q = 3, 4$ and increasing colloid densities ρ_C^r.

is developed. The curves of the free energy show, which parameter combination lead to a phase separation (cf. Figs.(5.11a, 5.11b). The figures show, how the attractive part of the free energy changes the appearance of the total free energy for an increasing colloid reservoir density ρ_C^r and a fixed functionality $f = 214$. While for $q = 3$ the free energy changes its appearance strongly for higher colloid densities, the curves stay convex for $q = 4$ even for high colloidal densities, and so no phase separation occurs. By finding the common tangent on the total free energy curve $f(\rho_S)$, one can construct now a binodal line in the density-density plane; in Fig. 5.12 we show, how such a common-tangent-construction is performed. In principle, we enforce that the pressure P and chemical potential μ of the two species are the two quantities, that are equal across phase boundaries, when phase boundaries in first-oder transitions are considered. This is represented by the common-tangent construction [111].

Finally, we show the binodal lines in Figs. 5.13, 5.14, depending on size ratios and functionalities. In agreement with [43] we find that the binodal line occurs at much lower colloid densities for smaller values of q than for higher values (meaning smaller colloids). Therefore a phase separation is observed at higher colloid reservoir densities for smaller colloids. Small particles can easier find a space, even in between the stars of the arm and therefore one can raise the density of the additive much higher. We have also tried to calculate a binodal line for $q = 8$ and we were not able to find a phase separation for this case, probably the necessary density is much higher, or the mixture is always stable. This confirms our recent predictions in Ref. [2]: Here, with the help of the non-additivity parameter, we were able to show, that a binary system consisting of polymer stars and colloids will easier undergo a demixing, if the stars are of high functionality or the colloids are of about the same size as the star polymers.
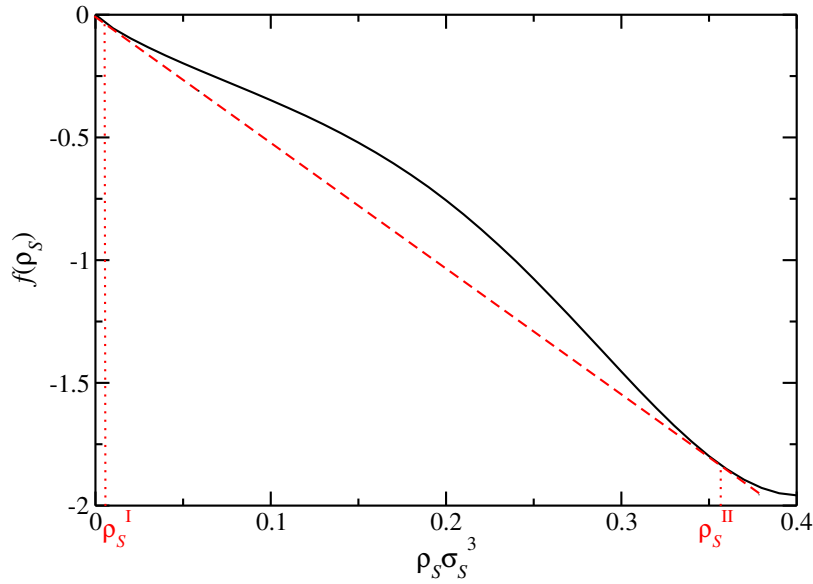
Figure 5.12: The binodal line is constructed by finding the tangent on the free energy curve for several colloid densities ρ_C. The points denoted with ρ_S^I and ρ_S^{II} show the two coexisting densities. This graphic representation is just an example, the calculations were done numerically.

The second observation, namely that for smaller functionalities it is easier to add colloids, is also very intuitive. Stars with many arms consume much more space in a solution than stars with less arms, and therefore additives can easier fill the space in between the star polymers. The state diagrams we have presented in Chapter 4 agree with this results for the binodal demixing line calculations. To give a first estimation of a demixing line there, we have presented the line, where the presented integral equation theory approach fails to converge because of an enormous increase in the partial star-star structure factor (see figures in Chapter 4). The state diagrams additionally also show that small colloidal particles, i.e., higher values of q, do not influence the polymer stars system and neither a demixing nor a polymer glass melting can be observed for the chosen parameters, which is in agreement with Fig. 5.13.

5.6   Conclusions and Outlook

Summarizing the results of this Chapter, we have calculated the depletion potential for a binary polymer star - colloid mixture for several parameters (i.e. functionality f, size ratio q and reservoir density of the colloids ρ_C^r), which we have calculated with the help
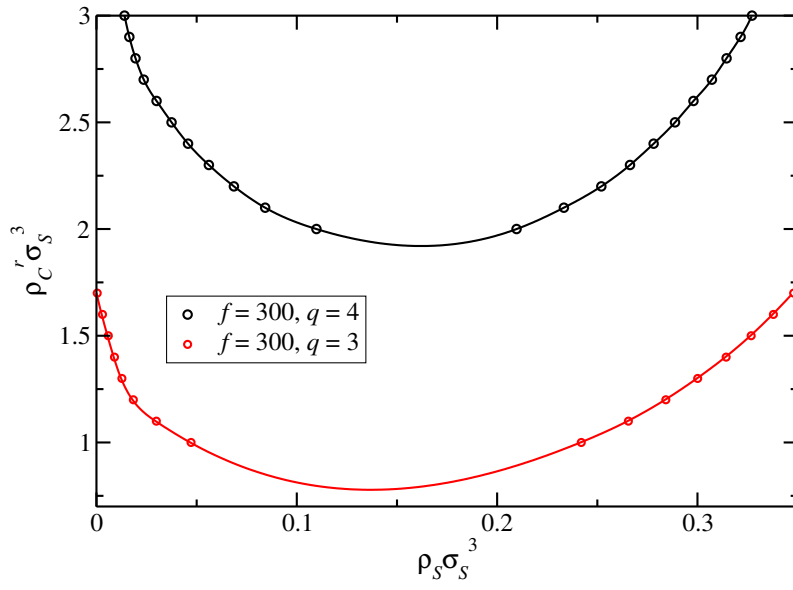
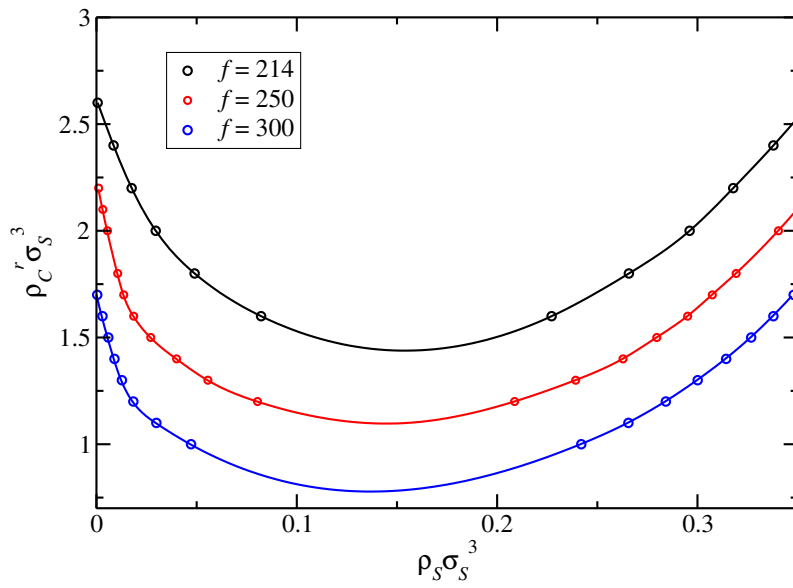Figure 5.13: The demixing binodal lines for changing size ratios q.

Figure 5.14: The demixing binodal lines for different functionalities f and $q = 3$.

of a Rogers-Young integral equation theory ansatz and the superposition approximation. We were able to show that the depletion potential becomes more attractive for larger functionalities and for larger reservoir densities of the colloidal additives. An increasing size ratio, meaning a decrease of the colloid size, leads to a less strong depletion effect and therefore to a well-mixed system, which we had already seen, when we investigated the non-additivity parameter in Ref. [2], while for similar sizes of polymer stars and colloids, the system demixes already for small amounts of additives. These observations are very important for the tuning of mixtures and to influence for example the softness of a glass just by the addition of small depletants. It would be an interesting starting point for experiments to take star polymers of a certain functionality and add colloids with different size ratios. While small colloids should not affect the mixture even for high densities, bigger colloids will probably drive the system very fast to a glass melting or even to a phase separation, since the colloids and stars are very likely to cluster then instead of well-mixing. Alternatively, also changing the functionality of the stars can lead to interesting experimental findings, since for stars with less arms, it should be possible to add bigger colloids than for a star with a higher number of arms, without leading necessarily to a phase separation. So an intensive studying of the parameters both in experiments as now also in effective computer simulations will pave the way for an understanding of tuning binary star-colloid mixtures.

The approach of a combination of the inversion of the Ornstein-Zernike equation together with the non-ergodicity factor has already proven to reflect results stemming from experiments [43] and we were able to present also binodal lines for the system by performing perturbation theoretical calculations. It is now possible to fully map a two-component star-polymer colloid mixture to an effective one-component description, which can lead to interesting possibilities when investigating large systems, e.g. in computer simulations. The perturbation theoretical investigations showed, that the binodal lines come down to small colloidal reservoir densities, when the size ratio is decreased or the functionality is increased. This is in agreement with the observations we have made in the previous Chapter 4.

Chapter 6

Summary and Conclusions

This Thesis provides investigations on mixtures between big, soft colloids, modelled as star polymers and small, hard, colloidal additives and presents results on effective interactions, mixing and demixing behaviour, structure and star polymer glass melting. While focusing on theoretical approaches, the results have been confirmed by using different theoretical methods, by computer simulations and even experiments. The developed coarse-grained model offers now the possibility of studying the structure of the mixture and comparing structural details with experiments. At the same time it offers a time-saving way of employing large systems in computer simulations to study structure and thermodynamics of polymer-colloid mixtures.

First we have introduced a coarse-grained description of the binary mixture and obtained effective pair interactions for various size ratios $q = R_{g,S}/R_C$ and star functionalities f. In dilute solutions, and up to a density that is close to the overlap star density, the pair potentials offer a good approximation for the overall interactions. The analytical calculations where the osmotic pressure of a star polymer exerted on a colloid was integrated to obtain the interaction force and the full monomer Monte Carlo simulations have shown an impressive agreement, paving the way for further investigations, which are relevant in experimental systems, but would have been computationally expensive in full monomer simulations. Now, having reliable effective interactions, it is possible to simulate even large systems with the help of coarse-grained simulations, comparing them to real experimental data.

The effective interaction in the so called nanocomposite limit i.e., the star size being much bigger than the colloid, already allows for predictions on the demixing behaviour of this binary mixtures, suggesting, that for colloids, much smaller than the stars, the mixture will be thermodynamically stable. This prediction was verified with advanced theoretical calculations.

The Ornstein Zernike equation was inverted by means of Rogers-Young integral equation theory using the effective pair interaction to obtain structural information on the

binary mixture, in particular pair radial distribution functions and pair structure factors, whose validity was again confirmed by means of Monte Carlo simulations. This time, we have used the effective interaction in a coarse-grained simulation instead of full-monomer representation, which allows to simulate also star polymers with a high functionality f and a high degree of polymerisation in a reasonable amount of time. With these pre-results we were able to provide a theoretical description of an experimental system by Truzzolillo and coworkers. In the experiments, treating mixtures of polymer stars with $f = 214$ arms and a size ratio of $q = 3$ (or $\xi = R_{H,S}/R_C = 4$), a structural polymer glass was melted by the addition of the small colloidal particles. Using Mode-Coupling theory with the static structure factors obtained from Rogers-Young integral equation calculations, we were able to find excellent parameter-free quantitative agreement, proving again the validity of our coarse-graining assumptions, which were also confirmed by Molecular Dynamics simulations using the effective interaction potentials. The agreement between simulations, experiments and theory show the reliability of the effective pair interactions. The relevant parameters in the experiment also motivated our parameter choice for further investigations, namely $f \in \{214, 250, 300\}$ and $q \in \{2, 3, 4, 8\}$. It should be noted that these choices are not due to any restrictions in the theoretic approach and in principle, arbitrary parameters can be considered. Using the same theoretical methods, the other systems were investigated by the same procedure of using effective interactions to gain structural information which can be used in the one-components mode-coupling theory to obtain information on glass or liquid states. Our findings confirm first predictions we have made on the phase separation, using the non-additivity parameter. While small colloidal additives ($q = 8$) neither cause a phase separation nor a glass melting in the density regime we have considered, intermediate size ratios of $q = 3, 4$ have interesting effects on the star polymer glass. Even smaller size ratios $q = 2$ lead immediately to a phase separation without an observable glass melting before, except for the softer star of $f = 214$, where it is possible to present a phase diagram. Nevertheless, it can be stated that intermediate size ratios are best candidates for observing a polymer glass melting, small size ratios lead to a phase separation for very small amounts of additives and very small additives have almost no effect on the polymers and mix well with them.

Finally, the two-component Rogers Young integral equation calculations were also used in the zero star density limit to split the total effective interaction into the interaction potential without any colloidal additives and a depletion interaction, caused by the colloids. The depletion effect leads at the end to an effective one-component description of the system, where the star-star pair interaction is modified by the colloids and thereby even further simplifying the complex binary system. Thus, with two different coarse-graining procedures, we were able to go from a monomer resolved star polymer colloid mixture to a description, where the "point-like" star polymers interact via a colloid-modified star-star
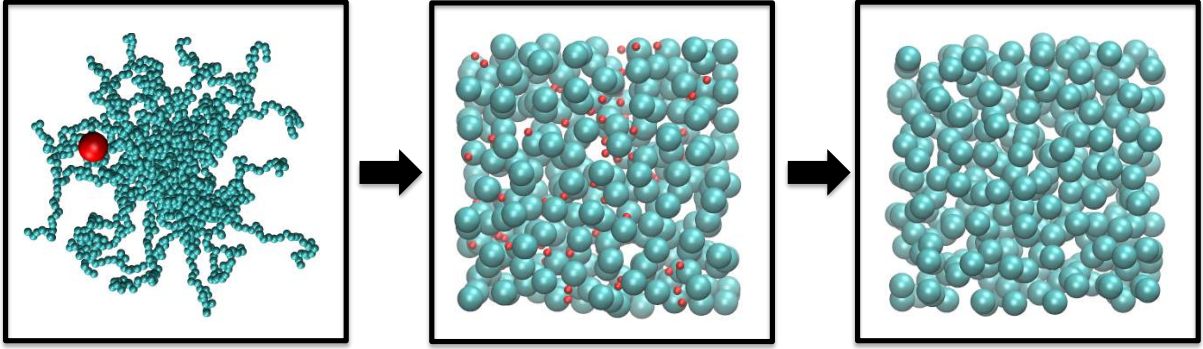
Figure 6.1: Coarse graining procedure: In a first step, the full-monomer stars are replaced by effective sphere-like particles with the help of scaling theory leading to a two component effective description (middle figure). The depletion picture and perturbation theoretical considerations lead to an effective one-component picture, where the effect of colloids on the stars is included in the effective star-star interaction (right figure).

effective interaction potential. This potential is the more pronounced, the smaller the size ratio is. For smaller colloids it tends to look the same as the effective star-star interaction we have started from.

The depletion interaction caused by the colloids on the stars is compared to results from the superposition approximation, again proving the validity of our theoretical approach. The depletion interactions are much stronger for smaller size ratios, showing again, that small colloids will not have a big effect on the polymers, while smaller size ratios lead to a strong depletion effect.

By employing perturbation theoretical calculations, demixing binodal lines were obtained, which confirmed the assumptions from the non-additivity parameter, that the system is well mixed for small colloidal particles and tends to demix faster for less asymmetric mixtures (smaller q) or a large number of arms f, since for the colloids in those cases it is more difficult to find a free space between the stars which at the end leads to a phase separation of the two components.

With the help of our coarse-graining results, it will now be possible to study systems of larger sizes also in computer simulations, where either the three pair interactions are used or only a system of stars will be considered, that interact via the colloid-modified star-star potential. Since we have already made predictions in which parameter ranges interesting effects like the glass melting can happen, experiments can be designed in this specific ranges, not having to search for interesting parameter combinations. Our description is not dependent on any fitting parameter, so it is possible for a wide range of functionalities or size ratios to predict results of experiments and simulations, paving the way for designing new, tuneable materials that are of high interest in material science and industrial applications.

In Figure 6.1 we show simulation snapshots that visualise the coarse-graining procedure. The left figure shows the complexity of full monomer simulations: only one star is simulated with 250 arms and 50 monomers per arm, meaning that all the interaction between the monomers and with the colloid have to be considered. The middle figure shows how the first coarse graining, that we have achieved by introducing effective interactions (Chapter 2), simplifies the representations and allows for much bigger systems, since each star is now represented by a sphere. The depletion considerations in Chapter 5 have led to an effective one-component description, where the colloid effect on the stars has been included in the effective star-star interaction.

Together with the considerations of Jusufi and coworkers [1], it is now possible to describe the full range of size ratios q and star functionalities f for binary systems of star polymers and colloids. While Jusufi *et al.* were treating systems, in which the star polymers deplete the stars, we have considered the opposite scenario and completed the calculations of effective pair interactions for such systems. The agreement of our results with computer simulations and experiments are excellent, although it is expected, that also effects like the possibility, that a star "wraps" its arms around a colloid, leading to attractive contributions in the effective interactions, become more and more important, when more dense systems are considered.

Possible further research would also be the influence of external fields of such systems, adopting the idea of Dzubiella and coworkers in [167]. In the opposite situation, where the colloids are bigger than the stars and the polymer stars act as depletants to the colloids, a "lane-formation" was observed, due to a non-equilibrium slip-stream effect and the effects on our mixture could easily be investigated with the help of coarse-grained simulations. External fields should offer even more possibilities of tuning the composite.

It should also be possible, to classify theoretically the arrested phase separation and glassy states, as the experiments that were done by Domenico Truzzolillo and his coworkers [43] already showed the experimental results for the classification of the glassy states. With the effective interactions, such systems should be investigated with computer simulations. Another possible research route is always the change of the solvent, which then has to be considered in the coarse graining procedure by using a different scaling approach for the osmotic pressure a star exerts on the colloid, but this would lead away from the tools we have already gained so far.

Appendices

Appendix A

Integral Equation Theories (IET)

In this Appendix, we present a short overview of how to employ a two-component integral equation approach to obtain structural information on a binary system with known effective pair interactions. More detailed information on integral equations, closure relations and correlation functions can be found in various books on simple liquids, e.g., in [164]. Following Hansen and McDonald [164], the formalism of distribution functions uses the probability of configurational grouping of two, three and more particles as a description of the system. Approximations for the radial distribution functions can be calculated by solving the Ornstein-Zernike equation, which is well-known for a homogeneous, isotropic system

$$h(r) = c(r) + \rho \int c(|\mathbf{r} - \mathbf{r}'|)h(r')\mathrm{d}^3 r', \tag{A.1}$$

where $c(r)$ is the direct and $h(r)$ the total correlation function.

Since $h(r)$ and the direct correlation function $c(r)$ are unknown, an additional closure relation is necessary to obtain a solution for this relation. There are several closure relations, that have been studied extensively in various systems and give , although they are approximations, good results for specific systems, i.e., the Percus-Yevick (PY) closure for hard sphere systems or the hypernettedchain closure (HNC) for soft, long-ranged interactions.

In Fourier space, the Ornstein-Zernike equation takes a simpler, multiplicative form:

$$\hat{\mathbf{H}}(k) = \hat{\mathbf{C}}(k) + \hat{\mathbf{C}}(k) \cdot \hat{\mathbf{D}} \cdot \hat{\mathbf{H}}(k), \tag{A.2}$$

where the tilde represents the Fourier transform, and

$$\hat{\mathbf{H}}(k) = \begin{pmatrix} \hat{h}_{SS}(k) & \hat{h}_{SC}(k) \\ \hat{h}_{SC}(k) & \hat{h}_{CC}(k) \end{pmatrix} \tag{A.3}$$

is the Fourier transform of the total correlation function matrix, and

$$\hat{\mathbf{C}}(k) = \begin{pmatrix} \hat{c}_{SS}(k) & \hat{c}_{SC}(k) \\ \hat{c}_{SC}(k) & \hat{c}_{CC}(k) \end{pmatrix} \tag{A.4}$$

is the Fourier transform direct correlation function matrix,

$$\hat{\mathbf{D}} = \begin{pmatrix} \rho_S & 0 \\ 0 & \rho_C \end{pmatrix} \tag{A.5}$$

is the matrix of the partial densities ρ_S and ρ_C in the system.

For the iteration method we use, it is more convenient to rewrite the Ornstein-Zernike equation in the following form:

$$\hat{\Gamma}(k) = [\mathbb{1} - \hat{C}(k) \cdot \hat{D}]^{-1} \cdot \hat{C}(k) \cdot \hat{D} \cdot \hat{C}(k). \tag{A.6}$$

Here, $\mathbb{1}$ is the identity matrix and

$$\hat{\Gamma}(k) = \begin{pmatrix} \hat{\gamma}_{SS}(k) & \hat{\gamma}_{SC}(k) \\ \hat{\gamma}_{SC}(k) & \hat{\gamma}_{CC}(k) \end{pmatrix}, \tag{A.7}$$

where $\hat{\gamma}_{ij}(k)$ is the Fourier transform of $\gamma_{ij}(r) = h_{ij}(r) - c_{ij}(r)$.

We have chosen to use the two-component Rogers-Young relation, which is a hybridisation of the two well known PY and HNC closures, and is known for its thermodynamic stability [34, 73, 164]. The Rogers-Young closure is given by

$$\gamma_{ij}(r) + c_{ij}(r) + 1 = \exp(-\beta V_{ij}(r)) \left(\frac{\exp[\gamma_{ij}(r)f(r)] - 1}{f(r)} \right), \tag{A.8}$$

where $V_{ij}(r)$ is the effective pair interaction between components i and j (the stars and colloids, respectively), and the mixing function $f(r) = 1 - \exp(-\alpha r)$, that enforces thermodynamic consistency [100, 164]. Note, that for $\alpha \to 0$, the Rogers-Young closure relation takes the form of the Percus-Yevick relation and for $\alpha \to \infty$ it represents the hypernetted chain closure.

With this closures the three pair radial distribution functions $g_{ij}(r)$ and the static structure factors $S_{ij}(k)$ can be calculated after the convergence of a Picard iteration as it is visualised in Fig. A.1. A good starting guess for the iteration of the direct correlation function $C_0(r)$ is the Mayer function of the pair potentials which are used as an input for the iteration. Once results are obtained it is recommended to use the old $C_n(r)$ as a guess of $C_0(r)$ for a new run.

After a sufficient convergence of the iteration routine, the total pair correlation function

$h_{ij}(r)$, the radial pair distribution function $g_{ij}(r)$ and the partial static structure factors $Sij(k)$ are calculated and can be compared to those from experiments or simulations as we have done in Chapters 4 and 5.
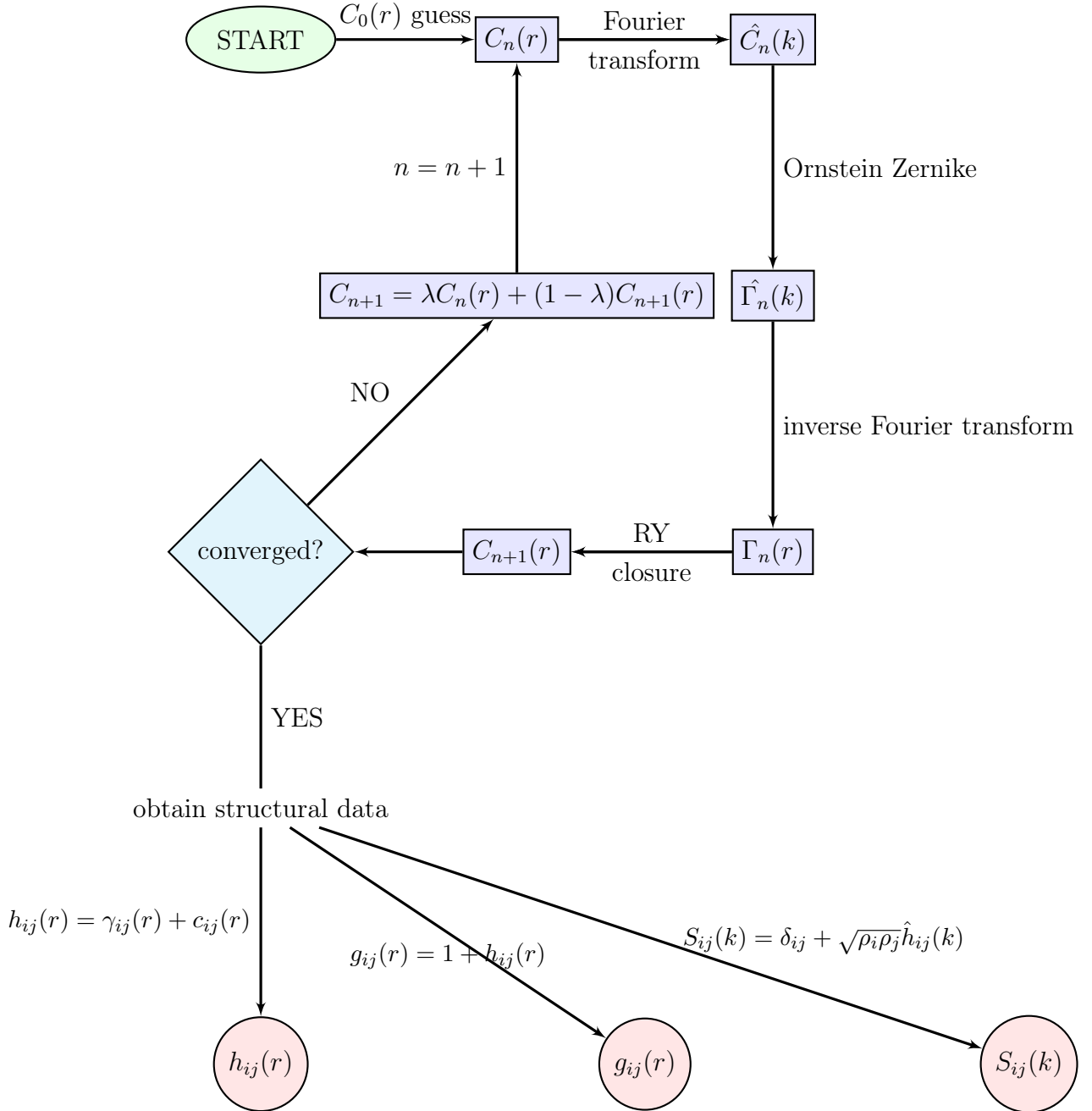

Figure A.1: A scheme for an integral equation approach: From a first guess of the matrix of direct correlation function $C_0(r)$ the iteration is started, after convergence, the total pair correlation function $h_{ij}(r)$, the radial pair distribution function $g_{ij}(r)$ and the partial static structure factors $Sij(k)$ are calculated.

Appendix B

The Mode-Coupling Theory of the Glass Transition (MCT)

Normally, when a liquid is (slowly) cooled, a transition to a crystalline phase occurs; to the contrary, by cooling or compressing the liquid fast, an amorphous phase can emerge. In such systems, relaxation times increase dramatically [164]. One control parameter is the decrease in temperature, which, for purely entropy systems corresponds to an increase in density or, equivalently, pressure. The glass transition temperature is smaller than the thermodynamic crystal freezing temperature, and below this temperature the system is in a *metastable* state that has a liquid-like structure but mechanical properties similar to a solid.

Since glass forming liquids are an important scientific subject, but the understanding of dynamics of supercooled glass-forming systems is an intellectual challenge, several theoretic approaches have been developed to explain the dynamics of such systems. Most of these theories are able to explain some experimental findings or fit experimental data - but there is also one theory, which is additionally able to make reliable predictions of the dynamics of glasses: the mode coupling theory of the glass transition, in short: MCT. If you approach the glassy state from the liquid region, it gives an description of the initial slowing down of the structural relaxation.

In principle, MCT makes use of experimental result in glass systems, that the structural properties in glass-forming dense liquids have a weak dependence on the temperature and at low temperatures the structural arrest of the system is formed by the strength of the nonlinear-feedback mechanisms in the microscopic dynamics. It therefore only considers slowly varying variables i.e., the structural relaxation.

Mode Coupling Theory (MCT) can for example describe the so-called "caging" – effect, which arises in dense liquids close to the triple point. The caging effect has been observed for dense liquids, where particles are temporarily trapped by a cage that is built by its

neighbors. For a specific system, i.e., spin glasses, MCT gives an exact description of the relaxation dynamics [112].

In this work, we have made use of the so-called one-component non-ergodicity factor $f(k)$, that allows us to decide whether our static structure factors stemming from the inversion of the Ornstein-Zernike equation represent a liquid or glassy state. In this Appendix, we give a brief exposure on how to derive it and how it can be used in our case.

Our starting point are the slowly changing density fluctuations and the time autocorrelation function:

$$\hat{\rho}_{\mathbf{k}}(t) = \sum_{j=1}^{N} \exp(i\mathbf{k} \cdot \mathbf{r}_j(t)) \tag{B.1}$$

$$F(k,t) = \frac{1}{N} \langle \hat{\rho}_{\mathbf{k}}(t) \hat{\rho}_{\mathbf{k}}^*(0) \rangle. \tag{B.2}$$

Important is, that these are slowly fluctuating variables and so the Zwanzig-Mori formalism (together with the mode-coupling approximations, that are imposed for slowly changing variables) which is not explained here, but can be found in references [112, 164, 168], is used to obtain an equation of motion for $F(k,t)$.

In mode coupling theory memory functions play an important role. For the response of a quantity $\alpha(t)$ which depends on the history, the memory function $M(t - t')$ can be understood with the following relation:

$$\alpha(t) = \int_{-\infty}^{t} dt' M(t - t') \beta(t'). \tag{B.3}$$

Various examples and explanations of how the *memory function* is approximated are presented in [112]. In this reference, it is also shown how in MCT a memory function is approximated by a product of two modes. The MCT approach gives for example reasonable theoretic results for experimental observations of critical phenomena (e.g. for the dynamics of density fluctuations or the dynamics in magnetic systems) and is a valuable tool to study effects which occur close to the critical point.

In a first step, the Zwanzig-Mori formalism leads to the Laplace transform $\Phi(k, z)$ of the normalised correlator $F(k,t)/F(k,0) = F(k,t)/S(k)$, where $S(k)$ is the static structure factor that we can obtain from integral equation algorithms. The quantity $\Phi(k, z)$ reads as

$$\Phi(k,z) = \frac{-1}{z - \frac{\Omega_k^2}{z + \Omega_k^2 \{\widehat{M}^{\mathrm{reg}}(k,z) + \widehat{M}(k,z)\}}}, \tag{B.4}$$

where the frequency Ω_k is defined as:

$$\Omega_k^2 = \frac{k^2}{\beta m S(k)}, \tag{B.5}$$

with m being the particle mass. This expression is an approximation, since a hierarchy of continued fractions has been truncated at a second level. In principle, it would be possible to make an iteration and by that get a more and more accurate expression for $\Phi(k, z)$, but it would involve heavy calculations. The truncation at this level has been used in several applications and seems to be a good approximation for a wide range of situations.

The quantity $\{\widehat{M}^{\mathrm{reg}}(k, z) + \widehat{M}(k, z)\}$ is the Laplace transform of the memory function. We have split it in two parts, the regular part, which describes the time dependence of $\Phi(k, z)$ for short times and the, in this chapter important, part $\widehat{M}(k, z)$, that describes the long time dependence. The regular part is always present, also in the case of non-glass forming liquids, where the relaxation dynamics is not slow. It therefore is a problem of the investigation of standard liquids. It can be approximated by a Gaussian function in time, but finding an accurate description for $\widehat{M}^{\mathrm{reg}}(k, z)$ is an own topic of research.

The back transformation of $\Phi(k, z)$ leads to the *full set of equations of MCT*:

(i) The equation of motion:

$$\ddot{\Phi}(k, t) + \Omega_k^2 \Phi(k, t) + \Omega_k^2 \int_0^t [M^{\mathrm{reg}}(k, t - t') + M(k, t - t')] \dot{\Phi}(k, t') \mathrm{d}t', \tag{B.6}$$

(ii) with the memory function for the long time relaxation dynamics, without the regular part $\widehat{M}^{\mathrm{reg}}(k, z)$:

$$M(k, t) = \frac{1}{2(2\pi)^3} \int \mathrm{d}\mathbf{q} V^{(2)}(k, q, |\mathbf{k} - \mathbf{q}|) \Phi(q, t) \Phi(|\mathbf{k} - \mathbf{q}|, t), \tag{B.7}$$

(iii) and the vertex

$$V^{(2)}(k, q, |\mathbf{k} - \mathbf{q}|) = \frac{\rho}{q^2} S(k) S(q) S(|\mathbf{k} - \mathbf{q}|) \left(\frac{\mathbf{k}}{k} [\mathbf{q}c(q) + (\mathbf{k} - \mathbf{q})c(\mathbf{k} - \mathbf{q})] \right). \tag{B.8}$$

In these equations, $\rho = V/N$ is the particle density and $c(q)$ the direct correlation function [164]

$$c(q) = \rho(1 - 1/S(q)). \tag{B.9}$$

For us, the important feature of MCT is the qualitative change of the solutions of this MCT equations for long times. To see these changes, we first make use of a generic

property of the Laplace transform:

$$-\lim_{z\to 0} z\widehat{C}(z) = -\lim_{z\to 0} i\int_0^\infty z\exp(izt)C(t)\mathrm{d}t \tag{B.10}$$

$$= -\lim_{z\to 0}\int_0^\infty iz\exp(izt)C(t)\mathrm{d}t \tag{B.11}$$

$$= -\lim_{z\to 0}\int_0^\infty \mathrm{d}(\exp(izt))C(t) \tag{B.12}$$

$$= -\lim_{z\to 0}\left[\exp(izt)C(t)\right]_{t=0}^{t\to\infty} - \int_0^\infty \dot{C}(t)\exp(izt)\mathrm{d}t \tag{B.13}$$

$$\overset{z\to 0}{=} C(t\to 0) + C(t\to\infty) - C(t\to 0) \tag{B.14}$$

$$= C(t\to\infty). \tag{B.15}$$

Therefore, $-\lim_{z\to 0} z\widehat{C}(z) = \lim_{t\to\infty} C(t)$.

We use this relation in the Laplace transform of the correlation function $F(k,t)$ (see eq. B.4) and make use of the fact that the regular part of the memory function $M^{\mathrm{reg}}(k,t)$ vanishes in the long time limit $t\to\infty$ and thus we only consider the part of the memory function, that is responsible for the long time relaxation dynamics:

$$f(k) := \lim_{t\to\infty}\frac{F(k,t)}{F(k,0)} \tag{B.16}$$

$$= -\lim_{z\to 0} z\Phi(k,z) \tag{B.17}$$

$$= -\lim_{z\to 0}\frac{-z}{z - \frac{\Omega_k^2}{z+\Omega_k^2\widehat{M}(k,z)}} \tag{B.18}$$

$$= \lim_{z\to 0}\frac{z^2 + z\Omega_k^2\widehat{M}(k,z)}{z^2 + z\Omega_k^2\widehat{M}(k,z) - \Omega_k^2} \tag{B.19}$$

$$= \lim_{z\to 0}\frac{z\widehat{M}(k,z)}{z\widehat{M}(k,z) - 1} \tag{B.20}$$

$$= \frac{-\mathcal{F}(k)}{-\mathcal{F}(k) - 1} \tag{B.21}$$

$$= \frac{\mathcal{F}(k)}{\mathcal{F}(k) + 1} \tag{B.22}$$

where we have defined

$$\mathcal{F}(k) = \lim_{t\to\infty} M(k,t) = -\lim_{z\to 0} z\widehat{M}(q,z). \tag{B.23}$$

With the help of the definition of the memory function (see Eq. B.7), one gets:

$$\frac{f(k)}{1 - f(k)} = \mathcal{F}(k) = \frac{1}{2(2\pi)^3}\int \mathrm{d}\mathbf{q}\,V^{(2)}(k,q,|\mathbf{k}-\mathbf{q}|)f(q)f(\mathbf{k}-\mathbf{q}). \tag{B.24}$$

In principle, this is the only equation we used in our investigations of the glass-transitions We have used it to decide whether we are in the glassy or liquid regime. It is easy to see that $f(k) = 0$ is always a solution of this set of implicit equations, corresponding to an ergodic fluid. Götze et al [23] have shown, that for sufficiently large vertices, there exist also solutions $f(k) > 0$ and it implies, that the system is no longer ergodic, since the long time value of the correlation function is then this value, *the nonergodicity parameter $f(k)$,* and no longer zero.

This is only one particular property of MCT and there has been a lot of research both on the mathematical and computational aspects [23, 169–171] and the advanced use of this theory, where it is no longer used as a theory to describe experiments, but also to predict phenomena [25, 93, 102, 132, 172–178] - an important advantage of MCT over all other theories that aim to describe the dynamics of glass-forming liquids.

Bibliography

[1] A. Jusufi, J. Dzubiella, C. N. Likos, C. V. Ferber, and H. Löwen, J. Phys.: Condens. Matter, **13**, 6177 (2001).

[2] D. Marzi, C. N. Likos, and B. Capone, J. Chem. Phys., **137**, 014902 (2012).

[3] R. J. Hunter, *Foundations of Colloid Science* (Oxford University Press, Oxford, 1989).

[4] R. A. L. Jones, *Soft Condensed Matter* (Oxford University Press, Oxford, 2002).

[5] C. N. Likos, Phys. Rep., **348**, 267 (2001).

[6] I. Coluzza, P. D. J. van Oostrum, B. Capone, E. Reimhult, and C. Dellago, Phys. Rev. Lett., **110**, 075501 (2013).

[7] Y. Kakizawa and K. Kataoka, Adv. Drug. Del. Rev., **54**, 203 (2002).

[8] P. J. Flory, *Principles of Polymer Chemistry*, Baker lectures 1948 (Cornell University Press, 1953).

[9] G. Odian, *Principles of Polymerization* (Wiley, 2004).

[10] N. Hadjichristidis, A. Hirao, Y. Tezuka, and F. Du Prez, *Complex Macromolecular Architectures: Synthesis, Characterization, and Self-Assembly* (Wiley, 2011).

[11] A. R. Denton, in *Nanostructured Soft Matter: Experiment, Theory, Simulation and Perspectives*, edited by Zvelindovsky (Springer, Dordrecht, 2007).

[12] M. Wilson, Soft Matter, **5**, 4355 (2009).

[13] A. Y. Grosberg and A. R. Khokhlov, *Statistical Physics of Macromolecules* (American Institute of Physics Press, New York, 1994).

[14] D. C. Rapaport, *The Art of Molecular Dynamics Simulation* (Cambridge University Press, Cambridge, 1995).

[15] D. Frenkel and B. Smit, *Understanding Molecular Simulation* (Academic Press, San Diego, 1996).

[16] M. P. Allen and D. J. Tildesley, *Computer Simulation of Liquids* (Oxford University Press, Oxford, 1987).

[17] A. C. Balazs and J. M. Yeomans, Soft Matter, **6**, 703 (2010).

[18] M. A. C. Stuart, W. T. S. Huck, J. Genzer, M. Müller, C. Ober, M. Stamm, G. B. Sukhorukov, I. Szleifer, V. V. Tsukruk, M. Urban, F. Winnik, S. Zauscher, I. Luzinov, and S. Minko, Nat. Mater., **9**, 101 (2010).

[19] W. B. Russel, D. A. Saville, and W. R. Schowalter, *Colloidal Dispersions*, Cambridge Monographs on Mechanics and Applied Mathematics (Cambridge University Press, 1989).

[20] S. Asakura and F. Oosawa, J. Polym. Sci., **33**, 183 (1958).

[21] V. J. Anderson and H. N. W. Lekkerkerker, Nature, **416**, 811 (2002).

[22] E. Zaccarelli, J. Phys.: Condens. Matter, **19**, 323101 (2007).

[23] W. Götze, in *Liquids Freezing and the Glass Transition: Les Houches Session LI*, edited by J. Hansen, D. Levesque, and J. Zinn-Justin (North-Holland, Amsterdam, 1991).

[24] F. Sciortino, Nat. Mater., **1**, 145 (2002).

[25] F. Sciortino, E. La Nave, and P. Tartaglia, Phys. Rev. Lett., **91**, 155701 (2003).

[26] F. Sciortino and P. Tartaglia, Adv. Phys., **54**, 471 (2005).

[27] J. Stellbrink, M. Allgaier, M. Monkenbusch, D. Richter, A. Lang, C. Likos, M. Watzlawek, H. Löwen, G. Ehlers, and P. Schleger, Progr. Coll. Polym. Sci., **115**, 88 (2000).

[28] D. Vlassopoulos, T. Pakula, G. Fytas, M. Pitsikalis, and N. Hadjichristidis, J. Chem. Phys, **111**, 1760 (1999).

[29] J. Roovers, L. L. Zhou, P. M. Toporowski, M. V. D. Zwan, H. Iatrou, and N. Hadjichristidis, Macromolecules, **26**, 4324 (1993).

[30] P. G. de Gennes, *Scaling Concepts in Polymer Physics* (Cornell University Press, Ithaca, 1979).

[31] M. Daoud and J. P. Cotton, J. Phys. (Paris), **43**, 531 (1982).

[32] C. N. Likos, H. Löwen, M. Watzlawek, B. Abbas, O. Jucknischke, J. Allgaier, and D. Richter, Phys. Rev. Lett., **80**, 4450 (1998).

[33] M. Watzlawek, *Phase Behavior of Star Polymers* (Shaker Verlag, Aachen, 2002).

[34] M. Watzlawek, C. N. Likos, and H. Löwen, Phys. Rev. Lett., **82**, 5289 (1999).

[35] G. S. Grest, K. Kremer, and T. A. Witten, Macromolecules, **20**, 1376 (1987).

[36] T. Voigtmann and J. Horbach, Phys. Rev. Lett., **103**, 205901 (2009).

[37] D. Truzzolillo, D. Vlassopoulos, and M. Gauthier, Macromolecules, **44**, 5043 (2011).

[38] R. Tuinier, J. Rieger, and C. de Kruif, Adv. Colloid Interface Sci., **103**, 1 (2003).

[39] J. Dzubiella, A. Jusufi, C. Likos, C. von Ferber, H. Löwen, J. Stellbrink, J. Allgaier, D. Richter, A. Schofield, P. Smith, W. Poon, and P. Pusey, Phys. Rev. E, **64**, 010401 (2001).

[40] A. A. Louis, R. Finken, and J. Hansen, Phys. Rev. E, **61**, R1028 (2000).

[41] M. Camargo and C. N. Likos, J. Chem. Phys., **130**, 204904 (2009).

[42] W. C. K. Poon, J. Phys.: Condens. Matter, **14**, R859 (2002).

[43] D. Truzzolillo, D. Marzi, J. Marakis, B. Capone, M. Camargo, A. Munam, F. Moingeon, M. Gauthier, C. N. Likos, and D. Vlassopoulos, Phys. Rev. Lett., **111**, 208301 (2013).

[44] R. Verma, J. C. Crocker, T. C. Lubensky, and A. G. Yodh, Phys. Rev. Lett., **81**, 4004 (1998).

[45] Y. N. Ohshima, H. Sakagami, K. Okumoto, A. Tokoyoda, T. Igarashi, K. B. Shintaku, S. Toride, H. Sekino, K. Kabuto, and I. Nishio, Phys. Rev. Lett., **78**, 3963 (1997).

[46] C. Bechinger, D. Rudhardt, P. Leiderer, R. Roth, and S. Dietrich, Phys. Rev. Lett., **83**, 3960 (1999).

[47] W. Poon, Science, **304**, 830 (2004).

[48] A. Louis, P. Bolhuis, J. Hansen, and E. Meijer, Phys. Rev. Lett., **85**, 2522 (2000).

[49] P. G. Bolhuis, A. A. Louis, J. P. Hansen, and E. J. Meijer, J. Chem. Phys., **114**, 4296 (2001).

[50] P. G. Bolhuis, A. A. Louis, and J.-P. Hansen, Phys. Rev. Lett., **89**, 128302 (2002).

[51] P. G. Bolhuis and A. A. Louis, Macromolecules, **35**, 1860 (2002).

[52] S. Asakura, N. Imai, and F. Oosawa, J. Polym. Sci., **13**, 499 (1954).

[53] M. Dijkstra, J. M. Brader, and R. Evans, J. Phys.: Condens. Matter, **11**, 10079 (1999).

[54] J. M. Brader, R. Evans, and M. Schmidt, Mol. Phys., **101**, 3349 (2003).

[55] D. G. A. L. Aarts, R. P. A. Dullens, H. N. W. Lekkerkerker, D. Bonn, and R. van Roij, J. Chem. Phys., **120**, 1973 (2004).

[56] R. L. C. Vink, A. Jusufi, J. Dzubiella, and C. N. Likos, Phys. Rev. E, **72**, 030401 (2005).

[57] G. A. Vliegenthart, J. S. van Duijneveldt, and B. Vincent, Farad. Discuss., **123**, 65 (2003).

[58] P. G. Bolhuis, E. J. Meijer, and A. A. Louis, Phys. Rev. Lett., **90**, 14 (2003).

[59] Y. Hennequin, M. Evens, C. M. Quezada Angulo, and J. S. van Duijneveldt, J. Chem. Phys., **123**, 054906 (2005).

[60] K. J. Mutch, J. S. van Duijneveldt, and J. Eastoe, Soft Matter, **3**, 155 (2007).

[61] M. Fuchs and K. S. Schweizer, Europhys. Lett., **51**, 621 (2000).

[62] T. Wang and J. L. Keddie, Adv. Colloid Interface Sci., **147-148**, 319 (2009).

[63] J. B. Hooper, K. S. Schweizer, T. G. Desai, R. Koshy, and P. Keblinski, J. Chem. Phys., **121**, 6986 (2004).

[64] J. B. Hooper and K. S. Schweizer, Macromolecules, **38**, 8858 (2005).

[65] L. M. Hall and K. S. Schweizer, J. Chem. Phys., **128**, 234901 (2008).

[66] B. J. Anderson and C. F. Zukoski, Macromolecules, **40**, 5133 (2007).

[67] B. J. Anderson and C. F. Zukoski, Macromolecules, **41**, 9326 (2008).

[68] B. J. Anderson and C. F. Zukoski, Macromolecules, **42**, 8370 (2009).

[69] B. J. Anderson and C. F. Zukoski, J. Phys.: Condens. Matter, **21**, 285102 (2009).

[70] B. J. Anderson and C. F. Zukoski, Langmuir, **26**, 8709 (2010).

[71] L. M. Hall, B. J. Anderson, C. F. Zukoski, and K. S. Schweizer, Macromolecules, **42**, 8435 (2009).

[72] J. Dzubiella, C. N. Likos, and H. Löwen, Europhys. Lett., **58**, 133 (2002).

[73] J. Dzubiella, C. N. Likos, and H. Löwen, J. Chem. Phys., **116**, 9518 (2002).

[74] C. von Ferber, A. Jusufi, C. N. Likos, H. Löwen, and M. Watzlawek, Eur. Phys. J. E, **2**, 311 (2000).

[75] B. Lonetti, M. Camargo, J. Stellbrink, C. N. Likos, E. Zaccarelli, L. Willner, P. Lindner, and D. Richter, Phys. Rev. Lett., **106**, 228301 (2011).

[76] E. Stiakakis, D. Vlassopoulos, C. Likos, J. Roovers, and G. Meier, Phys. Rev. Lett., **89**, 208302 (2002).

[77] G. Foffi, F. Sciortino, P. Tartaglia, E. Zaccarelli, F. L. Verso, L. Reatto, K. A. Dawson, and C. N. Likos, Phys. Rev. Lett., **90**, 238301 (2003).

[78] E. Zaccarelli, S. V. Buldyrev, E. La Nave, A. J. Moreno, I. Saika-Voivod, F. Sciortino, and P. Tartaglia, Phys. Rev. Lett., **94**, 218301 (2005).

[79] C. Mayer, E. Zaccarelli, E. Stiakakis, C. N. Likos, F. Scortino, A. Munam, M. Gauthier, N. Hadjichristidis, H. Iatrou, P. Tartaglia, H. Löwen, and D. Vlassopoulos, Nat. Mater., **7**, 780 (2008).

[80] I. Coluzza and D. Frenkel, ChemPhysChem, **6**, 1779 (2005).

[81] R. Faller, Q. Yan, and J. de Pablo, J. Chem. Phys., **116**, 5419 (2002).

[82] D. Frenkel, Proc. Natl. Acad. Sci. USA, **101**, 17571 (2004).

[83] C. Mayer and C. N. Likos, Macromolecules, **40**, 1196 (2007).

[84] P. Pincus, Macromolecules, **24**, 2912 (1991).

[85] D. Trombly and V. Ganesan, J. Polym. Sci., 2566 (2009).

[86] J. A. Barker, J. Chem. Phys., **47**, 4714 (1967).

[87] A. A. Louis and R. Roth, J. Phys.: Condens. Matter, **13**, L777 (2001).

[88] T. Biben and J.-P. Hansen, Physica, **235**, 142 (1997).

[89] M. Dijkstra, Phys. Rev. E, **58**, 7523 (1998).

[90] A. L. Frischknecht and A. Yethiraj, J. Chem. Phys., **134**, 174901 (2011).

[91] J. Mewis and N. J. Wagner, *Colloidal Suspension Rheology* (Cambridge University Press, 2012) p. 416.

[92] P. Pusey, in *Liquids Freezing and the Glass Transition: Proceedings of the Les Houches Summer School*, edited by J. Hansen, D. Levesquie, and J. Zinn-Justin (Amsterdam, 1991) pp. 763–942.

[93] K. N. Pham, A. Puertas, J. Bergenholtz, S. U. Egelhaaf, A. Moussaïd, P. N. Pusey, A. B. Schofield, M. E. Cates, M. Fuchs, and W. C. K. Poon, Science (New York, N.Y.), **296**, 104 (2002).

[94] A. Imhof and J. K. G. Dhont, Phys. Rev. Letters, **75**, 1662 (1995).

[95] D. Vlassopoulos and G. Fytas, in *High Solid Dispersion*, Adv.Polym. Sci., Vol. 236, edited by M. Cloitre (Springer Berlin Heidelberg, 2010) pp. 1–54.

[96] M. Gauthier and A. Munam, Macromolecules, **43**, 3672 (2010).

[97] K. N. Pham, G. Petekidis, D. Vlassopoulos, S. Egelhaaf, W. Poon, and P. Pusey, J. Rheol., **52**, 649 (2008).

[98] C. Mayer, F. Sciortino, C. N. Likos, P. Tartaglia, H. Löwen, and E. Zaccarelli, Macromolecules, **42** (2009).

[99] A. Jusufi, M. Watzlawek, and Löwen, Macromolecules, **32**, 4470 (1984).

[100] F. J. Rogers and D. A. Young, Phys. Rev. A, **30**, 999 (1984).

[101] E. Zaccarelli, H. Löwen, P. P. F. Wessels, F. Sciortino, P. Tartaglia, and C. N. Likos, Phys. Rev. Lett., **92**, 225703 (2004).

[102] K. Dawson, G. Foffi, M. Fuchs, W. Götze, F. Sciortino, M. Sperl, P. Tartaglia, T. Voigtmann, and E. Zaccarelli, Phys. Rev. E, **63**, 011401 (2000).

[103] A. M. Puertas, M. Fuchs, and M. E. Cates, J. Phys. Chem. B, **109**, 6666 (2005).

[104] A. M. Puertas, M. Fuchs, and M. E. Cates, J. Phys.: Condens. Matter, **19**, 205140 (2007).

[105] N. A. Mahynski and A. Z. Panagiotopoulos, J. Chem. Phys., **139**, 024907 (2013).

[106] A. Stradner, H. Sedwick, F. Cardinaux, W. Poon, S. Egelhaaf, and P. Schurtenberger, Nature, **432**, 7016 (2004).

[107] G. Foffi, C. D. Michele, F. Sciortino, and P. Tartaglia, Phys. Rev. Lett., **94**, 078301 (2005).

[108] E. Zaccarelli, I. Saika-Voivod, S. V. Buldyrev, A. J. Moreno, P. Tartaglia,   and F. Sciortino, J. Chem. Phys., **124**, 124908 (2006).

[109] F. Cardinaux, T. Gibaud, A. Stradner,   and P. Schurtenberger, Phys. Rev. Lett., **99**, 118301 (2007).

[110] P. J. Lu, E. Zaccarelli, F. Ciulla, A. B. Schofield, F. Sciortino, and D. A. Weitz, Nature, **453**, 499P503 (2008).

[111] M. Dijkstra, R. van Roij, and R. Evans, Phys. Rev. Lett., **82**, 117 (1999).

[112] K. Binder and W. Kob, *Glassy Materials and Disordered Solids: An Introduction to Their Statistical Mechanics* (World Scientific Publishing Company, Singapore, 2005).

[113] M. Fuchs and K. S. Schweizer, Europhys. Lett. (Europhys. Lett.), **51**, 621 (2000).

[114] C. Mayer, E. Stiakakis, E. Zaccarelli, C. N. Likos, F. Sciortino, P. Tartaglia, H. Löwen, and D. Vlassopoulos, Rheol. Acta, **46**, 611 (2006).

[115] E. Zaccarelli, G. Foffi, F. Sciortino, and P. Tartaglia, Phys. Rev. Lett., **91**, 108301 (2003).

[116] T. Voigtmann, Europhys. Lett., **96**, 36006 (2011).

[117] M. Sellitto, J. Chem. Phys., **138**, 224507 (2013).

[118] G. Das, N. Gnan, F. Sciortino, and E. Zaccarelli, J. Chem. Phys., **138**, 134501 (2013).

[119] F. Höfling and T. Franosch, Rep. Prog. Phys., **76**, 046602 (2013).

[120] T. Sentjabrskaja, E. Babaliari, J. Hendricks, M. Laurati, G. Petekidis, and S. U. Egelhaaf, Soft Matter, **9**, 4524 (2013).

[121] W.-S. Xu, Z.-Y. Sun, and L.-J. An, J. Chem. Phys., **137**, 104509 (2012).

[122] F. T. Nya, A. Ayadim, P. Germain, and S. Amokrane, J. Phys.: Condens. Matter, **24**, 325106 (2012).

[123] J. Kurzidim, D. Coslovich, and G. Kahl, J. Phys.: Condens. Matter, **23**, 234122 (2011).

[124] J. Kurzidim and G. Kahl, Mol. Phys., **109**, 1331 (2011).

[125] J. Kurzidim, D. Coslovich, and G. Kahl, Phys. Rev. Lett., **103**, 138303 (2009).

[126] S. Lang, R. Schilling, V. Krakoviack, and T. Franosch, Phys. Rev. E, **86**, 021502 (2012).

[127] R. Seyboldt, D. Hajnal, F. Weysser, and M. Fuchs, Soft Matter, **8**, 4132 (2012).

[128] E. Zaccarelli, C. Mayer, A. Asteriadi, C. N. Likos, F. Sciortino, J. Roovers, H. Iatrou, N. Hadjichristidis, P. Tartaglia, H. Löwen, and D. Vlassopoulos, Phys. Rev. Lett., **95**, 268301 (2005).

[129] E. Stiakakis, B. M. Erwin, D. Vlassopoulos, M. Cloitre, A. Munam, M. Gauthier, H. Iatrou, and N. Hadjichristidis, J. Phys.: Condens. Matter, **23**, 234116 (2011).

[130] J. Bergenholtz and M. Fuchs, Phys. Rev. E, **59**, 5706 (1999).

[131] E. Zaccarelli, G. Foffi, K. Dawson, F. Sciortino, and P. Tartaglia, Phys. Rev. E, **63**, 031501 (2001).

[132] E. Zaccarelli, in *Physics of Complex Colloids*, International School of Physics Enrico Fermi, edited by C. Bechinger, F. Sciortino, and P. Ziherl (IOS Press, 2013) pp. 95–154.

[133] R. Roth, B. Götzelmann, and S. Dietrich, Phys. Rev. Lett., **83**, 448 (1999).

[134] R. Tuinier, E. ten Grotenhuis, C. Holt, P. A. Timmins, and C. G. de Kruif, Phys. Rev. E, **60**, 848 (1999).

[135] B. Götzelmann, R. Roth, S. Dietrich, M. Dijkstra, and R. Evans, Europhys. Lett., **47**, 398 (1999).

[136] R. Roth, R. Evans, and S. Dietrich, Phys. Rev. E, **62**, 5360 (2000).

[137] Roth, R. and Evans, R., Europhys. Lett., **53**, 271 (2001).

[138] R. Roth and P.-M. König, Pramana, **64**, 971 (2005).

[139] R. Roth and M. Kinoshita, J. Chem. Phys., **125**, 084910 (2006).

[140] M. Oettel, H. Hansen-Goos, P. Bryk, and R. Roth, Europhys. Lett., **85**, 36003 (2009).

[141] D. J. Ashton, N. B. Wilding, R. Roth, and R. Evans, Phys. Rev. E, **84**, 061136 (2011).

[142] R. Tuinier, J. K. G. Dhont, and C. G. De Kruif, Langmuir, **16**, 1497 (2000).

[143] A. A. Louis, E. Allahyarov, H. Löwen, and R. Roth, Phys. Rev. E, **65**, 061407 (2002).

[144] A. A. Louis, P. G. Bolhuis, E. J. Meijer, and J. P. Hansen, J. Chem. Phys., **117**, 1893 (2002).

[145] R. Tuinier, G. A. Vliegenthart, and H. N. W. Lekkerkerker, J. Chem. Phys., **113**, 10768 (2000).

[146] R. Tuinier and A. V. Petukhov, Macromol. Theory Simul., **11**, 975 (2002).

[147] R. Tuinier, J. K. G. Dhont, and T.-H. Fan, Europhys. Lett., **75**, 929 (2006).

[148] P.-M. König, R. Roth, and S. Dietrich, Phys. Rev. E, **74**, 041404 (2006).

[149] S. Jungblut, R. Tuinier, K. Binder, and T. Schilling, J. Chem. Phys., **127**, 244909 (2007).

[150] C. Gögelein, G. Nägele, J. Buitenhuis, R. Tuinier, and J. K. G. Dhont, J. Chem. Phys., **130**, 204905 (2009).

[151] G. J. Fleer, A. M. Skvortsov, and R. Tuinier, Macromolecules, **36**, 7857 (2003).

[152] P. Bryk, R. Roth, M. Schoen, and S. Dietrich, Europhys. Lett., **63**, 233 (2003).

[153] R. Roth, J. Phys.: Condens. Matter, **15**, S277 (2003).

[154] R. Tuinier and H. Lekkerkerker, Eur. Phys. J. E, **6**, 129 (2001).

[155] R. Tuinier and T. Taniguchi, J. Phys.: Condens. Matter, **17**, L9 (2005).

[156] D. Kleshchanok, R. Tuinier, and P. R. Lang, Langmuir, **22**, 9121 (2006).

[157] T. Taniguchi, Y. Arai, R. Tuinier, and T.-H. Fan, Eur. Phys. J. E, **35**, 1 (2012).

[158] G. J. Fleer, A. M. Skvortsov, and R. Tuinier, Macromol. Theory Simul., **16**, 531 (2007).

[159] M. Camargo and C. N. Likos, Phys. Rev. Lett., **104**, 078301 (2010).

[160] J. Dzubiella, H. Löwen, and C. N. Likos, Phys. Rev. Lett., **91**, 248301 (2003).

[161] S. Belli, M. Dijkstra, and R. van Roij, J. Phys.: Condens. Matter, **24**, 284128 (2012).

[162] S. Abbas and T. P. Lodge, Phys. Rev. Lett., **99**, 137802 (2007).

[163] F. Sciortino, S. Mossa, E. Zaccarelli, and P. Tartaglia, Phys. Rev. Lett., **93**, 055701 (2004).

[164] J. P. Hansen and I. McDonald, *Theory of Simple Liquids* (Academic, London, 1990).

[165] P. Attard, J. Chem. Phys., **91**, 3083 (1989).

[166] M. Dijkstra, R. van Roij, and R. Evans, Phys. Rev. E, **59**, 5744 (1999).

[167] J. Dzubiella, G. Hoffmann, and H. Löwen, Phys. Rev. E, **65**, 021402 (2002).

[168] U. Balucani, *Dynamics of the Liquid State*, Oxford Series on Neutron Scattering in Condensed Matter (Clarendon Press, 1995).

[169] M. Fuchs, W. Götze, I. Hofacker, and A. Latz, J. Phys.: Condens. Matter, **3**, 5047 (1991).

[170] S. P. Das, Rev. Mod. Phys., **76**, 785 (2004).

[171] W. Götze, *Complex Dynamics of Glass-Forming Liquids : A Mode-Coupling Theory*, International Series of Monographs on Physics (OUP Oxford, 2008).

[172] F. Mallamace, P. Gambadauro, N. Micali, P. Tartaglia, C. Liao, and S.-H. Chen, Phys. Rev. Lett., **84**, 5431 (2000).

[173] G. Foffi, K. A. Dawson, S. V. Buldyrev, F. Sciortino, E. Zaccarelli, and P. Tartaglia, Phys. Rev. E, **65**, 050802 (2002).

[174] S.-H. Chen, W.-R. Chen, and F. Mallamace, Science, **300**, 619 (2003).

[175] M. Sperl, Phys. Rev. E, **68**, 031405 (2003).

[176] V. Krakoviack, Phys. Rev. Lett., **94**, 065703 (2005).

[177] G. Biroli, J.-P. Bouchaud, K. Miyazaki, and D. R. Reichman, Phys. Rev. Lett., **97**, 195701 (2006).

[178] P. Ghosh, A. Shit, S. Chattopadhyay, and J. R. Chaudhuri, Phys. Rev. E, **81**, 061112 (2010).

Acknowledgements

Curriculum Vitae – Daniela Marzi

Ausbildung

ab 10/2011
Universität Wien, Österreich
Doktoratsstudium im Bereich Computational Physics
Voraussichtlicher Abschluss: **Dr. rer. nat**. im Fach Physik
Thema: *Coarse-graining, structure and rheology of polymer colloid nanocomposites*

10/2008 bis 12/2010:
Heinrich-Heine Universität, Düsseldorf , Deutschland
Masterstudium im Fach Physik, Abschluss: **„Master of Science"** (*Note 1,4*)
Thema: *Computer Simulations of Polarizable Colloids*

10/2005 bis 9/2008:
Heinrich-Heine Universität, Düsseldorf, Deutschland
Bachelorstudium der Physik, Abschluss: „**Bachelor of Science**" (*Note: 1,8*)
Thema: *Information theoretic properties of spin systems in moving reference frames*

08/1996 bis 05/2005:
Lise-Meitner-Gymnasium, Leverkusen, Deutschland
Abschluss: Abitur (*Note: 1,5*)

Stipendien:

- 10/2010 – 09/2013: *Marie-Curie Stipendiatin* im EU-Netzwerk

- 08/2009 bis 09/2009: Stipendiatin der *Ben-Gurion Universität,* Beer Sheva, Israel zur Teilnahme an der internationalen Sommeruniversität (inkl. Intensivsprachkurs Hebräisch)
- Wintersemester 2008/09: Basisstipendium der *Heinrich-Heine Universität,* Düsseldorf
- 31.01. bis 04.02.2005: Reisestipendium der *Carl-Duisberg Stiftung* zum Deutschen Museum in München

Präsentationen:

- September 2013: Posterpräsentation, *Soft Matter Conference,* Rom, Italien
- Mai 2013: Posterpräsentation, *Comploids Conference,* Ljubljana, Slowenien
- Mai 2012: Vortrag, *Comploids Annual Meeting*, Edinburgh, Schottland
- Juli 2012: Posterpräsentation, *Varenna Summer School* Physics of Complex Colloids*, International School of Physics „Enrico Fermi", Varenna, Italien
- Februar 2012: Posterpräsentation, Gordon Research Conference, Ventura, Kalifornien, USA
- Februar 2012: Vortrag, *Prof. Randall Kamien Group meeting*, University of Pennsylvania, USA
- Mai 2011: Vortrag, *MidTerm Review Comploids*, Wien
- September 2011: Posterpräsentation, *Liquid Matter Conference*, Wien
- Wintersemester 09/10: Vortrag, *Gruppenseminar Prof. Likos*, Heinrich-Heine Universität, Düsseldorf
- November 2008: Posterpräsentation, *Deutsche Physikerinnentagung*, Münster